MODIFICATION OF BARIUM TITANATE FOR POSITIVE TEMPERATURE
COEFFICIENT OF RESISTIVITY APPLICATIONS

A THESIS SUBMITTED TO
THE GRADUATE SCHOOL OF NATURAL AND APPLIED SCIENCES
OF
THE MIDDLE EAST TECHNICAL UNIVERSITY

BY

HÜSEYİN YILMAZ

IN PARTIAL FULFILLMENT OF THE REQUIREMENTS FOR

THE DEGREE OF MASTER OF SCIENCE

IN

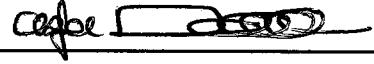THE DEPARTMENT OF METALLURGICAL AND MATERIALS ENGINEERING

JANUARY 1997

Approval of the Graduate School of Natural and Applied Sciences
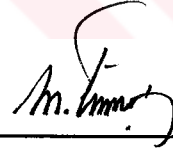
Prof.Dr. Tayfur ÖZTÜRK

Director

I certify that this thesis satisfies all the requirements as a thesis for the degree of Master of Science.

Prof.Dr. Mustafa DORUK

Head of Department

This is to certify that we have read this thesis and that in our opinion it is fully adequate, in scope and quality, as a thesis for the degree of Master of Science.

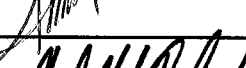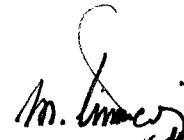Prof.Dr. Muharrem TİMUÇİN

Supervisor

Examining Committee Members

Prof.Dr. Muharrem TİMUÇİN

Prof.Dr. Macit ÖZENBAŞ

Prof.Dr. Güngör GÜNDÜZ

Assist.Prof.Dr. Ali KALKANLI

Assist.Prof.Dr. Abdullah ÖZTÜRK

ABSTRACT

MODIFICATION OF BARIUM TITANATE FOR POSITIVE TEMPERATURE COEFFICIENT OF RESISTIVITY APPLICATIONS

Yılmaz, Hüseyin

M.S.,Department of Metallurgical and Materials Engineering

Supervisor: Prof.Dr. Muharrem Timuçin

In this study, semiconducting $BaTiO_3$ ceramics were produced by doping barium titanate with La^{+3} ions. The powders prepared had the composition of $Ba_{1-x}La_xTiO_3$, where the La^{+3} ion concentrations were varied from 0.0 to 0.5 atomic percent at 0.05 atomic percent steps. 2 mol % excess TiO_2 and 2 mol % SiO_2 were added to ensure liquid phase sintering. Sintering at 1360°C for two hours gave densities in the range 90-95% of the theoretical value in all samples. From the plot of resistivity versus La^{+3} ion concentration it was found that 0.25 atomic percent of La^{+3} ion addition yielded maximum conductivity. The samples cooled directly from the sintering temperature showed poor PTCR effect. Therefore, the PTCR behavior was improved by heat treatment and by manganese additions. Finally, the effect of lead titanate additions on the electrical properties of barium titanate were studied.

Keywords: Perovskite, Barium Titanate, Electrical Resistivity, PTCR, Thermistor

ÖZ

BARYUM TİTANATIN PTC UYGULAMALARI İÇİN MODİFİKASYONU

Yılmaz, Hüseyin

Yüksek Lisans, Metalurji ve Malzeme Mühendisliği Bölümü

Tez Yöneticisi: Prof.Dr. Muharrem Timuçin

Ocak 1997, 141 sayfa

Bu tezde, yarıiletken $BaTiO_3$ seramikleri La^{+3} iyonlarıyla dop edilerek üretilmişlerdir. Üretilen $Ba_{1-x}La_xTiO_3$ tozları yüzde 0.0 - 0.5 aralığında La^{+3} iyonları içermektedir. Bu aralık 0.05 yüzdelik basamaklarla değiştirilmiştir. Sıvı faz sinterlenmesini gerçeklestirebilmek amacıyla her birinden yüzde 2 olmak suretiyle fazladan TiO_2 ve SiO_2 eklemesi yapılmıştır. Örnekler 1360°C de 2 saat sinterlenmiştir. Sinterlenme sonucunda örneklerin yüzde 90-95 kuramsal yoğunluğa ulaştıkları görülmüştür. La^{+3} iyonları derişimine göre özdirencin değişimi incelendiğinde, 0.25 La^{+3} iyon derişimi yüzdesinin en yüksek iletkenliği sağladığı görülmüştür. Sinterlenmenin ardından doğrudan oda sıcaklığına soğutulan örnekler zayıf PTC etkisi göstermişlerdir. Bu nedenle PTC etkisini geliştirebilmek için ısıl işleme ek olarak mangan eklemesi de yapılmıştır. Son olarak kurşun titanat eklenmesinin, baryum titanatın elektriksel özelliğini nasıl etkilediği araştırılmıştır.

Anahtar Kelimeler: Perovskit, Baryum Titanat, Elektriksel Özdirenç, PTC, Termistör.

iv

To My Family

ACKNOWLEDGMENTS

TABLE OF CONTENTS

LIST OF TABLES

LIST OF FIGURES

LIST OF SYMBOLS

PTCR	Positive temperature coefficient of resistivity
ρ	Electrical resistivity, ohm-cm
T_c	Curie temperature
C	Curie constant
ϕ	Grain boundary potential barrier height
ε	Dielectric permittivity
ε_r	Dielectric constant
P_s	Spontaneous polarization
GGIT	Grain growth inhibition threshold
N_s	Density of surface states
E_g	Band gap energy
R_{min}	Minimum resistivity
R_{max}	Maximum resistivity

CHAPTER 1

INTRODUCTION

Barium titanate has been regarded as one of the most prominent ceramic materials in the modern age ever since its discovery as a highly dielectric constant material during World war II. The material is a compound with equimolar combination of BaO and TiO_2 in a crystal lattice known as perovskite structure, the molecular formula being represented as $BaTiO_3$.

Because of its unusually high dielectric permittivity barium titanate has become the basic ceramic capacitor material in use today. The class II dielectrics which are characterized by dielectric constants in the range 2000 to 20000 are manufactured with compositions that are dominated by $BaTiO_3$. The X7R and Z5U dielectrics falling into this particular class find a wide range of applications in modern electronic and electrical circuits.

Soon after the discovery of high dielectric constant it was realized that high permittivity was related to the ferroelectric nature of $BaTiO_3$. This was followed by the invention of the poling process which lead to the development of piezoelectric ceramics. The first commercial ceramic piezoelectric devices were the phonograph pickups made from $BaTiO_3$. Barium titanate enjoyed the leading position in the piezoelectric transducer market until the appearance of lead zirconate titanate compositions.

In the June of 1955, a German patent was issued which disclosed a new application area for $BaTiO_3$ [1]. This was related with an invention of

imparting electrical conductivity to the barium titanate which was normally an insulator. This discovery has led to the opening of two new broad areas of application to the $BaTiO_3$. These are the humidity sensing devices based on porous barium titanate and the thermistors based on the positive temperature coefficient of resistivity effect observed in doped $BaTiO_3$ ceramics. The latter has been the subject of numerous studies in the past and happens to be the subject of the present thesis work as well.

As mentioned above, barium titanate has the crystal structure of perovskite. This structure may be described as a simple cubic unit cell with the large cation (Ba^{+2}) on the corners, the smaller cation (Ti^{+4}) in the body center, and oxygen (O^{-2}) in the centers of the faces, as shown in Figure 1.1. The structure is a network of corner-linked oxygen octahedra, with the smaller cation filling the octahedral holes and the large cation filling the dodecahedral holes [2].

Barium titanate has four polymorphs depending on the temperature. At temperatures above 130°C the unit cell is cubic. Below 130°C, the cell of the perovskite form elongates along an edge, and is then tetragonal with c/a ratio equals to 1.01. The temperature at which the transition from tetragonal to cubic transformation occurs is of special importance and has a specific name, the Curie temperature, T_c. At this temperature ferroelectricity comes into force and the centro-symmetric cubic structure is replaced by a polar one. Upon further cooling, another polymorphic transformation occurs at 0°C. The cube elongates along the face diagonal rather than an edge. This structure is called pseudomonoclinic, but is actually orthorhombic, the axes enclosing the shear angle being equal in length. At even lower temperatures, a third displacive transformation occurs, this time the unit cell elongates along a body diagonal to give rhombohedral symmetry. Figure 1.2 shows the relationships among these polymorphs. In each temperature range the direction of the ferroelectric dipole parallels the elongation of the unit cell [2].
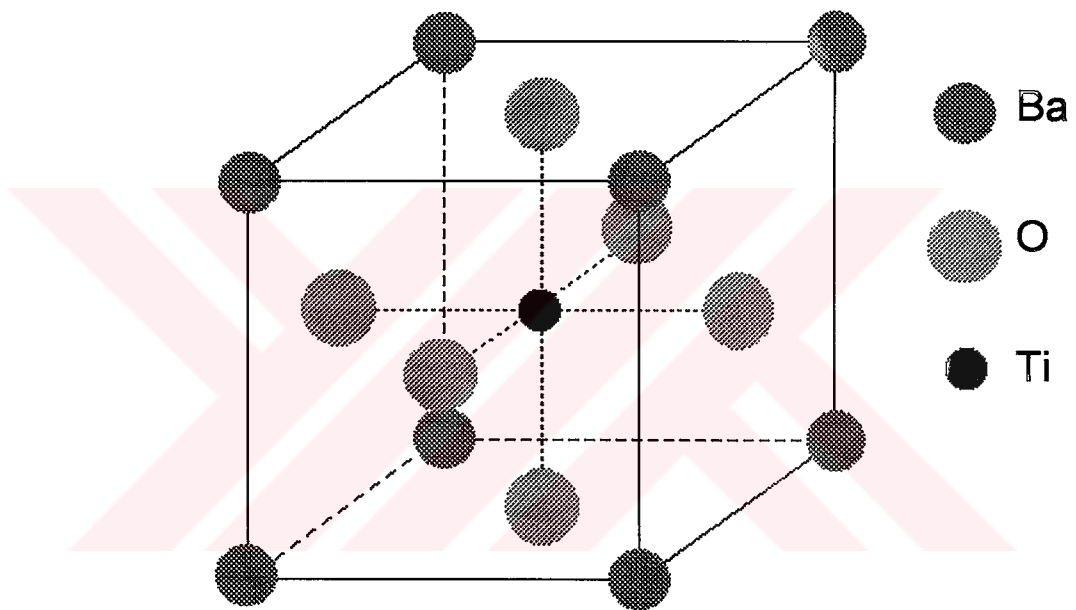
Figure 1.1. Cubic perovskite crystal structure of $BaTiO_3$.

Cubic

at 130°: $a_1 = a_2 = a_3 = 4.009$ Å

130° C

Tetragonal

$a_1 = a_1$ of cubic form
$a = a_2$ of cubic form
$c \neq a_3$ of cubic form

at 130° $\begin{cases} a_1 = a_2 = 4.003 \text{ Å} \\ c = 4.022 \end{cases}$

at 0° $\begin{cases} a_1 = a_2 = 3.992 \\ c = 4.035 \end{cases}$

Monoclinic
(Except that $a_3 = a_1$)

$a_1 = a_1$ of tetragonal form
$c = a_2$ of tetragonal form
$a_3 = c$ of tetragonal form

at 0° $\begin{cases} a_1 = a_3 = 4.012 \text{ Å} \\ c = 3.989 \\ \beta = 89° 51.6' \end{cases}$

at -90° $\begin{cases} a_1 = a_3 = 4.013 \\ c = 3.976 \\ \beta = 89° 51' \end{cases}$

0°C

at 0°

at -90°

Rhombohedral

Orthorhombic

$c = c$
$a' = 2a \sin(\beta/2)$
$b' = 2a \cos(\beta/2)$

at 0° $\begin{cases} a' = 5.667 \text{ Å} \\ b' = 5.681 \\ c = 3.989 \end{cases}$

at -90° $\begin{cases} a' = 5.668 \\ b' = 5.683 \\ c = 3.976 \end{cases}$

-90° C

$a_1 = a_1$
$a_2 = c$ of orthorhombic form
$a_3 = a_3$ of orthorhombic form

at -90° $\begin{cases} a = a_2 = a_3 = 3.998 \text{ Å} \\ \alpha = 89° 52.5' \end{cases}$

Figure 1.2. Distortion of BaTiO$_3$ unit cell in its polymorphic forms [2].

4

The reason for the appearance of these polymorphic transformations originate from the presence of TiO_6-octahedra in barium titanate [3]. When the temperature is lowered below T_c, the position of the Ti^{+4} ion and the octahedral structure changes from cubic to tetragonal symmetry with the Ti^{+4} ion in an off-center position corresponding to a permanent dipole. These dipoles are ordered, giving a domain structure with a net spontaneous polarization within the domains [3].

The transition to the off-center position at T_c results in a series of important physical consequences. The crystal structure changes from cubic (T>130°C) via tetragonal (+5°C<T<130°C) and orthorombic (-90°C<T<+5°C) to rombohedral (T<-90°C). At the same time a spontaneous polarization P_s appears [4]. This large spontaneous polarization gives rise to a large dielectric constant and large temperature dependence of the dielectric constant as shown in Figure 1.3. The spontaneous polarization is considerably stronger in the c-direction which results in the larger dielectric constant in this orientation.

The transition points mentioned above are not fixed. They are variable by doping. This ability of barium titanate is of great importance especially in industrial applications, because by compositional modification a dielectric material suitable for specific application can be produced. The Curie point shifters and their shifting directions are indicated on Figure 1.4.

Pure barium titanate has a band gap of about 2.9 eV, therefore normally it is a resistor with a resistivity of about 10^{10} Ω-cm at room temperature. By doping with ions of higher valency, e.g. La^{+3} instead of Ba^{+2} or Nb^{+5} for Ti^{+4}, [5a], the resistivity of the material can be lowered to around 10^2 Ω-cm at room temperature, making it a semiconductor. In the case for lanthanum doped $BaTiO_3$, the La^{+3} ions incorporated at Ba^{+2} sites carry an excess positive charge which must be compensated for the maintenance of

5
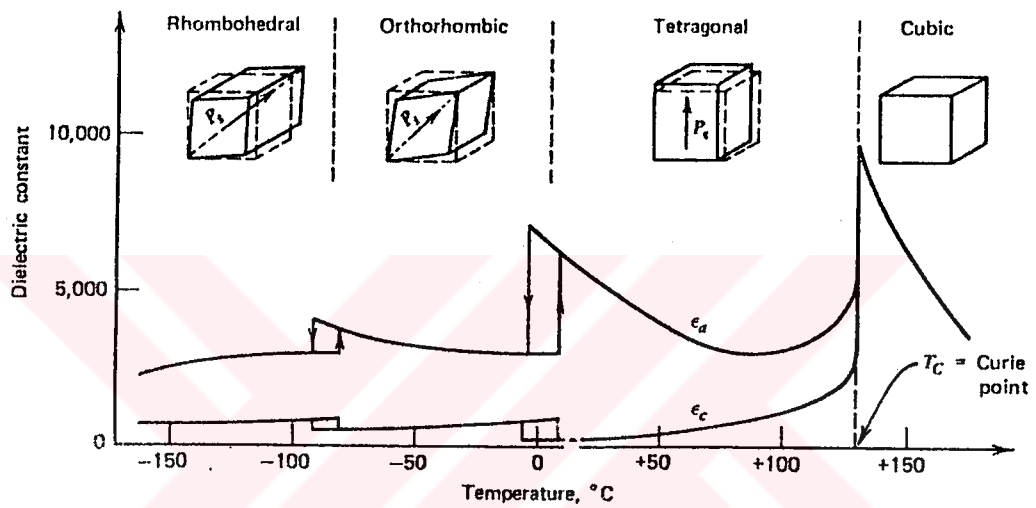
Figure 1.3. Crystal structure; lattice distortion of the unit cell and direction of spontaneous polarization; dielectric constant in dependence on temperature for a $BaTiO_3$ single crystal. The subscript a and c relate to orientations parallel and perpendicular to the tetragonal axis, respectively [4].
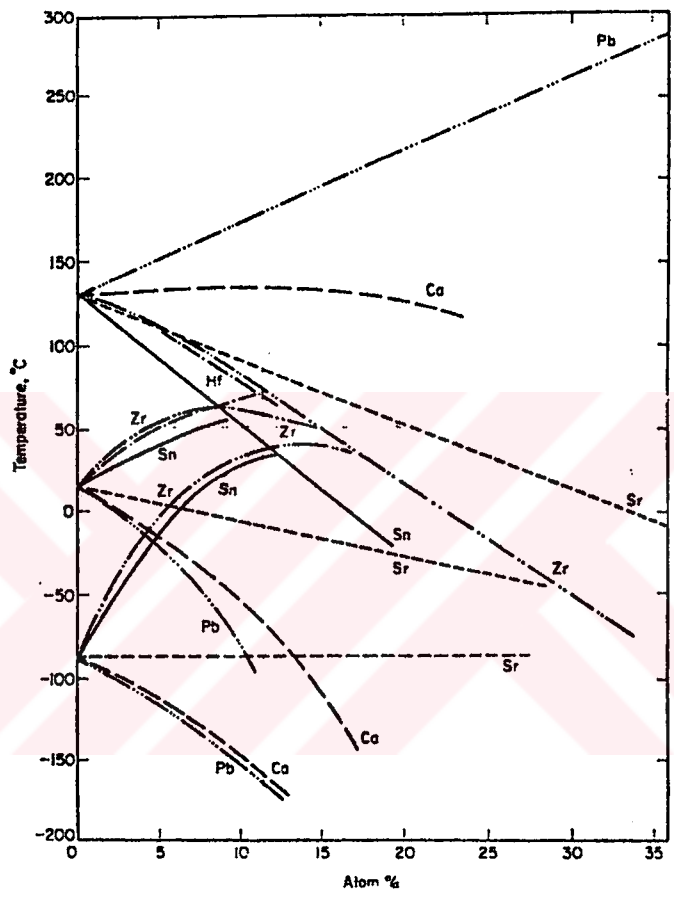
Figure 1.4. Effect of several isovalent substitutions on transition
temperatures of ceramic barium titanate [2].

electrical neutrality. This can be done in two different manners, either by the formation of conducting electrons, (electron compensation) or metal vacancies (vacancy compensation). At room temperature, electron compensation will lead to a conductive material, whereas vacancy compensation leads to insulating material [5a].

When lanthanum doped $BaTiO_3$ is electron compensated it becomes an n-type semiconductor expressed by the formula:

$$Ba_{1-x}La_x TiO_3 = Ba^{+2}_{1-x} La^{+3}_x Ti^{+4}_{1-x} Ti^{+3}_x O^{-2}_3, \qquad (1.1)$$
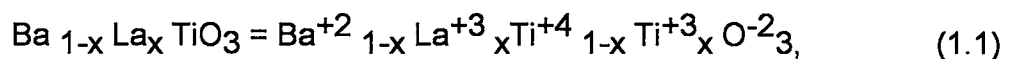
with conduction taking place via transfer of electrons generated by the equilibrium, $Ti^{+4} + e^- = Ti^{+3}$. Thus, the barium titanate grains in the sintered ceramic become conducting on cooling to room temperature [6].

PTCR barium titanate has two basic properties: (i) it is semiconductor around room temperature, (ii) it shows a very steep rise in resistivity above its Curie point which is known as the PTCR (Positive Temperature Coefficient of Resistivity) effect [7]. The so called PTCR effect is characterized as follows: when temperature rises to just above the Curie point, T_c, the resistivity of the ceramic increases sharply with temperature, as shown in Figure 1.5. This curve has three main portions indicated as (a-b), (b-c), and (c-d). In the first portion (a-b), barium titanate is semiconductor and its electrical resistivity decreases gradually with increasing temperature up to point b. Between point b and c the electrical resistivity increases sharply and reaches a maximum at point c; this steep rise is called the PTCR anomaly. In the third portion of the PTCR curve, the resistivity decreases with increasing temperature beyond point c.
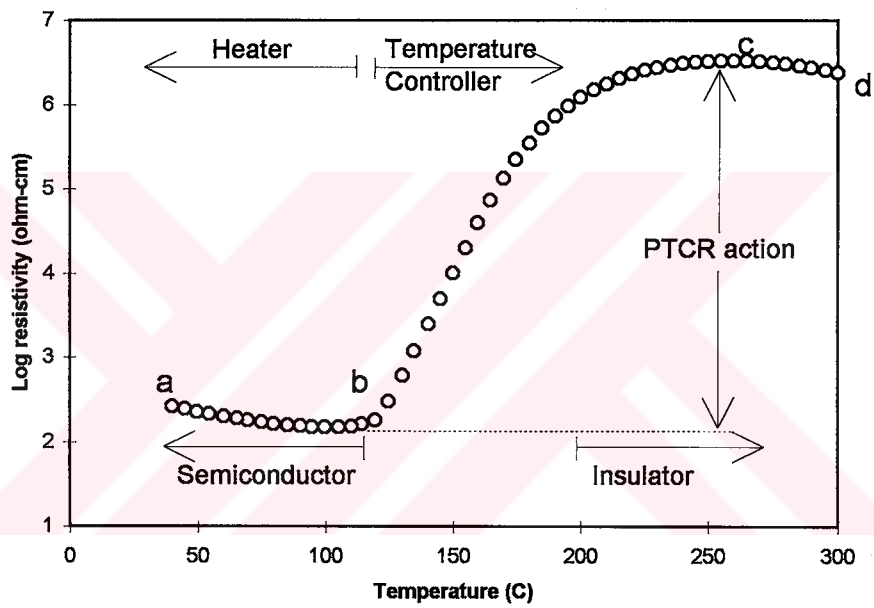
Figure 1.5. A typical resistivity-temperature characteristics of a PTCR
element.

Modified barium titanate for PTCR applications is also called positive temperature coefficient thermistor due to being a thermally sensitive resistor. PTCR materials find applications in many areas.

After the discovery of PTCR action several unique properties were introduced in Japan in the late 1960s and early 1970s: specialty heaters for food processing (rice steamers) and room air heating (harmonica and honey comb type) being typical examples. In addition, temperature utilization was extended to as high as 300°C with the development of $(Ba,Pb)TiO_3$ formulations [8]. Important automotive applications were developed at Texas Instruments, Inc., in the 1970s. A low voltage honeycomb heater employed to assure complete evaporation of the fuel droplets in the colt carburetors was introduced in the 1979. This component, when properly matched with an even faster PTCR heated choke system, has resulted in excellent four-cylinder-cold-start engine performance and lower hydrocarbon and nitrous oxide (NO_x) emission [8]. As a heating element it is superior to metal heating elements because it can apply a faster heating rate, avoid dangerous overheating, and economize electric energy.

A significant effort to develop sensing systems utilizing small PTCR elements as resistance switches has been undertaken in Europe. The introduction of system designs that use these elements in liquid level detection, thermal protection, and other control applications by Phillips is particularly noteworthy [8]. Currently, development efforts are focusing on the high performance PTCR elements. The short term dissipation of larger than 1000 W of energy in small elements and the low cost manufacture of high performance devices should have a significant impact on motor controls, industrial heater, and consumer market [8]. The application tree shown in Figure 1.6. describes pictorially various major application areas of PTCR devices.
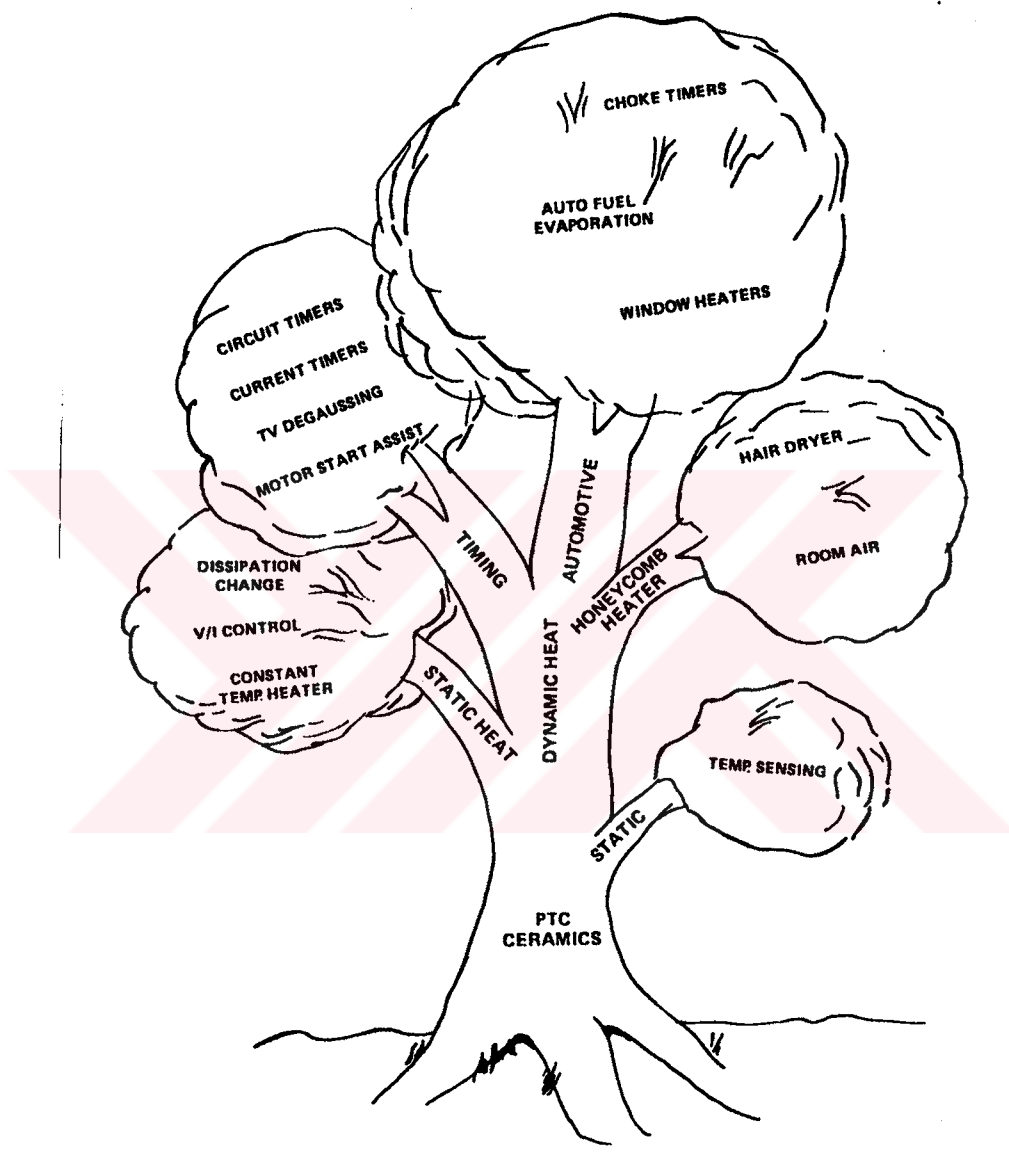
Figure 1.6. Application tree for PTCR elements [8].

Doping barium titanate with an isovalent cation, like Pb^{+2} or Sr^{+2} for Ba^{+2}, produces solid solution with random distribution of cations throughout the crystal. The ability of barium titanate to form solid solutions allow the technologist to produce a wide variety of materials with continuously changing electrical properties in the polycrystalline ceramic state. The Curie point of barium titanate can be shifted to lower temperatures by the substitution of Sr^{+2} for Ba^{+2}, or Sn^{+4} or Zr^{+4} for Ti^{+4}. T_c can be shifted to higher temperatures by the substitution of Pb^{+2} for Ba^{+2}. Lead is the only known element that shifts the Curie point to higher temperatures, as shown in Figure 1.7. This is a significant advantage for barium titanate based PTCR materials in practice [4].

Undoped barium titanate could be made semiconducting by giving it a reduction heat treatment in a gaseous atmosphere which contains H_2 or CO [9]. The increased conductivity has been attributed to the partial reduction of Ti^{+4} ions to Ti^{+3} state whereby excess conduction electrons were generated. Although atmospheric reduction has been conceived as an alternative process for reducing $BaTiO_3$ semiconductor, the PTCR effect was never observed in these samples. Therefore much of the previous studies on PTCR barium titanate were centered on the dopants which produced the PTC action. These studies contributed greatly to the understanding of the mechanism of the PTCR behavior.

Many studies have been reported on the fabrication of PTC thermistors [10, 11, 12, 13] and dopant effects [14, 15, 16, 17]. Great many doping elements which make barium titanate ceramics semiconductive are known, like yttrium, lanthanum and their rare-earth family or bismuth, antimony, niobium and tantalum, [12]. The conductivity phenomena prove to be independent of the kind of donor ions. In Table 1.1 electrical conductivity character of doped barium titanate are given with the ionic radii of dopants. It is generally found that the doping elements should be chosen from those
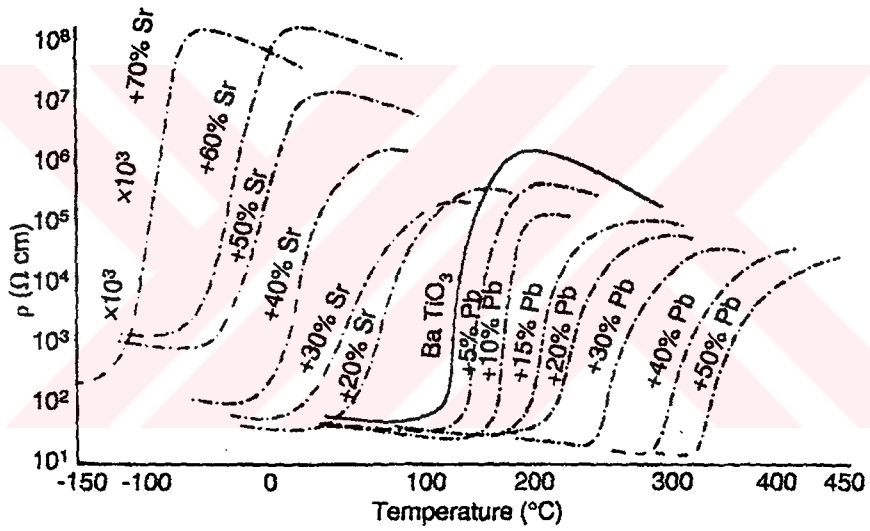
Figure 1.7. Shift of the Curie point of $BaTiO_3$ by substitution of Ba^{+2} ions by Pb^{+2} ions [8].

Table 1.1. Electrical conductivity character of lanthanide-doped BaTiO$_3$ [15]. S = Semiconducting, I = Insulating, GGIT = Grain growth inhibition threshold.

Dopant	GGIT (at.%)	R.T. electrical resistivity	
		Low content	High content
La (0.114)	0.30	S	I
Ce (0.107)	0.25	S	I
Pr (0.106)	0.45	S	I
Nd (0.104)	0.35	S	I
Sm (0.098)	0.45	S	I
Eu (0.098)	0.40	S	I
Gd (0.097)	0.40	S	I
Tb (0.093)	0.40	S	I
Dy (0.092)	0.45	S	I
Ho (0.091)	0.55	S	I
Er (0.089)	2.50	S	I
Tm (0.087)	no GGIT up to 2.0 %	I	I
Yb (0.086)	1.50	I	I
Lu (0.085)	0.50	I	I

which have radii similar to Ba^{+2} and valences larger than two, or from those of dopants which have radii similar to Ti^{+4} and valences larger than four.

Prior to the discovery of the PTCR effect, titanate ceramics were made from raw materials of the type in which Al, Si, and other impurities did not unduly influence the nonlinear dielectric functions for which they were intended. As PTCR developments progressed, however, the impact of certain impurities at less than 100 ppm on PTCR performance became known. At least certain poisonous elements such as Na^+ and Fe^{+3} should be below certain concentrations. Otherwise the resistivity of the obtained ceramics rises abruptly [12]. In commercial raw materials a wide range of impurities, like Na, K, Fe, Cu, Mn, V, are usually found. Ueoka [12, 14] qualified the effects of Na, V, Cr, Mn, and Fe + Mn and concluded that exact control of impurities as well as additives were very important for industrial manufacturing of high-quality PTC thermistors. Therefore, it is desirable to use the highest-purity raw material sources and dope the base composition with the desired conduction generator, modifiers and/or sintering aids [8]. It is also very important to avoid contamination as much as possible throughout the whole ceramic processing process.

Ueoka [12] listed some key steps for successful manufacturing of high quality PTC thermistors with the first two steps being: (i) the use of high-purity raw materials and (ii) controlling the amount of effective additives. This indicates that an understanding of the influence of contaminating impurities and the interactions among additives and impurities is a necessity for manufacturing PTC thermistors.

The resistivity behavior of barium titanate as a function of donor dopant concentration is as follows: at low donor dopant concentration the material is insulator but with increasing dopant concentration the resistivity decreases and reaches a minimum at a certain point. When the critical

15

donor dopant concentration is exceeded the resistivity starts to increase and after a certain point the material is no longer semiconductor. It is claimed that this U-shaped behavior is independent of parameters like powder characteristics and sintering conditions. But the minimum of the resistivity curve changes with the kind of donor dopant used, as shown in Figure 1.8.

The aim of the present thesis study was to examine the effects of doping on the resistivity of barium titanate ceramics and the ensuing PTCR behavior. The dopants selected were lanthanum and manganese; the former was chosen for including semiconductivity and the latter for modifying the PTC anomaly. An additional goal was to study the extent of the Curie temperature shifts and associated changes in the conductivity and PTC anomaly when lead titanate was introduced into the basic ceramic composition. Although the general trends could be anticipated from published literature, the study had to be done in order to generate the processing information for the selected raw materials so that some of the proprietary processing knowledge could be uncovered.
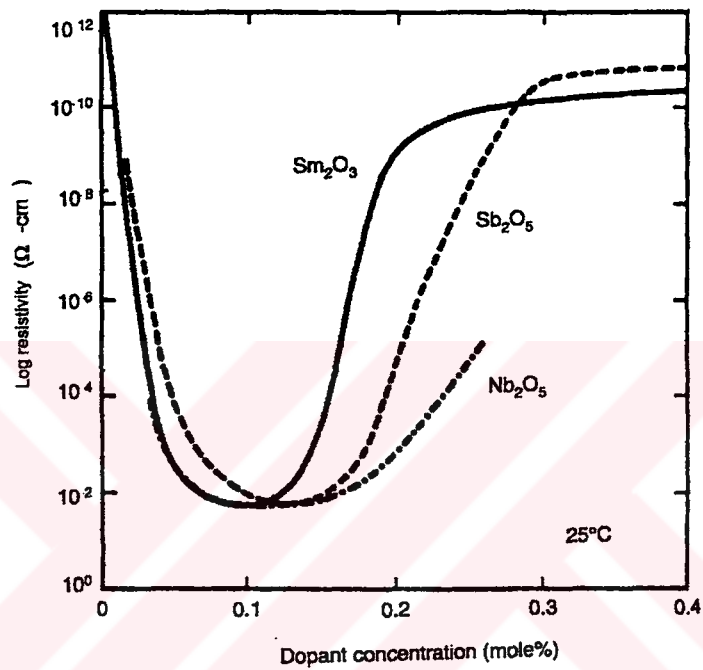
Figure 1.8. The position of the log resistivity versus donor dopant concentration curves for donor doped barium titanate [18].

CHAPTER 2

LITERATURE REVIEW

2.1. Processing

2.1.1. Production

The most widely used process for PTC thermistor fabrication is the carbonate-TiO_2 slurry method. In this method, the raw materials are selected carefully for chemical purity, dispersed in deionized water, and mixed intimately in a ball mill using high density grinding ZrO_2 media. After milling, the slurry is filtered and dried, then calcined at ~1100°C to achieve the desired titanate crystallite agglomerates. The agglomerates are reduced to the desired particle size and sintering reactivity using a wet ball milling method similar to that described above. At this stage, binder and lubricants are added and the slurry is spray dried into free flowing granulates, then compacted using uniaxial pressing. Pressed compacts were then sintered, after careful binder removal, at temperatures between 1300°-1400°C [18].

There are several chemical methods that may be used for PTC powder synthesis, including sol-gel, co-precipitation, and the more popular carbonate-TiO_2 slurry method. These co-precipitation methods lead to higher purity products than are normally produced in the $BaCO_3$-TiO_2 solid state thermochemical reaction, but they are more costly than a properly prepared ceramic reacted from $BaCO_3$ and TiO_2 [2].

18

2.1.2. Additives

2.1.2.1. Modifier/Acceptor Addition

Acceptor additives are not essential for the occurrence of the PTCR effect but they generally increase the magnitude of PTCR action [19b]. Donor-acceptor co-doped ceramics were found to be much more durable against the applied voltage than the usual one [12]. However, the exact way in which these elements modify the PTCR behavior is still not very well understood. There are conflicting interpretations in the literature.

Manganese is of special interest for PTCR thermistors since it is considered to be particularly effective in enhancing the resistivity change at the Curie point [19a]. Manganese was tought to substitute for Ti^{+4} ions at low valency state, and therefore act as an acceptor. Early models for improvement of the PTCR effect proposed segregation of 3d transition metal acceptor impurities at the grain boundaries [20], leading to an increase in their concentration at the grain surfaces. Charge compensation of such acceptor dopants can occur via anion vacancies or holes. The transition metal skin layer surrounding the grains would also provide more favorable oxygen adsorption sites [21]. Heywang [20] and Brauer [22] also observed the segregation of manganese in the intergranular glassy second phase (added to provide liquid phase) and proposed an explanation based on the potential barrier model. According to Heywang and Brauer the increased concentration of the 3d transition elements at the grain-boundary region results in an increase in the surface-state acceptor density and the consequent enhancement of the PTCR effect.

Other authors [5, 23], however, assumed a homogeneous distribution of acceptors through the lattice. Using their studies of the defect formation in these materials at elevated temperatures, Daniels and Wernicke [5]

attributed the effect of the 3d transition elements to the formation of an insulating grain boundary layer, rich in Ba vacancies (acting as acceptors), arising as a consequence of the incorporation of the 3d elements into the lattice.

Most of the previous investigations show that manganese occupies the Ti^{+4} site [24], but they did not specify the valence state of manganese after normal furnace cooling in air. The change in oxidation state of manganese as a function of oxygen partial pressure has been reported by some authors. However, very little attention has been paid to the valence state of manganese with temperature [24]. Although there are some doubt about the change of valance state of manganese with temperature, some authors still insist on the valance change with temperature [24].

The electron spin resonance (ESR) was employed to examine the valence state of manganese ions in barium titanate, [24]. It is reported that the predominant valence state of manganese at room temperature was +3, and that the valence state of manganese changed from +3 in tetragonal phase to +2 in the cubic phase. Due to the similarity in ionic radii of Mn^{+2} (0.67 nm) and Mn^{+3} (0.58 nm) with that of Ti^{+4} (0.61 nm), it was reasonable to assume that manganese doped the titanium site in the perovskite structures. Manganese with +2 or with +3 valence state resulted in the formation of defects like Mn_{Ti}'' or Mn_{Ti}' respectively [17]. The valence change of manganese ions segregated on grain boundaries played the leading role in improving the PTCR effect by joining with existing acceptors at grain boundaries such as cation vacancies [5] or adsorbed oxygen [25]. As a result, manganese doping raises the potential barrier of the grain boundary, owing to enhancement of surface acceptor states [24].

Ting and his co-workers [17] found by experiments that the change of resistivity of barium titanate with lanthanum doping depended on the

manganese addition as well. Following correlation (1) was derived between the concentrations of La^{+3} and Mn^{+x} (where +x represents +2 or +3) for the position of the minimum point in the resistivity curve shown in Figure 1.8

$$[La^{+3}] - 2[Mn^{+x}] \sim 0.15, \tag{2.1}$$

2.1.2.2. Sintering Aids and Liquid Phase Sintering

Liquid phase sintering aids are commonly employed in the preparation of ceramic materials to enhance the densification of samples via dissolution and precipitation mechanisms [26].

Examination of the BaO-TiO_2 phase diagram shows that a eutectic temperature on the TiO_2 excess side of $BaTiO_3$ occurs at 1317°C as shown in Figure 2.1 and in Figure 2.2. The liquid phase created at temperatures above the eutectic is quite fluid, it wets the titanate grains readily, and induces rapid densification of the powder compacts [8]. A slight excess of TiO_2 from stoichiometry does not effect the resistivity of the end product [11].

Negas [27] reported that below 1317°C, the adjacent phase on the TiO_2-rich side of $BaTiO_3$ is $Ba_6Ti_{17}O_{40}$. The solubility of TiO_2 in the $BaTiO_3$ phase is less than 100 ppm, indicating that TiO_2 is practically insoluble in $BaTiO_3$ [28].

In addition to excess TiO_2 a small amount of silica promotes the sintering of ceramics [11]. The approximate addition of SiO_2 decreases the temperature at which barium titanate ceramics become semiconductive, and moreover, this is effective to make ceramic grains the same size; This prevents fluctuations of electrical properties and also improves the durability against applied voltage [12]. The addition of small amounts of SiO_2 reduces

21
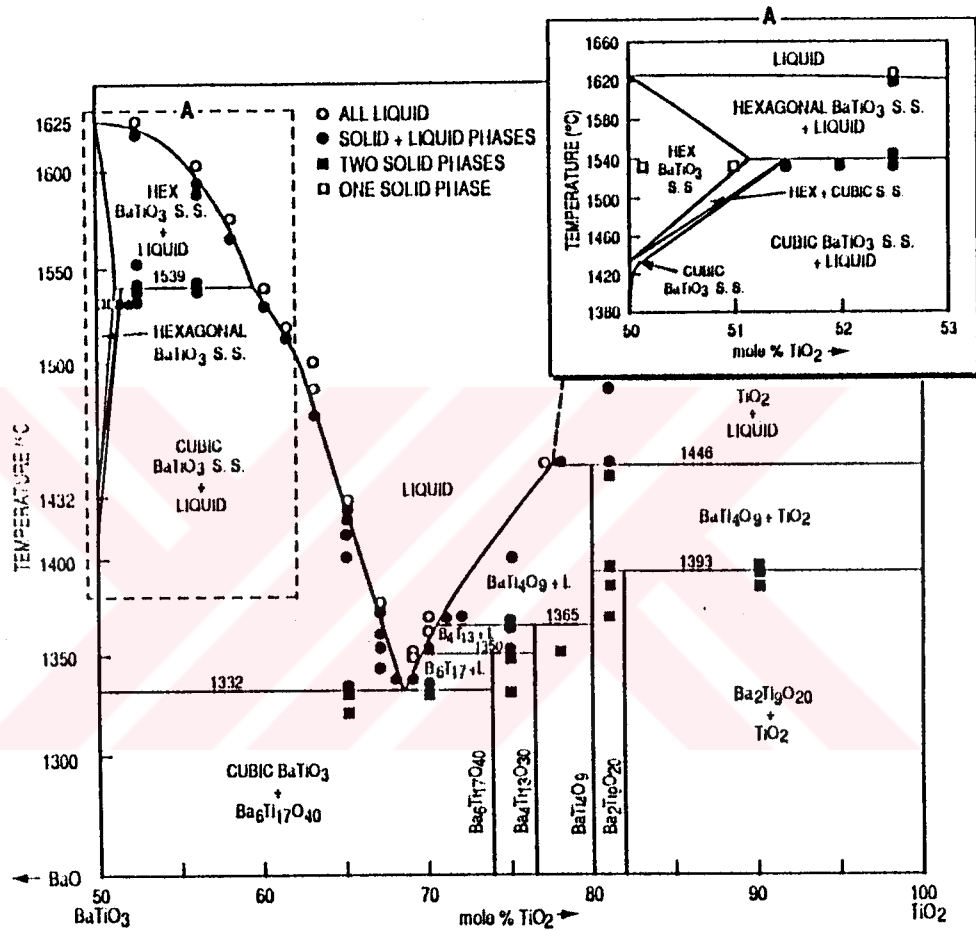
Figure 2.1. BaTiO₃-TiO₂ equilibrium phase diagram. Composition is given in terms of the components BaO and TiO₂ [27].
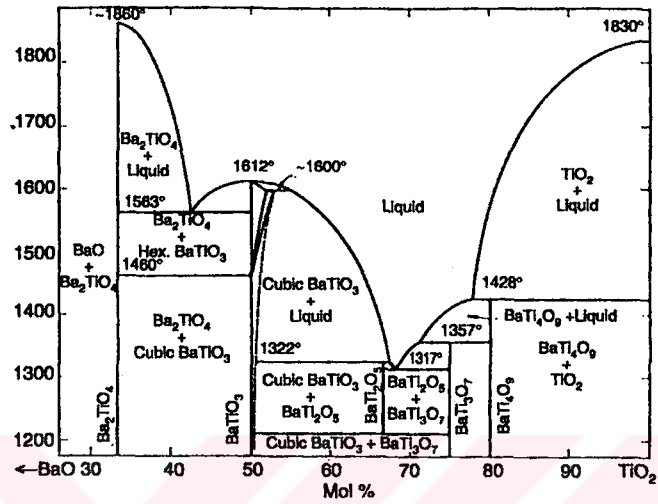
Figure 2.2. BaO-TiO$_2$ equilibrium phase diagram [18].
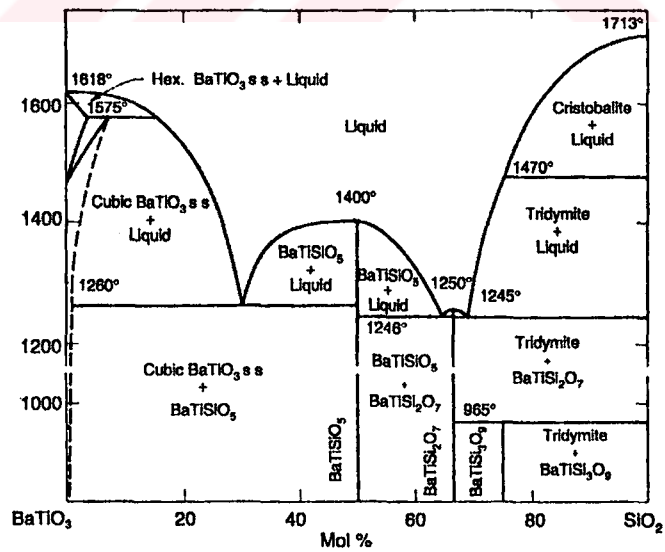
Figure 2.3. BaTiO$_3$-SiO$_2$ equilibrium phase diagram [18].

the eutectic temperature further. The $BaTiO_3$-SiO_2 liquid phase has a melting temperature of ~1260°C as shown in Figure 2.3 [29].

The boundary liquid phase is believed to serve an additional function besides aiding in sintering. The (BaTi) silicate liquid phase can serve as a host for alkali, Al, Mg, P, and other potential poisons that influence PTCR performance (i.e., the collection of other impurities that could adversely affect grain resistivity and depletion of carriers immediately adjacent to the boundary interface). As the boundary surfaces sweep across the crystallites, impurities are segregated to the liquid phase and remain isolated from the crystallized semiconducting perovskite grains [8].

Very small amounts of dopants are added to convert $BaTiO_3$ into a semiconductor. Recent investigations demonstrate that the liquid phase present during densification for TiO_2 excess and SiO_2 containing samples incorporate dopants more efficiently without decreasing the resistivity jump at the Curie temperature [30].

2.1.2.3. Annealing

Kahn found that the PTCR anomaly in doped $BaTiO_3$ appeared only after thermal treatment in oxidizing atmosphere [31]. Therefore, it is accepted that the PTCR effect is related to the oxygen absorption and subsequent trapping of conduction electrons at the grain boundaries [25]. Photoemissivity measurements indicate possibly related chemisorption of oxygen on the surface of barium titanate crystals [32]. There is evidence that grain boundary trapping centers can also be due to the presence of other elements like manganese.

With reference to Figure 2.4, the extra oxygen ion adsorbed at the grain surface functions as follows: it attracts electrons from nearby Ti^{+3} ions,

24
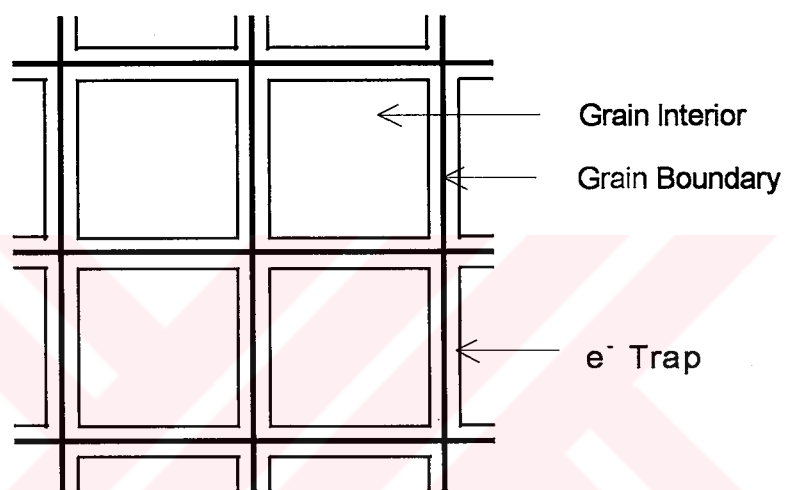
Figure 2.4. Grain boundary structure of doped BaTiO$_3$ in oxidizing atmosphere [6].

thereby creating an insulating layer between grains [6]. The oxidation process can be described by the following formula:

$$Ba^{+2}_{1-x} La^{+3}_{x}) (Ti^{+4}_{1-x+2y} Ti^{+3}_{x-2y}) O^{-2}_{3+y}, \qquad (2.2)$$
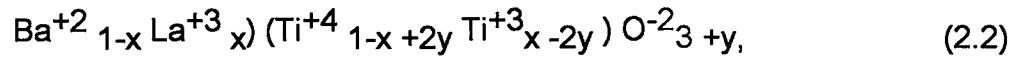
It is reported that the grain boundary region immediately adjacent to the grain boundary surface becomes depleted of carriers. This change is associated with a metastable equilibrium being established upon cooling the PTCR composition from the sintering temperature through the oxidation region between 1260°C and 1000°C. It is obvious that oxidation can proceed quickly along grain boundaries to establish a barrier region of very thin dimensions adjacent to the boundary interface [8]. Experimental evidence indicates that boundary layer oxidation is nearly complete below 1000°C. Further cooling does not effect electrical properties until the Curie point is approached [8].

The free carrier depletion in the boundary layer region is dependent on the microstructure and grain size of the PTCR element and the ratio between the grain boundary and bulk diffusion rates of the species that cause free carrier depletion. The addition of modifiers allow the materials technologist to control the oxidation of the grain boundary region and thus optimize PTCR properties [8].

2.2. Behavior Models

The PTCR effect and the defect chemistry of $BaTiO_3$ have been especially studied and monographs dealing with these themes have been published. Despite this, some of the factors which govern the process of the formation of semiconducting ceramics exhibiting the PTCR effect and some of the resulting electrical properties are not clear. Therefore, there exists several models that explains the PTCR effect.

2.2.1. Heywang's Model

A widely accepted explanation for the PTCR effect of $BaTiO_3$ was first given by W. Heywang [33]. He assumed the presence of surface states with an acceptor character at the grain boundaries. These surface states take up conduction electrons from the immediate vicinity, thus giving rise to a negatively charged boundary layer with, on both sides, a positive space charge that forms a symmetrical potential barrier for the remaining conduction electrons. According to the Heywang's model the electrical resistivity (ρ) is exponential function of the barrier height and is given as:

$$\rho = \rho_o \exp[\phi / kT], \tag{2.3}$$

where ρ_o is a constant and ϕ is the height of the potential barrier defined by:

$$\phi \propto N_s^2 / \varepsilon n, \tag{2.4}$$

where N_s is the density of surface states, ε is the dielectric permittivity and n is the concentration of conduction electrons. At temperatures above the Curie point the permittivity ε follows the Curie-Weiss law:

$$\varepsilon = C / (T-T_c), \tag{2.5}$$

where C is the Curie constant and T_c is the Curie temperature. Since ϕ is inversely proportional to the dielectric constant, the height of the potential barrier increases rapidly at a temperature above the Curie point, where the dielectric constant decreases sharply, Figure 2.5 and this would therefore explain the steep rise in the electrical resistivity above the Curie point. Thus, according to Heywang, the steep rise in the electrical resistivity above the Curie point is a result of surface barriers which are very sensitive to the value of the dielectric constant.

27
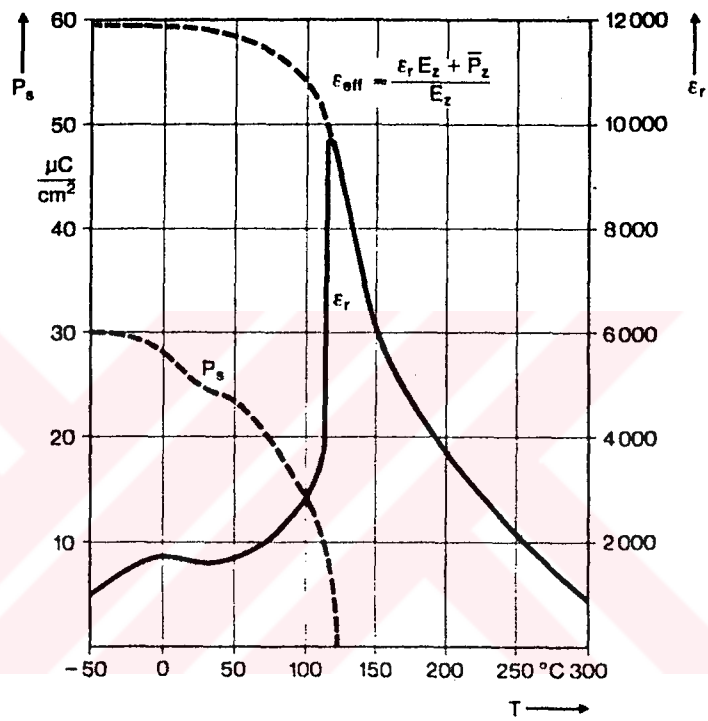
Figure 2.5. Dielectric properties of BaTiO₃. P_s is spontaneous polarization, ε_r is the small field permittivity, ε_{eff} is the AC high field permittivity [34].

About 10°C above T_c a spontaneous polarization P_s develops combined with a distortion of the cubic lattice by about 1%. Due to this distortion the relative permittivity decays to about 2000. This decay does not occur when the applied voltage is high enough to orient the spontaneous polarization, this means when its average field strength is higher than about 10^3 V/cm. This is shown by the curve of ε_{eff}. In this high field strength case there are contributions both from a field induced polarization $\varepsilon_r E_z$ and from an oriented spontaneous polarization P_z.

The observation, that the slope of ε_{eff} and the measured resistance are closely related has led to the development of the grain boundary model of the PTCR resistors. It explains the whole behavior of the material and is described in the band diagram of Figure 2.6 [20, 33, 34].

Heywang's model explained the marked change in resistivity as being due to potential barriers (depletion layers) at the grain boundaries. The above model supports that, the resistivity anomaly is due to a decrease in carrier density and not due to a decrease in carrier mobility. This agrees very well with investigations of the Hall effect made by Ryan and Subbarao [35]. The height of these barriers is controlled by the electric constant ε and by the spontaneous ferroelectric polarization. The potential barriers are thought to be caused by acceptor-type surface states, the nature of which has not yet been adequately explained. Heywang assume impurities which segregate preferentially at the grain boundaries. Without an understanding of the surface states it is not possible to derive statements from the Heywang model in which way the PTCR properties can be influenced by an appropriate treatment of the specimens [5e].

This model is unable to the formation of grain boundary acceptor states. However, among the theories proposed to explain the electrical
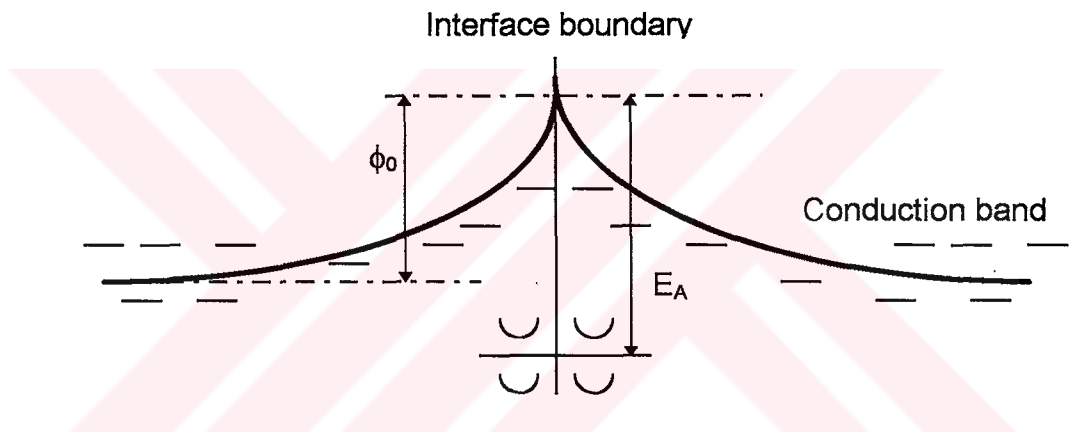
Figure 2.6. Energy level diagram near the boundary after Heywang [34].

structure of the grain boundary, Heywang's model of treating the potential in the depletion region as a Shottky barrier type is the most widely accepted.

2.2.2. Jonker's Model

Jonker's model differs from Heywang's model in that the former considered the ferroelectric nature of $BaTiO_3$ originally as the main cause of the disappearance of grain boundary resistance below the Curie point. In addition to that, he proposed the presence of a thin adsorbed layer of oxygen at the grain boundary as the nature of acceptors responsible for the increase in resistivity above the Curie point [25].

In a polycrystalline ferroelectric sample each crystal is split up into ferroelectric domains which are spontaneously polarized. The particular domain pattern formed is a result of the stresses created at the Curie point, uncompensated surface charges, and physical imperfections [2]. The polarization direction is along the tetragonal axis, which change in direction from domain to domain. At the contact between two crystals of different orientation, the domain structures do not fit. As a result, there would be a non-continuos normal component of the polarization through the surface. As this is impossible, domain structures are formed which fit as well as possible, but the surface layers must be strained in order to get a complete fit.

The difficulty of non-fitting domains in neighbor crystals does not exist, as there is the possibility of compensation by surface charges. These would form a pattern of positive and negative charged surface layers as given in Figure 2.7. This leads at once to the disappearance of the contact resistance. In the case of a compensation by a negative surface charge, this charge fills up more or less the depletion layer. This happens in roughly 50 per cent of the boundary layer and this may be considered as enough for a good contact. In the other 50 per cent of the surface the contact is even

31
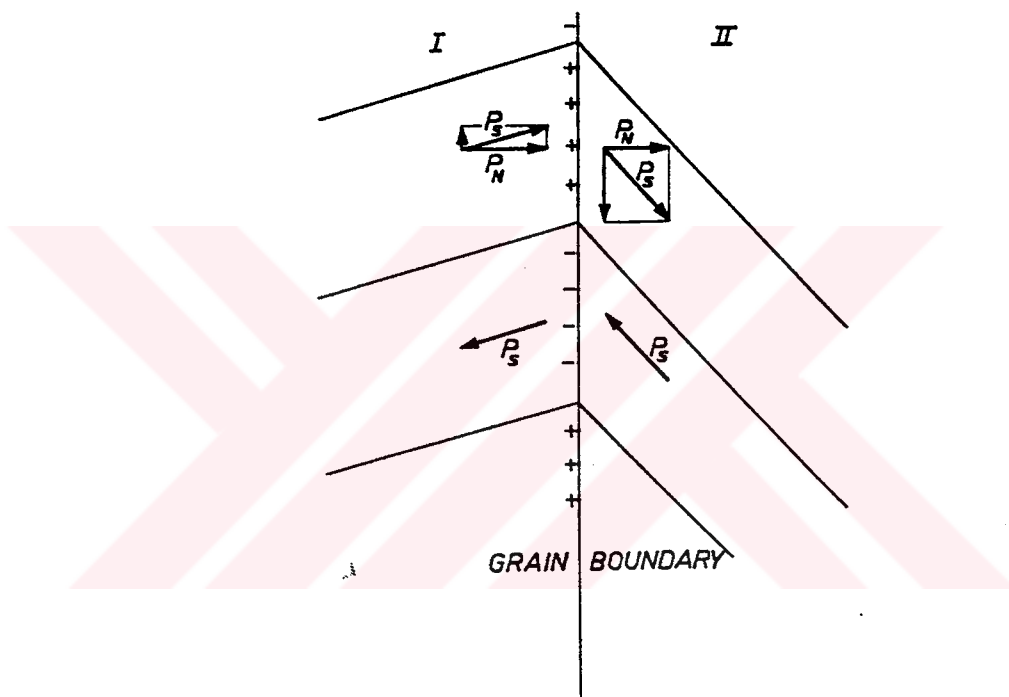
Figure 2.7. Polarization of ferroelectric domains at the grain boundary [36].

worse, but this does not matter. Once this picture is accepted, it is perhaps better to consider this effect the other way around: by assuming that the domain pattern below the Curie point is built up in such a way that the surface charge-electrons trapped in the surface states-forms the compensation of the difference in normal component of the polarization on both sides of the boundary, and that no depletion layer is formed [36].

$$\Delta P_n = en_s, \tag{2.6}$$

where ΔP_n is non continuous normal component of the polarization and n_s is electrons trapped in the surface states at a distance E_s below the conduction band. Here the order of magnitude of ΔP and en_s should be compared. At the Curie point P_s is equal to $18\mu C/cm^2$. This corresponds to 1.3×10^{14} electrons/cm^2. This is indeed the order of magnitude of the surface charge found in Jonker's samples [36].

2.2.3. Defect Model of Barium Titanate

J. Daniels and K. H. Hardtl [7, 5.a] developed a defect model for donor doped barium titanate to explain the PTCR anomaly. They proposed the barium vacancies at the grain boundary as the nature of acceptor postulated in Heywang's model, which trap the conduction electrons and thus give rise to the potential barriers.

It should be mentioned that it will be almost impossible to draw up an exact model of all defects that may occur in $BaTiO_3$. Nevertheless, the attempt of Daniels seems useful to describe the phenomena with the smallest possible set of different defects. In his attempt all interstitial lattice defects were excluded, most probably an admissible assumption on the account of the high packing density of the perovskite lattice of $BaTiO_3$.

Furthermore defect clusters and all effects originating from an interaction of the defects of high concentrations were not taken into account [5a].

In doping, it is assumed that there are no defects in the system considered other than neutral and singly or doubly ionized (positively charged) oxygen vacancies (V_o, $V_o^{\cdot}$, $V_o^{\cdot\cdot}$), and neutral as well as singly or doubly (negatively charged) barium vacancies (V_{Ba}, V_{Ba}', V_{Ba}''). It is also to be assumed that the presence of titanium vacancies in the system may be treated as negligible [5d].

With these assumptions the electroneutrality equation is:

$$n + [\, V_{Ba}'\,] + 2[\, V_{Ba}''\,] = p + [\, V_o^{\cdot}\,] + 2[\, V_o^{\cdot\cdot}\,] + [\, La^{\cdot}\,], \qquad (2.7)$$

where n represents the concentration of conduction electrons, p the concentrations of holes, and [$La^{\cdot}$] the concentrations of the La^{+3} atom substituted and subsequently ionized at Ba^{+2} sites [7].

The defects that take part in the reaction equations listed in the left-hand column of Table 2.1, and their equilibrium conditions are given by the law of mass action are listed in the right-hand column. Relation (2.14) applies to any semiconductor, and relation (2.15) is the modified Schottky equation [5d]

Combination of these nine equations yield the relation between the electron concentration, the oxygen partial pressure, the La^{+3} concentration and the equilibrium constants. Based on the equations in Table 2.1 the calculated concentrations of all the defects considered in the doped material are given in Figure 2.8.

Table2.1. Defect reaction equations and their equilibrium constants [7].

Reaction equation	Equilibrium condition
(2.8) $O_x \leftrightarrow V_o + 1/2O_2$ (g)	$[V_o]Po_2^{1/2} = K_1 = N_1\exp(-E_1/kT)$
(2.9) $V_o \leftrightarrow V_o^{\cdot} + e$	$[V_o^{\cdot}]n/[V_o] = K_2 = N_2\exp(-E_2/kT)$
(2.10) $V_o^{\cdot} \leftrightarrow V_o^{\cdot\cdot} + e$	$[V_o^{\cdot\cdot}]n/[V_o^{\cdot}] = K_3 = N_3\exp(-E_3/kT)$
(2.11) $V_{Ba} \leftrightarrow V_{Ba}{}' + h$	$[V_{Ba}{}']p/[V_{Ba}] = K_4 = N_4\exp(-E_4/kT)$
(2.12) $V_{Ba}{}' \leftrightarrow V_{Ba}{}'' + h$	$[V_{Ba}{}'']p/[V_{Ba}{}'] = K_5 = N_5\exp(-E_5/kT)$
(2.13) $La \leftrightarrow La^{\cdot} + e$	$[La^{\cdot}]n/[La] = K_D = N_D\exp(-E_D/kT)$
(2.14) $e + h = 0$	$np = K_i = N_cN_v\exp(-E_g/kT)$
(2.15) $BaTi_3O_7 + 2Ba_x + 2O_x \leftrightarrow$ $3BaTiO_3 + 2V_{Ba} + 2V_o$	$[V_o][V_{Ba}] = K_s$
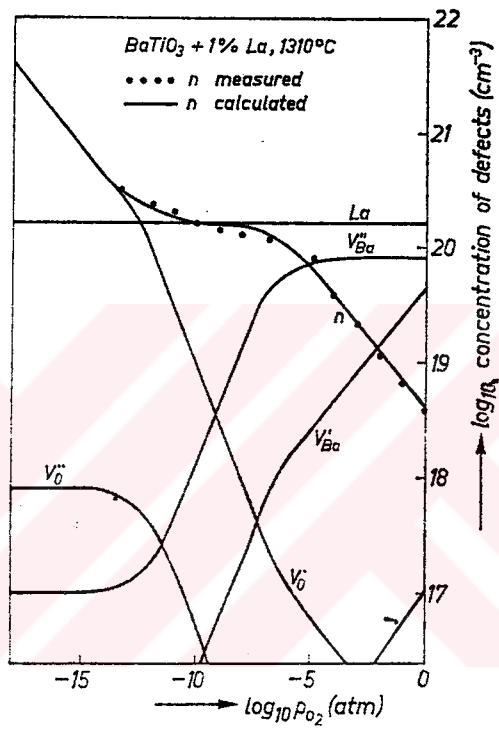
Figure 2.8. The concentrations c of all defects taken into account in the above model [5].

From the findings of Daniels and his co-workers [7, 5] the following three different neutrality conditions apply to the doped material in the pressure regions I, II, and III, shown in Figure 2.8. The great concentration of barium vacancies $[V_{Ba}'']$ at high oxygen partial pressures means that in region I the electrons are trapped. The ionized donors are compensated by the twofold negatively ionized barium vacancies (vacancy compensation), so that the electroneutrality equation reduces to:

$$2[V_{Ba}''] = [La^{\cdot}], \qquad (2.16)$$

and the material tends to vacancy compensation.

In region II the ionized donors are the predominant defects. Their number is equal to the total number of incorporated La^{+3} atoms (electron compensation). The concentration of electrons is independent of the partial pressure, and the neutrality equation here reduces to:

$$n = [La^{\cdot}], \qquad (2.17)$$

In region III the singly ionized oxygen vacancies are predominant defects and the neutrality equation reduces to:

$$n = [V_o^{\cdot}], \qquad (2.18)$$

Both in region II and in region III the charge is compensated by electrons, and the transition from vacancy compensation (high-ohmic) to electron compensation (low-ohmic), which is so important with respect to the resistance properties at room temperature, takes place during the transition from region I to region II [5a].
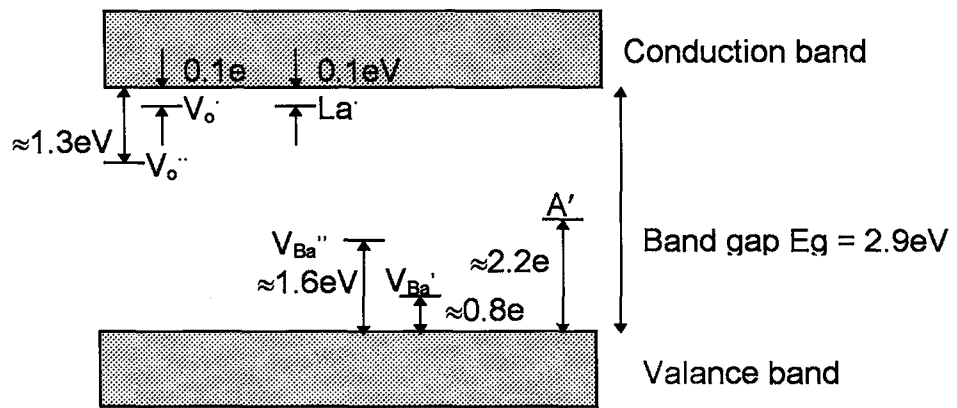
Figure 2.9. Energy level-sheme of $BaTiO_3$ [5].
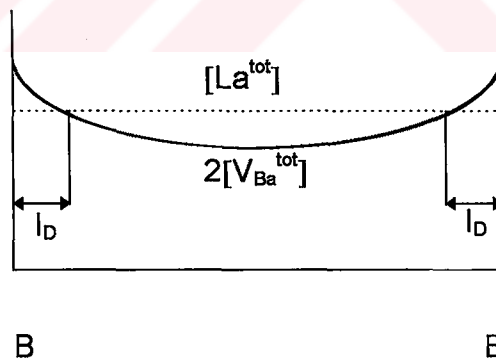
Figure 2.10. Schematic profile of the defect concentrations relevant to the PTCR effect, as found in a grain of La-doped $BaTiO_3$ [7].

38

The position of the energy levels corresponding to the various defects of $BaTiO_3$ are given in Figure 2.9. This diagram shows why the p-type conduction found at room temperature is so much lower than the n-type conduction. The acceptor like energy levels of the defects, such as the barium vacancies, are located about half-way across the band gap, the levels of the donor-like defects, such as the La^{+3} ions and the singly charged oxygen vacancies, are situated close to the bottom of the conduction band.

In doped $BaTiO_3$ under the condition considered in region I the barium vacancies occur in the largest concentration, and hence their behavior determines the rate of equilibrium restoration. From experimental measurements [5] it is found that the diffusion coefficients of the barium vacancies are many order of magnitude smaller than those of the oxygen vacancies. The same investigation also revealed that the barium vacancies unlike the oxygen vacancies, reach their new state of equilibrium by diffusion from the grain boundaries, and not by diffusion to the surface. This is due to the special manner in which these vacancies are formed.

In the defect model proposed by Daniels [7] barium vacancies are given as the fundamental causes of the PTCR effect in donor doped barium titanate. Due to the excess TiO_2 added to promote the sintering process, there is a second titanium rich phase present at the grain boundaries in which the barium ions can find a site to occupy. A conceivable reaction scheme could then be the following:

$$BaTi_3O_7 + 2Ba(lattice) + 2O(lattice) \leftrightarrow 3BaTiO_3 + 2V_{Ba} + 2V_o, \qquad (2.19)$$
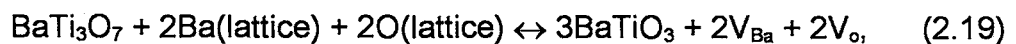
By means of a reaction proposed above barium vacancies could then form at the grain boundaries and then diffuse from there to the interior until the new equilibrium state is reached throughout the grain. During the cooling a diffusion front rich in barium vacancies penetrates the bulk of the grain from the grain boundary, but that after some time the front loses its speed of

39

propagation and comes to a standstill. The result is a heterogeneous distribution of the barium vacancy concentration within each grain as shown in Figure 2.10. This means that while the barium vacancies retain their equilibrium concentrations in the region near the grain boundaries down to fairly low temperatures, this is no longer the case in the bulk of the grain when the temperature has dropped.

The distance l_D over which the diffusion front of the barium vacancies penetrates the grain depends mainly on the cooling rate and on the coefficient. In this way one arrives at an insulating boundary layer, with a thickness of l_D, while the interior of the grain a high conductivity is maintained. The total conductivity is then a function of the ratio of the width of the boundary layer to the grain size [7].

Here the barium vacancies in the outer layer are postulated as the source that trap the conduction electrons and give rise to the potential barrier. The narrower this zone at the grain boundary becomes, the closer the limiting case postulated by the Heywang model is approached.

This model also explains why the PTCR effect is not found in the undoped $BaTiO_3$ that has been made n-type by a reducing treatment. Under reducing atmosphere the material has become n-type due to the formation of oxygen vacancies, and there are no or hardly any barium vacancies present, whose behavior is a necessary condition for the formation of grain-boundary layers.

The thickness of the diffusion layer determined by the cooling rate also influences the PTCR behavior. Roughly speaking, the wider the zone the higher the concentration of barium vacancies at the grain boundary. This implies that the wider the zone the less able will the ferroelectric polarization be to compensate these acceptors which leads to an increase in the resistivity of the grain boundary layer below the curie point [7].

With this model the shape of the conductivity versus percent donor dopant curve can be understood if one also takes into account the changes taking place in the grain size. After a certain limit the grain size becomes smaller, as also does the conductivity. At practical cooling rates the insulating boundary layer has a with of 1-3μm. If the donor concentrations has increased to such an extent that the grain size has acquired about the same value, the material has then become a complete insulator [7, 5].

From the investigation of the thermodynamic and the kinetic behavior of the defects in donor doped $BaTiO_3$, Daniels, deduced that the surface acceptor states postulated by Heywang have the character of an insulating layer at the grain boundary caused by diffusion of barium vacancies. The high concentration of barium vacancies in the layer leads to the full compensation of donors, resulting in an n-i-n structure at the grain boundaries. This finding has, however, been disputed by a number of other studies. For example, Kuwabara [37] used porous semiconducting barium titanate ceramics with small grain sizes to show the influence of stoichiometry. He rationalized that the exhibition of large PTCR effect by barium titanate ceramics with Ba-rich compositions contradicted the barium vacancy model. Amarakoon [30] used a combination of Auger electron spectroscopy and argon ion sputtering to observe Ba excess layer in the grain boundary regions even for titania excess PTCR compositions. Lewis, [38], undertook a comprehensive survey using theoretical techniques of the defect structure of $BaTiO_3$ to suggest that the predominant compensating cation vacancy in the PTCR effect is the titanium vacancy, which is in agreement with the experiments of Jonker and Hevinga [39] on the BaO-TiO_2-La_2O_3. These conflicting evidences prove that the theory underlying the PTCR effect is still not understood completely [30].

There exists a variety of models to explain the origin of the grain boundary states, none of which have been unequivocally proved. It may be

that a number of different defects are effective grain boundary acceptors and can form a useful electrical barrier. Previously proposed models that explain PTCR barrier formation as the result of acceptor impurity segregation, cation vacancy formation, or chemisorbed oxygen do allow for the formation the necessary uncompensated acceptor states. For these space charge defects to become active (uncompensated) acceptor states, donor defects in the grain boundary core must be otherwise compensated and this occurs by grain boundary oxidation. Additional defect changes upon oxidation are necessary to create uncompensated acceptor states and a barrier to electron conduction.

All models of the PTCR barrier agree that oxidation is required to form acceptor states. But, they differ in the interpretation of the defect that is considered responsible, and in the mechanism by which it forms. In what Jonker [36] and later Kuwabara [40] described as "oxygen-chemisorption" at the boundary during the cooling process, the acceptor defect was not explicitly stated, but it is inferred to be an oxygen ion at the boundary core $(O"_{gb})$. The creation of acceptor states by halogenation might similarly be viewed as the grain boundary adsorption of halogen ions, or as the substitution of the halogen for oxygen in an oxidation reaction [25]. In the barium vacancy model of Daniels [5] the vacancies were believed to form during oxidation in donor doped compositions [19b].

In all of the models, the surface acceptor states (N_s) at the grain boundary as the reason for the PTCR effect of semiconducting barium titanate is common. They only disagree about the nature of these surface states.

2.3. Barium-Lead Titanate

The anomalous resistivity-temperature characteristics found in semiconducting barium titanates were studied extensively in relation to their composition by Saburi [41]. The resistivity and impedance characteristics and the crystal structures were investigated for different compositions in the system $(Ba,Sr)(Ti,Sn)O_3$, $(Ba,Ca,Sr)TiO_3$, $(Ba,Pb)TiO_3$, $Ba(Ti,Si)O_3$, and $Ba(Ti,Zr)O_3$ doped with 0.1 mole percent of Ce and also in the system $(Ba,Mg,Ce)TiO_3$.

These studies showed that the ferroelectric Curie point, T_c, of barium titanate is not fixed and can be varied by compositional modification. Complete solid solution occurs between $BaTiO_3$ and $PbTiO_3$. The substitution of Pb^{+2} for Ba^{+2} has the effect of rising the Curie point monotonically towards that of $PbTiO_3$ (490°C) [42, 21].

Barium titanate doped with lanthanites has n-type electrical conductivity. In lead titanate, over a wide temperature range below the Curie point, p-type conductivity has been recorded. This may be explained by the formation of additional acceptor levels in the forbidden band due to the vaporization of lead and the formation of vacancies [43].

CHAPTER 3

EXPERIMENTAL PROCEDURE

3.1. General Procedure

The PTCR ceramics examined in the present study were produced in the laboratory from perovskite barium titanate powders made in accordance with the mixed oxide technique. The ceramics were rendered n-type semiconductor by doping the powders with lanthanum. The sintering process was conducted at a fixed temperature of 1360°C. In order to obtain the PTC anomaly the sintered samples were heat treated in the temperature interval 1150 to 1225°C for selected durations. The basic semiconducting barium titanate composition was modified by additions of manganese and /or lead with the aim of enhancing the PTCR behavior and shifting the PTC action to temperatures above the Curie point of pure $BaTiO_3$ ceramics.

Electrical resistivity measurements were performed on the electroded ceramic disks by the two-point probe technique. The data were taken as a function of temperature in order to characterize the temperature dependence of resistivity. The structural features of the sintered samples were examined by x-ray diffraction and by SEM analyses.

3.2. Details

3.2.1. Preparation of Ceramic Powders

Powders required for making the barium titanate ceramics were produced by the classical mixed oxide route. The basic composition $BaTiO_3$ was prepared by thermal synthesis in which an intimate mixture of $BaCO_3$ and TiO_2 powders, containing equal moles of these components, was pressed like a cylindrical slug and then heated to 1075°C. The slug was kept at this temperature for 4 hours. It was then cooled in the furnace, ground and milled into fine powder form, pressed as a slug again and then heated at 1075°C for an additional 4 hours. The product, as verified by x-ray diffraction, was essentially pure $BaTiO_3$.

The semiconducting $BaTiO_3$ powder was prepared by the same procedure described above with certain differences in the details of the processing steps. Because stringent purity requirements prevail in the production of the semiconducting grade barium titanate powder, reagent grade $BaCO_3$ and TiO_2 were selected as the starting materials. Barium carbonate was Merck grade 1712 and titanium dioxide was Merck 808. These were weighed in accordance with the following number of moles:

$$BaCO_3 = 1\text{-}x$$
$$La_2O_3 = x/2$$
$$TiO_2 = 1$$

In this formulation, La_2O_3 was the source of La^{+3} ion to make the barium titanate semiconductor. The powders $BaCO_3$ and TiO_2 were weighed in the desired proportions and then, together with lanthanum, these were blended for 6 hours in a plastic jar by a milling action. Lanthanum additions were made in the form of an aqueous lanthanum nitrate solution. This was prepared by dissolving Merck 12220 La_2O_3 powder in Merck grade nitric acid

followed by neutralization with evaporation to dryness twice. This way a stock solution of lanthanum with 10 mg/cc La^{+3} concentration was made ready for use as the donor source.

Milling was conducted with the aid of 8 mm diameter stabilized zirconia balls in a medium of ethyl alcohol. Following the blending/milling steps, the slurry was dried in an oven and the powder mixture was pressed in a 30 mm steel die into the form of a cylindrical tablet. The tablet was heated in the muffle furnace to 1075°C and soaked at this temperature for 8 hours in order to allow the calcination of $BaCO_3$ and permit the formation of barium titanate compound through solid state reactions between BaO and TiO_2. At the end of this calcination process, the reacted tablet was cooled in the furnace to room temperature.

The cooled tablet was crushed in a mortar and pestle and then ball milled in a plastic jar with zirconia balls and alcohol. The milling duration was kept sufficiently long to obtain fine powders suitable for pressing and sintering into a dense ceramic. The specific surface area of the milled powder determined by a Quantasorb Surface Area Analyzer (Quantachrome Inc.) from a typical milling duration of 16 hours was 2.617 m^2/gm, corresponding to an average spherical particle diameter of 0.381 micron.

The powder x-ray diffraction (XRD) study done for $Ba_{0.9975}La_{0.0025}Ti_{1.02}O_3$ (containing 2 percent SiO_2 and 0.03 percent manganese) which was calcined at 1075°C for 8 hours is shown in Figure 3.1. From the XRD trace it was found that phases other than barium titanate were absent.

During the weighing stage, excess TiO_2 and SiO_2 additions were made to the powder batch in order to promote liquid phase sintering. The amounts of each of these were 2 percent of the intended molar compositions of barium titanate. Manganese additions, aimed for enhancing the PTC
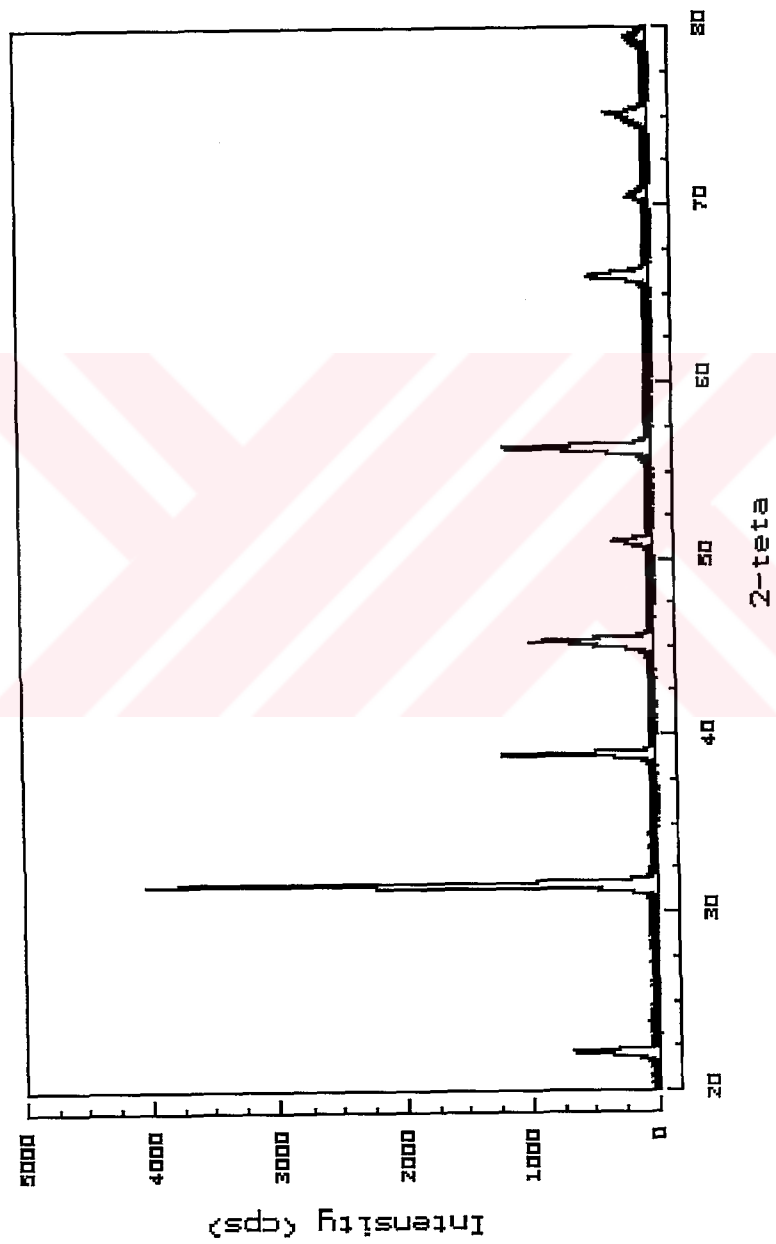
Figure 3.1. XRD trace of $Ba_{0.9975}La_{0.0025}Ti_{1.02}O_3$ (with 2 percent SiO_2 and 0.03 percent manganese) after calcination at 1075°C for 8 hours.

anomaly, were also made during the powder blending stage. For this purpose, a dilute aqueous solution of Mn^{+2} was prepared by dissolving crystals of Merck 5940 $Mn(NO_3)_2.4H_2O$ in dionized water. The concentration of the manganese solution was adjusted to 1 mg/cc.

The reasons for choosing lanthanum as the donor were: (i) the stability of the trivalent state of this cation which assures its incorporation into the barium titanate lattice as La^{+3}, (ii) the negligible volatility of La_2O_3 which precluded the possibility of the loss of lanthanum by evaporation even at high sintering temperatures, (iii) the similarity of the ionic radius of La^{+3} (1.14 A) with that of Ba^{+2} (1.34 A) which permit easy replacement of the barium ion with lanthanum.

The basic chemical composition of the powders prepared by the procedure described above can be expressed rigorously as $Ba_{1-x}La_xO_{3+x/2}$. For the sake of brevity, in the reminder of the thesis we shall drop the x/2 in the suffix of oxygen and write the basic formula of the powder as $Ba_{1-x}La_xO_3$. The La^{+3} ion concentration of the barium titanate powders prepared in this thesis ranged from 0.0 to 0.5 atomic percent with 0.05 atomic percent increments so that nine compositions were at hand for examining the effect of La^{+3} content on semiconduction of barium titanate.

The procedure followed in preparing the doped or undoped $BaTiO_3$-$PbTiO_3$ solid solution powders were similar to the one described above except that $BaTiO_3$ part of the solid solution was synthesized first at 1075°C and the additions of PbO, TiO_2, and $La(NO_3)_3$ were made to the milling batch prior to the second stage calcination. The lead oxide used for making the titanate solid solutions was Merck 5658 grade high purity PbO. The second stage calcination, which allowed the formation of total barium-lead titanate solid solution, was conducted at 950°C for 90 minutes. The charge for calcination was pelletized and then it was placed in an alumina crucible in order to prevent losses of lead by evaporation. Flow sheets, which show the

unitary steps taken in the preparation of barium titanate and barium-lead titanate powders are given in Figure 3.2 and Figure 3.3, respectively.

3.2.2. Sample Preparation and Sintering

The titanate powders were brought into dense ceramic form by sintering the disc compacts prepared from them in a high temperature muffle furnace. The white sample disc was produced by pressing approximately 1 gram of the powder in a hardened steel die with 11 mm diameter. The thickness of white disc was about 3 mm. Prior to pressing, was mixed with 2 drops of a binder/plasticizer solution containing 2.5 percent each of polyvinyl alcohol and ethylene glycol in order to obtain a uniform pressure distribution and a sample free from lamination.

The pressed disc was dried in an oven at 105°C for a few hours and then sintered in a Thermolyne 46200 muffle furnace at 1360°C for 2 hours. The temperature controller of the furnace was programmable so that following schedule could be exercised automatically for the barium titanate compositions:

1) Heating from room temperature to 800°C at a rate 7°C/min,

2) Heating from 800°C to 1100°C at 12°C/min,

3) Heating from 1100°C to 1360°C at 15°C/min,

4) Keeping at 1360°C for 2 hours,

5) Furnace cooling to room temperature.

The first stage of the schedule, carried at lower heating rate, was for binder removal. After removal of the organics, the heating rate was increased stepwise, so that arrival to the peak sintering temperature was hastened. This was important, because the formation of PTCR ceramic is

MIXED OXIDE PROCESSING

BARIUM TITANATE PTCR POWDER PRODUCTION

⇓

WEIGHING

($BaCO_3$, TiO_2 , SiO_2, $La(NO_3)_3$ & $Mn(NO_3)_2.4H_2O$)

⇓

MIXING

(Ball Milling under Ethyl Alcohol in ZrO_2 Media for 6 hours)

⇓

PELLET PRESSING

(Uniaxial pressing, 186 kg/cm^2)

⇓

CALCINATION

(1075 °C, 8 hrs.)

⇓

GRINDING

(Ball Milling under Ethyl Alcohol in ZrO_2 Media for 16 hours)

⇓

PTCR POWDER

(Ready for Shaping and Sintering)
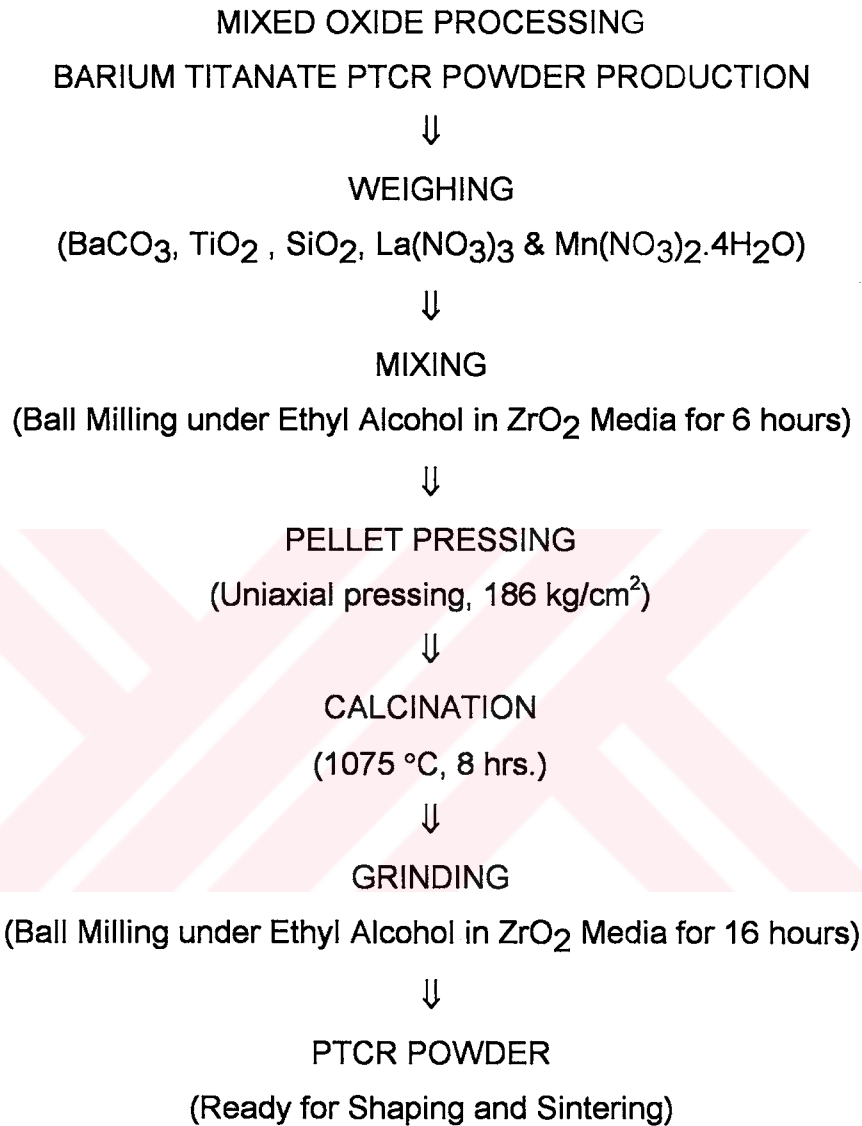
Figure 3.2. A typical flowsheet for PTCR powder production via mixed oxide process for barium titanate powders.

MIXED OXIDE PROCESSING

BARIUM-LEAD TITANATE PTCR POWDER PRODUCTION

⇓

WEIGHING

($BaCO_3$, TiO_2, & $La(NO_3)_3$)

⇓

MIXING

(Ball Milling under Ethyl Alcohol in ZrO_2 Media for 6 hours)

⇓

PELLET PRESSING

(Uniaxial pressing, 186 kg/cm^2)

⇓

CALCINATION

(1075 °C, 8 hrs.)

⇓

GRINDING

(Ball Milling under Ethyl Alcohol in ZrO_2 Media for 16 hours)

⇓

WEIGHING

($Ba_{1-x}La_xTiO_3$, PbO, TiO_2, $La(NO_3)_3$ & $Mn(NO_3)_2.4H_2O$)

⇓
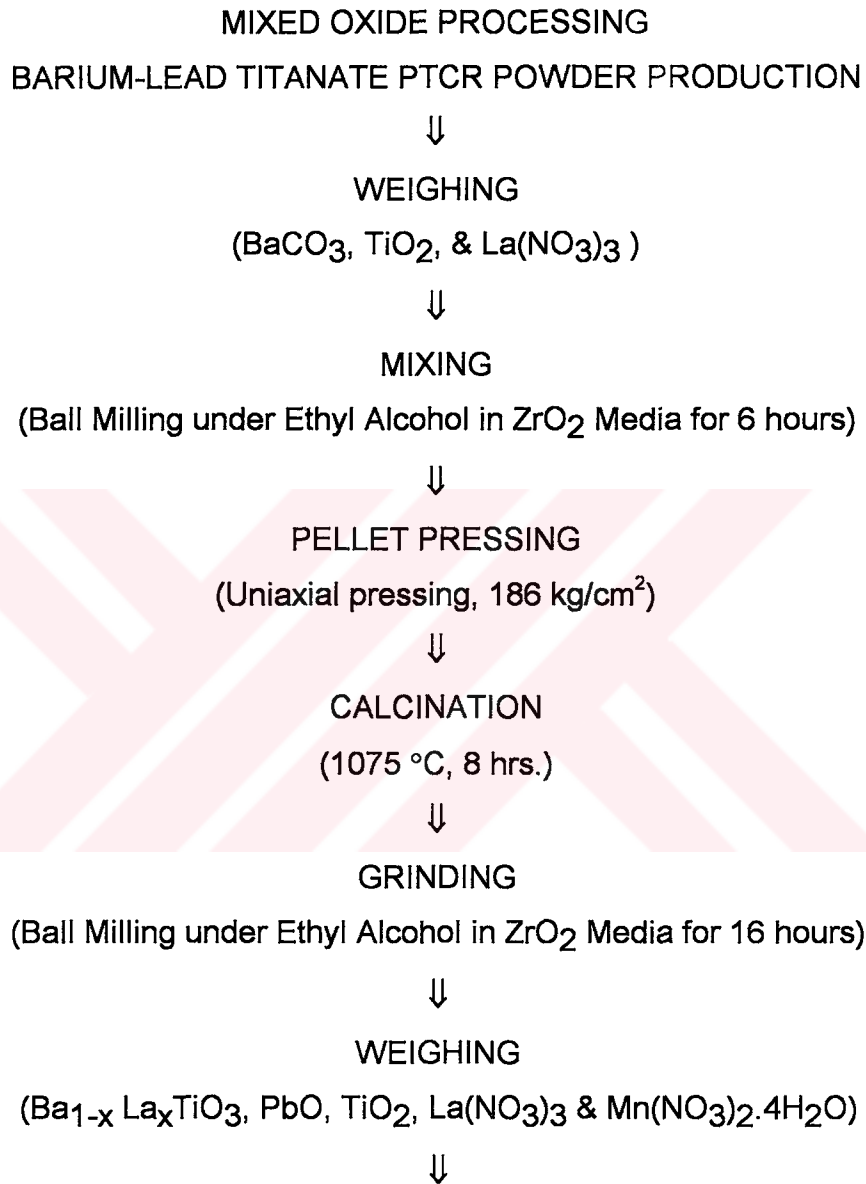
Figure 3.3. A typical flowsheet for PTCR powder production via mixed oxide process for barium titanate - lead titanate solid solutions.

$\Downarrow$

MIXING

(Ball Milling under Ethyl Alcohol in ZrO_2 Media for 6 hours)

$\Downarrow$

PELLET PRESSING

(Uniaxial pressing, 186 kg/cm^2)

$\Downarrow$

CALCINATION

(550 °C, 1 hr.)

(700 °C, 1 hr.)

(850 °C, 1 hr.)

(950 °C, 2 hrs.)

$\Downarrow$

GRINDING

(Ball Milling under Ethyl Alcohol in ZrO_2 Media for 16 hours)

$\Downarrow$

PTCR POWDER

(Ready for Shaping and Sintering)
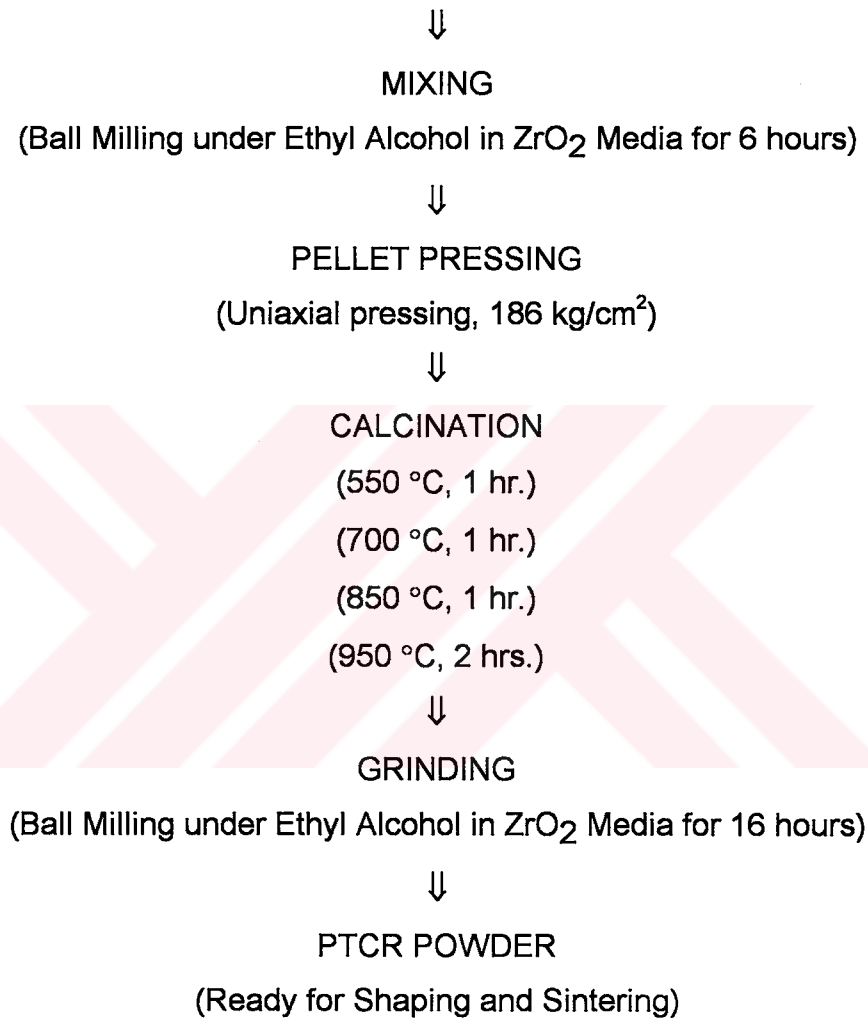
Figure 3.3. (Continued).

stated to be a non-equilibrium event and diminishing results may be obtained with slow heating rates. The schedule outlined above was applied when sintering was the only objective. In cases where an annealing heat treatment was involved, this was included in to the schedule by modifying the sequence after the 4th step as follows:

5) Cooling to the annealing temperature at a rate of 15°C/min,

6) Holding isothermally at the annealing temperature for 30 or 60 minutes,

7) Cooling to room temperature at 15°C/min.

Lead containing samples were sintered in dense alumina crucibles covered with a lid, and the lid was sealed with alumina cement so that a tight enclosure was forming preventing lead losses to the atmosphere. A constant PbO activity was maintained inside the enclosure by making a bed at the bottom of the crucible from the powder having the same composition of the sample. The weight of the powder was the same as the weight of the sample disc to be sintered. The barium-lead titanate samples were sintered at 1200°C or 1250°C for 30 minutes. The sintering schedule for ceramic discs containing lead was the same as the one described above for barium titanate discs except that the peak sintering temperature was lower and the soaking time at this temperature was shorter. The closed saggar used for sintering the lead containing discs is shown schematically in Figure 3.4: After sintering, bulk densities of sintered samples were measured by the liquid (Xylene) displacement technique and found to be about 90 percent of its theoretical value. The PTCR ceramic production flowsheet for barium titanate and barium-lead titanate are given in Figure 3.5 and Figure 3.6 respectively.
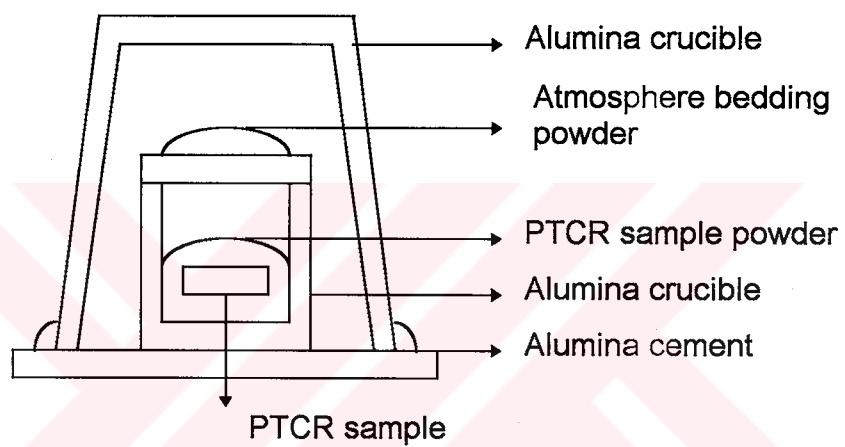
Figure 3.4. Sintering crucible configuration used for PbO content control and sintering experiments.

POWDER SHAPING, SINTERING AND CHARACTERIZATION

⇓

PVA-EG BINDER ADDITION

⇓

TABLETS PRESSING

(Uniaxial Pressing, 1578 kg/cm^2)

⇓

BINDER REMOVAL

(550 °C, 1 hr.)

⇓

SINTERING

(1360 °C, 2 hrs.)

⇓

ANNEALING

(1150 °C, 1175 °C, 1200 °C or 1225 °C, 30 or 60 mins.)

⇓

XRD PHASE CHARACTERIZATION

⇓

DENSITY MEASUREMENT

⇓

LAPPING

⇓

PROVIDING OHMIC CONTACT

(Electroless Ni-electrode Coating)

⇓

ELECTRICAL PROPERTY MEASUREMENT

(Resistivity versus Temperature)

Figure 3.5. A typical flowsheet for PTCR ceramic production for barium titanate.

POWDER SHAPING, SINTERING AND CHARACTERIZATION

⇓

PVA-EG BINDER ADDITION

⇓

TABLETS PRESSING

(Uniaxial Pressing, 1578 kg/cm^2)

⇓

BINDER REMOVAL

(550 °C, 1 hr.)

⇓

SINTERING

(1200 °C or 1250 °C, 30 mins., Controlled PbO Atm.)

⇓

XRD PHASE CHARACTERIZATION

⇓

DENSITY MEASUREMENT

⇓

LAPPING

⇓

PROVIDING OHMIC CONTACT

(Electroless Ni-electrode Coating)

⇓

ELECTRICAL PROPERTY MEASUREMENT

(Resistivity versus Temperature)

Figure 3.6. A typical flowsheet for PTCR ceramic production for barium titanate lead titanate solid solutions.

3.2.3. Characterization Studies

3.2.3.1. Phases and Microstructure

The phases present in the calcined powders and in the sintering ceramic discs were determined by powder x-ray diffraction methods using Rigaku Geigerflex XRD unit operated with Cu-Kα radiation. Powders of sintered samples were prepared for diffraction work by grinding them in a high speed Spec WC vibratory ball mill.

The sample powders and the microstructures of sintered ceramics were examined with scanning electron microscopy using a Jeol-JMS 6400 unit. The fracture surfaces of broken specimens were observed for grain texture. In order to reveal grain size and morphology better, the glassy phase in some of the polished ceramics was leached out in a molten pool of potassium hydroxide kept at 600°C.

3.2.3.2. Determination of Electrical Resistivity

The electrical resistance of the ceramics were measured by using the test system shown in Figure 3.7. The system contained a horizontal tube furnace (Lindberg Hevy Duty Type 59344) equipped with a PID controller which allowed to make electrical measurements at high temperatures. A picoampere/dc voltage source (HP 4140B) and a data acquisition/control unit (HP 3497A) were the elements of the measuring system. Both of the latter two units were the product of Hewlett Packard. These were coupled to Compaq 486 desk-top computer which functioned both as a controller and readout device.

The resistivity probe shown in Figure 3.8, was based on the four-terminal measurement principle. The probe had an alumina ceramic tube (30

A&B: Thermocouple 1

C&F: Thermocouple 2

D&E: Thermocouple 3

C&D: Connection to voltage source
for resistivity measurement
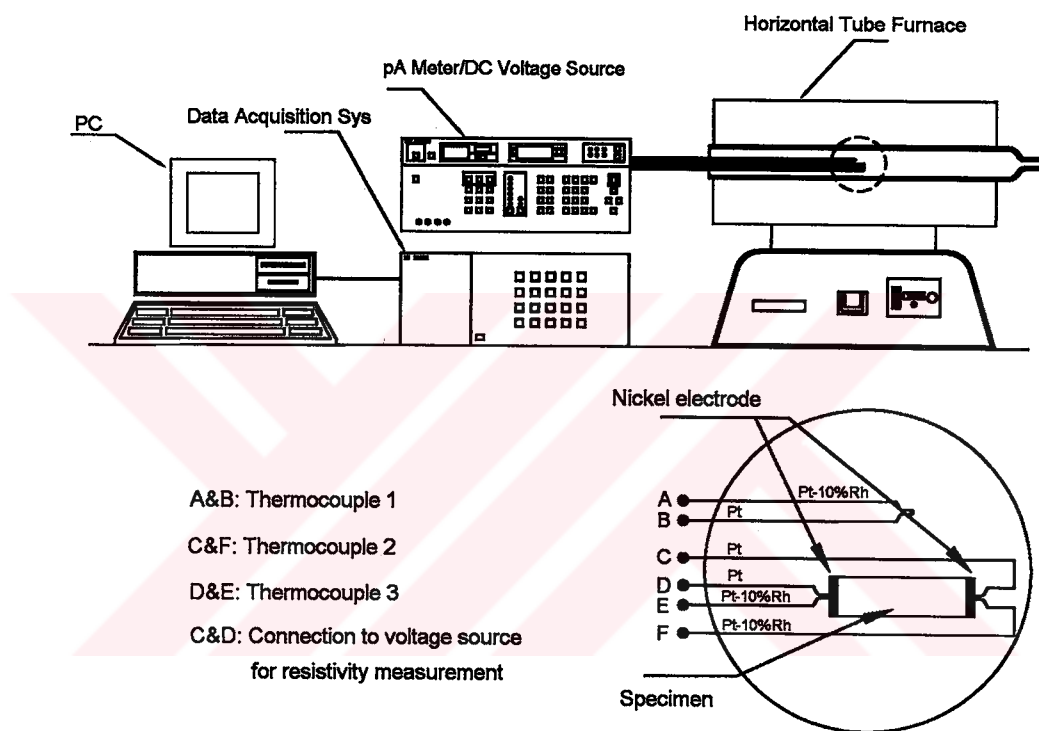
Figure 3.7. Data taking and processing setup

58
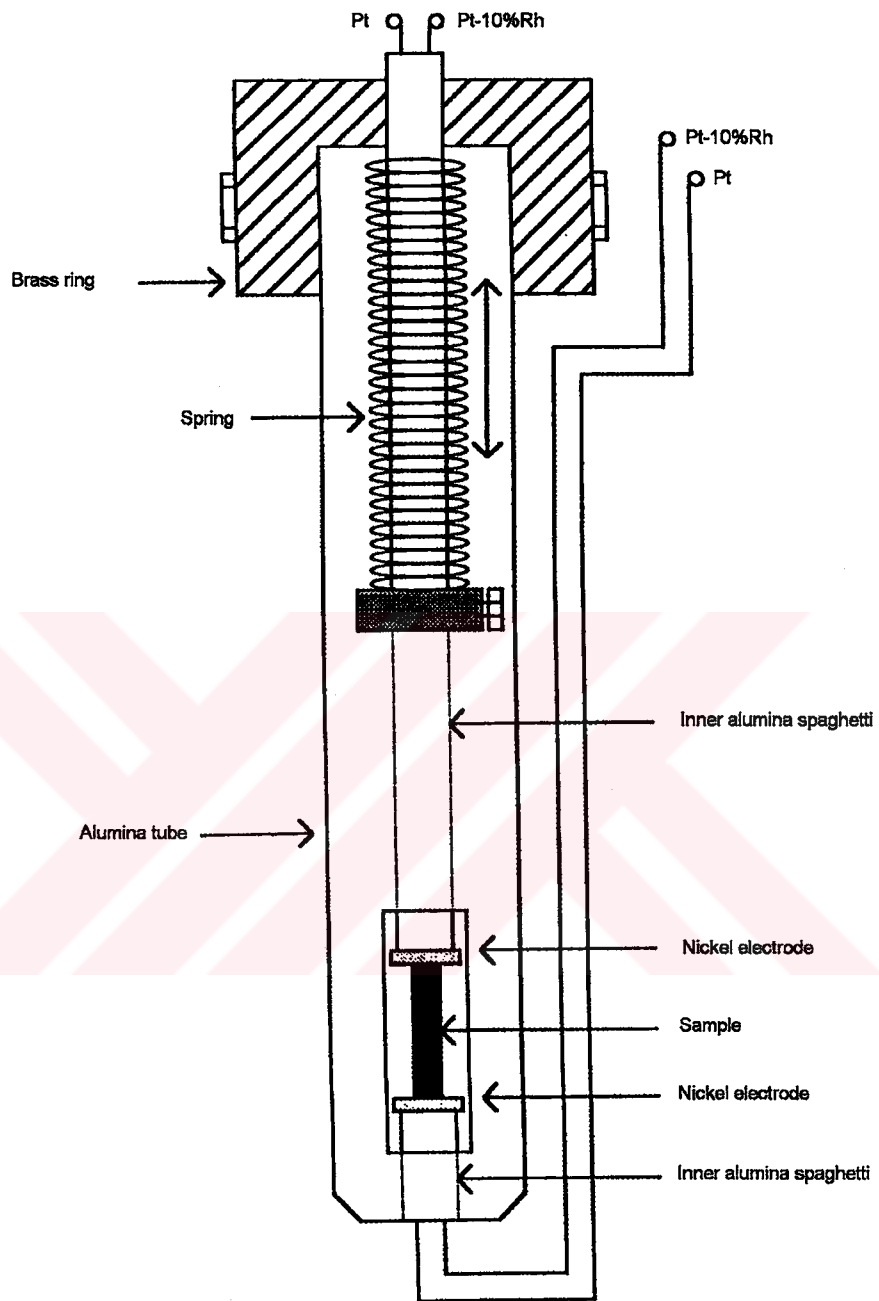
Figure 3.8. Resistivity probe for electrical resistivity measurement

cm long and 1.2 cm inside diameter) which housed the sample and the leads. The flat surfaces of the sintered ceramic disc was electroded properly with nickel so that ohmic metallic contacts were obtained. The sample was placed inside the alumina tube between two longitudinal alumina spaghetties. These alumina tubes were of double bore type; each tube carried a platinum-platinum 10 percent rhodium thermocouple with the beads touching the opposite metallized faces of the ceramic. A spring pressure applied to one of the spaghetties kept the sample firm and tight between the contacts.

For resistance measurements, the probe was placed in the furnace and then the furnace and its contents were heated to the desired temperature. The probe was allowed to equilibrate by holding it at the maximum temperature for about 6 hours. After thermal equilibrium the furnace power was cut and the system was allowed to cool slowly on its own. During cooling, a known voltage, was applied across the electroded faces of the sample and current flow through the ceramic as the result of this applied voltage was measured. The currents were measured by the HP 4140b unit, which is capable of measuring currents precisely down to pico-ampere range, by applying 0.5 V/cm. The HP 3497A data acquisition/control system was used just to measure the temperature from the sample surface.

The computer program was prepared by means of which the system described above was actuated and operated automatically by the Compaq 486. The data received by the computer was transferred directly to electrical resistivity by using the sample dimensions. These data could then be displayed, printed or stored.

The main problem encountered in electrical resistivity measurements was obtaining ohmic metallic contacts on the flat faces of the ceramic disc. The usual silver paste method, either air-dry or fired-on type electroding did not give adequate results; superfluously high resistivities were measured

due, probably, to the presence of an insulating barrier between the sample and the electrode. Indium-amalgam or indium-gallium alloys which are known to be used as electrode materials in many of previous studies are toxic, therefore their availability is increasingly banned.

In the present study, The solution of the electroding problem was obtained by the use of electroless nickel plating. The composition of the plating bath, developed particularly for barium titanate ceramics [44], was as follows.

Component	Amount of Component gm/lt
$NiCl_2$	11
$NaH_2PO_2.H_2O$	20
$NaH_2PO_2.H_2O$	20.8
NH_4OH	to adjust pH to 9

The sintered ceramic disc was prepared for nickel plating by cleaning its surfaces. For this purpose, the flat faces were polished by grinding successively on number 300 and number 600 emery papers. The specimen faces were activated by immersion in 0.07 M $SnCl_2.H_2O$ and then catalyzed by immersion in 0.0012 M $PdCl_2$ solution each for about 1 minute. The nickel was deposited on both faces by dipping the specimen into the plating bath for 15 minutes. The temperature of the bath was maintained at 90°C during plating. An electrode thickness of a few microns developed at the end of 15 minutes immersion time. The specimens electroded with nickel were rinsed and washed thoroughly in alcohol. They were dried in an oven at 105°C , this was followed by an annealing heat treatment done at 350°C for 10 minutes. The latter was found to improve the contact stability [45]. Prior to annealing, the nickel surfaces were coated with silver paste in order to prevent the oxidation of nickel.

CHAPTER 4

DATA AND RESULTS

4.1. Effect of La^{+3} Concentration on Semiconductivity

The data obtained from electrical resistivity measurements on sintered samples of barium titanate having increasing levels of lanthanum dopant are presented in Table 4.1. These data were converted to the resistivity values given in the third column of Table 4.1. From these data, the variation of resistivity with dopant concentration is shown by the graph in Figure 4.1. The figure reveals that there is indeed a resistivity well and the minimum resistivity occurs at 0.25 atomic percent of La^{+3}.

The color of the sintered samples could be taken as an indication of whether the ceramic was an insulator or semiconductor. The insulator ceramic was yellow, whereas the color turned to characteristic dark blue when the sample become semiconductor.

The U-shaped relation of the La^{+3} ion content and room temperature resistivity of semiconducting $BaTiO_3$ ceramic was described by Figure 4.1. The un-doped barium titanate was insulator with a resistivity of $10^{11.25}$ ohm-cm. The resistivity did not change much up to 0.1 percent lanthanum ion concentration. Lanthanum addition exceeding 0.1 percentage La^{+3} decreased resistivity sharply. Although the resistivity axis was logarithmic, the drop in resistivity was very dramatic. At 0.25 atomic percent lanthanum ion concentration the room temperature resistivity of $BaTiO_3$ was already

Table 4.1. Sample compositions and their resistivity characteristics as a function of lanthanum concentration

Sample Composition	%La^{+3} (mol %)	Resistivity (ohm-cm)	Log10 (ρ) (ohm-cm)
$Ba_1La_0Ti_{1.02}O_3$	0.00	1.78E+11	11.25
$Ba_{0.999}La_{0.001}Ti_{1.02}O_3$	0.10	3.70E+10	10.57
$Ba_{0.9985}La_{0.0015}Ti_{1.02}O_3$	0.15	3.94E+06	6.60
$Ba_{0.998}La_{0.002}Ti_{1.02}O_3$	0.20	3.71E+01	1.57
$Ba_{0.9975}La_{0.0025}Ti_{1.02}O_3$	0.25	2.35E+01	1.37
$Ba_{0.997}La_{0.003}Ti_{1.02}O_3$	0.30	7.15E+02	2.85
$Ba_{0.9965}La_{0.0035}Ti_{1.02}O_3$	0.35	4.09E+06	6.61
$Ba_{0.996}La_{0.004}Ti_{1.02}O_3$	0.40	4.52E+08	8.66
$Ba_{0.995}La_{0.005}Ti_{1.02}O_3$	0.50	7.73E+09	9.89
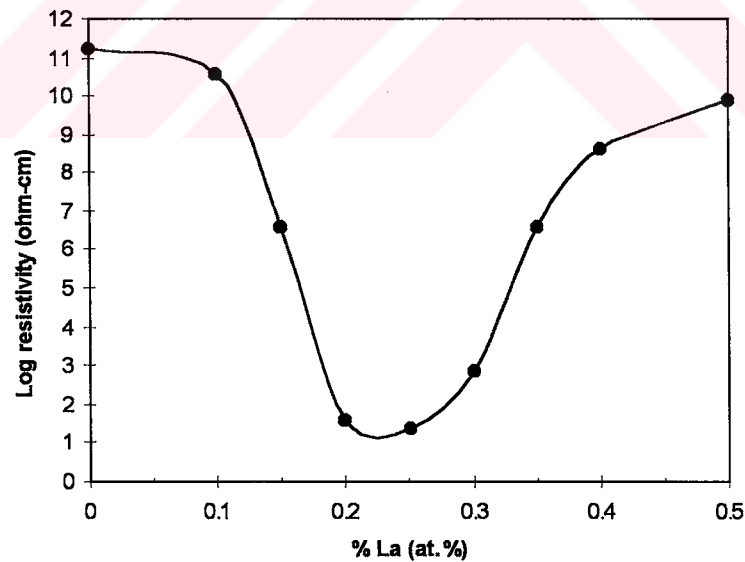
Figure 4.1. The dependence of room temperature resistivity on the La^{+3} concentration, sintered at 1360°C for 2 hrs.

approximately 25 ohm-cm, which was the value at the bottom of the well. Then, it showed a transition from conductive to insulating behavior with increasing donor dopant concentration. Above 0.4 atomic percent lanthanum ion the material was not semiconductor any longer.

4.2. Ceramics With 0.25 Atomic Percent Lanthanum Additions

4.2.1. Variation of Resistivity with Manganese Doping

The compositions of PTCR ceramics prepared for study in this thesis are given in Table 4.2. These compositions were subjected to heat treatment as explained in Chapter 3. The data related to the resistivity of sintered samples measured in the set up of Figure 3.9, are summarized in Table A of the Appendix as a function of temperature. These data were used to construct the log resistivity versus temperature graphs shown in Figures 4.2, 4.4, 4.6, 4.8, 4.10, 4.12, 4.14, 4.16 and 4.18. The sample designation used on in the construction of these and other figures is given in Table 4.3. In order to make the PTC anomaly more clear, the minimum resistivity (ρ_{min}), the maximum resistivity (ρ_{max}), and the PTC anomaly ($\log \rho_{max} - \log \rho_{min}$), are plotted as a function of manganese concentration and are given beneath the resistivity versus temperature figures in Figures 4.3, 4.5, 4.7, 4.9, 4.11, 4.13, 4.15, 4.17 and 4.19.

These figures revealed that all compositions which became semiconductor after sintering exhibited PTCR effect to a greater or lesser degree. All curves had similar features. For purposes of interpretation, let us consider Figure 4.2. as an example. The lowest curve represented the variation of resistivity in the ceramic containing 0.02 percent manganese addition. The remaining curves indicated that further additions of manganese promoted magnitude of the PTC anomaly up to 0.06 atomic percent manganese. Beyond this point the room temperature resistivity increased dramatically with a slight increase in the maximum resistivity. Due to these

increases the PTCR effect, defined as the difference between the log maximum resistivity and the log minimum resistivity, were affected adversely. This decay in the PTC anomaly was indicated by the curve at the center in Figure 4.3.

The increases in the slope of the resistivity curves above the Curie point with increasing manganese concentration were also noteworthy. Increasing the manganese concentration from 0.02 to 0.07 percent increased the positive temperature coefficient of resistance from ~6 percent per degree C to ~15 percent per degree C, respectively. The general trend observed was that, increasing manganese concentration the transition from semiconduction to insulation with increasing temperature occur over in a narrow temperature range. These figures revealed that, in general, the higher manganese content resulted in higher maximum resistivities and that the PTC anomaly was promoted.

Table 4.2. Chemical compositions of the PTCR ceramics studied

BaCO$_3$	TiO$_2$	La(NO$_3$)$_3$	Mn(NO$_3$)$_2$	SiO$_2$	Sample Composition
(mol%)	(mol%)	(mol%)	(mol%)	(mol%)	
100.00	102	0.00	0.02	2.00	Ba$_1$La$_0$Ti$_{1.02}$O$_3$ +2 mol % SiO$_2$ +0.02 mol % Mn
99.90	102	0.10	0.02	2.00	Ba$_{0.999}$La$_{0.001}$Ti$_{1.02}$O$_3$ +2 mol % SiO$_2$ +0.02 mol % Mn
99.85	102	0.15	0.02	2.00	Ba$_{0.9985}$La$_{0.0015}$Ti$_{1.02}$O$_3$ +2 mol % SiO$_2$ +0.02 mol % Mn
99.80	102	0.20	0.02	2.00	Ba$_{0.998}$La$_{0.002}$Ti$_{1.02}$O$_3$ +2 mol % SiO$_2$ +0.02 mol % Mn
99.75	102	0.25	0.02	2.00	Ba$_{0.9975}$La$_{0.0025}$Ti$_{1.02}$O$_3$ +2 mol % SiO$_2$ +0.02 mol % Mn
99.70	102	0.30	0.02	2.00	Ba$_{0.997}$La$_{0.003}$Ti$_{1.02}$O$_3$ +2 mol % SiO$_2$ +0.02 mol % Mn
99.65	102	0.35	0.02	2.00	Ba$_{0.9965}$La$_{0.0035}$Ti$_{1.02}$O$_3$ +2 mol % SiO$_2$ +0.02 mol % Mn
99.60	102	0.40	0.02	2.00	Ba$_{0.996}$La$_{0.004}$Ti$_{1.02}$O$_3$ +2 mol % SiO$_2$ +0.02 mol % Mn
99.80	102	0.20	0.03	2.00	Ba$_{0.998}$La$_{0.002}$Ti$_{1.02}$O$_3$ +2 mol % SiO$_2$ +0.03 mol % Mn
99.80	102	0.20	0.04	2.00	Ba$_{0.998}$La$_{0.002}$Ti$_{1.02}$O$_3$ +2 mol % SiO$_2$ +0.04 mol % Mn
99.80	102	0.20	0.05	2.00	Ba$_{0.998}$La$_{0.002}$Ti$_{1.02}$O$_3$ +2 mol % SiO$_2$ +0.05 mol % Mn
99.75	102	0.25	0.03	2.00	Ba$_{0.9975}$La$_{0.0025}$Ti$_{1.02}$O$_3$ +2 mol % SiO$_2$ +0.03 mol % Mn
99.75	102	0.25	0.04	2.00	Ba$_{0.9975}$La$_{0.0025}$Ti$_{1.02}$O$_3$ +2 mol % SiO$_2$ +0.04 mol % Mn
99.75	102	0.25	0.05	2.00	Ba$_{0.9975}$La$_{0.0025}$Ti$_{1.02}$O$_3$ +2 mol % SiO$_2$ +0.05 mol % Mn
99.75	102	0.25	0.06	2.00	Ba$_{0.9975}$La$_{0.0025}$Ti$_{1.02}$O$_3$ +2 mol % SiO$_2$ +0.06 mol % Mn
99.75	102	0.25	0.07	2.00	Ba$_{0.9975}$La$_{0.0025}$Ti$_{1.02}$O$_3$ +2 mol % SiO$_2$ +0.07 mol % Mn
99.75	102	0.25	0.08	2.00	Ba$_{0.9975}$La$_{0.0025}$Ti$_{1.02}$O$_3$ +2 mol % SiO$_2$ +0.08 mol % Mn

Table 4.3. The sample designations and their corresponding formula indicate on the resistivity versus temperature figures.

Sample Designation	Sample Composition
La0Mn2	$Ba_1La_0Ti_{1.02}O_3$ +2 mol % SiO_2 +0.02 mol % Mn
La10Mn2	$Ba_{0.999}La_{0.001}Ti_{1.02}O_3$ +2 mol % SiO_2 +0.02 mol % Mn
La15Mn2	$Ba_{0.9985}La_{0.0015}Ti_{1.02}O_3$ +2 mol % SiO_2 +0.02 mol % Mn
La20Mn2	$Ba_{0.998}La_{0.002}Ti_{1.02}O_3$ +2 mol % SiO_2 +0.02 mol % Mn
La25Mn2	$Ba_{0.9975}La_{0.0025}Ti_{1.02}O_3$ +2 mol % SiO_2 +0.02 mol % Mn
La30Mn2	$Ba_{0.997}La_{0.003}Ti_{1.02}O_3$ +2 mol % SiO_2 +0.02 mol % Mn
La35Mn2	$Ba_{0.9965}La_{0.0035}Ti_{1.02}O_3$ +2 mol % SiO_2 +0.02 mol % Mn
La40Mn2	$Ba_{0.996}La_{0.004}Ti_{1.02}O_3$ +2 mol % SiO_2 +0.02 mol % Mn
La20Mn3	$Ba_{0.998}La_{0.002}Ti_{1.02}O_3$ +2 mol % SiO_2 +0.03 mol % Mn
La20Mn4	$Ba_{0.998}La_{0.002}Ti_{1.02}O_3$ +2 mol % SiO_2 +0.04 mol % Mn
La20Mn5	$Ba_{0.998}La_{0.002}Ti_{1.02}O_3$ +2 mol % SiO_2 +0.05 mol % Mn
La25Mn3	$Ba_{0.9975}La_{0.0025}Ti_{1.02}O_3$ +2 mol % SiO_2 +0.03 mol % Mn
La25Mn4	$Ba_{0.9975}La_{0.0025}Ti_{1.02}O_3$ +2 mol % SiO_2 +0.04 mol % Mn
La25Mn5	$Ba_{0.9975}La_{0.0025}Ti_{1.02}O_3$ +2 mol % SiO_2 +0.05 mol % Mn
La25Mn6	$Ba_{0.9975}La_{0.0025}Ti_{1.02}O_3$ +2 mol % SiO_2 +0.06 mol % Mn
La25Mn7	$Ba_{0.9975}La_{0.0025}Ti_{1.02}O_3$ +2 mol % SiO_2 +0.07 mol % Mn
La25Mn8	$Ba_{0.9975}La_{0.0025}Ti_{1.02}O_3$ +2 mol % SiO_2 +0.08 mol % Mn
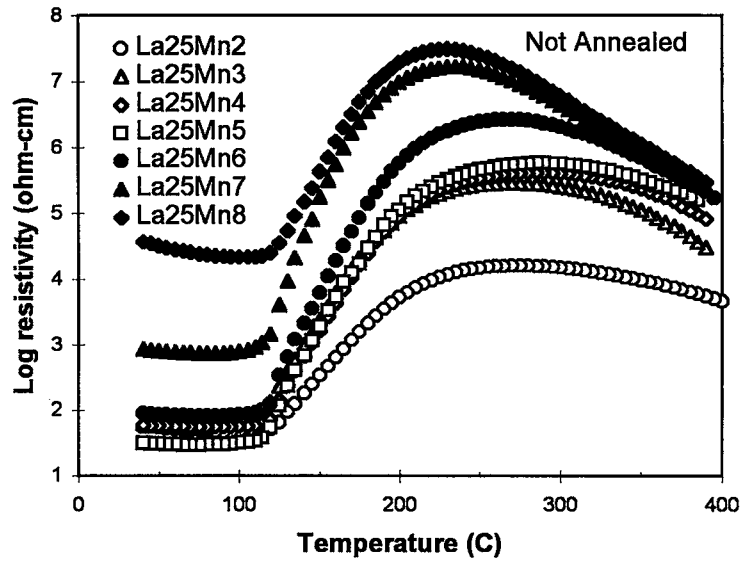
Figure 4.2. The resistivity versus temperature behavior of 0.25 percent La^{+3} doped BaTiO$_3$ without any annealing treatment at various Mn^{+2} concentration levels.
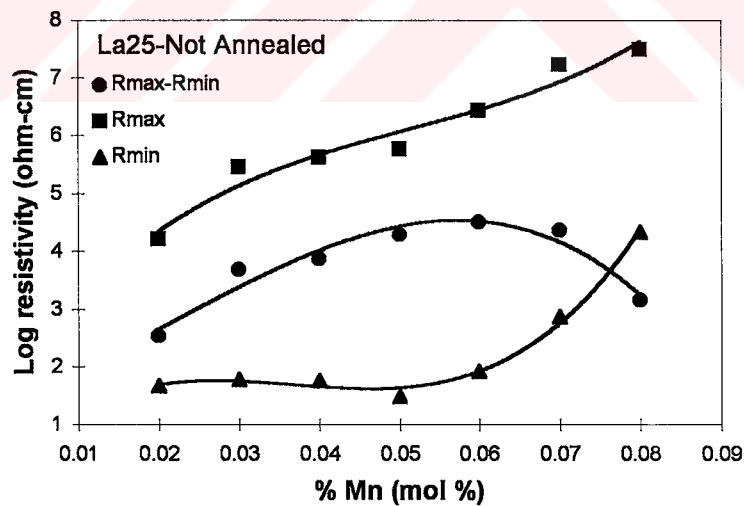
Figure 4.3. The plot of log R$_{min}$, log R$_{max}$ and (log R$_{max}$-log R$_{min}$) of 0.25 atomic percent La^{+3} doped BaTiO$_3$ as a function of Mn^{+2} concentration.
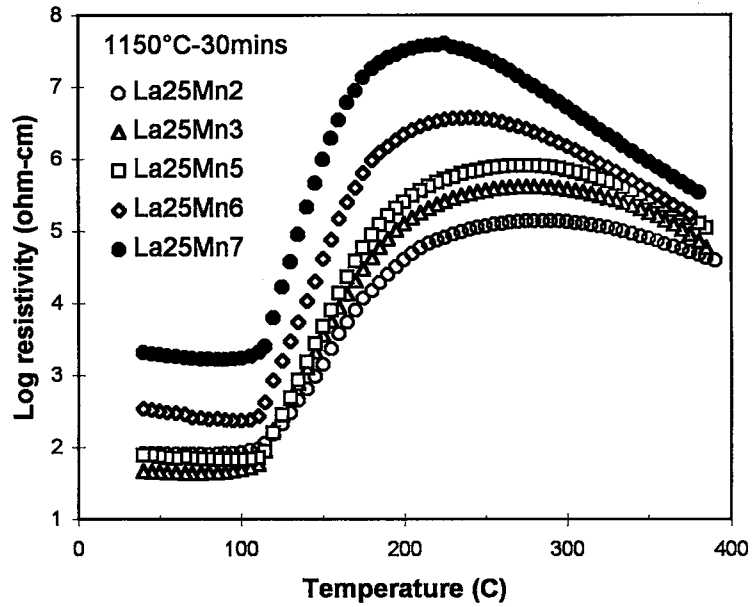
Figure 4.4. The resistivity versus temperature behavior of 0.25 percent La^{+3} doped BaTiO$_3$ after annealing at 1150°C for 30 minutes at various Mn^{+2} concentration levels.
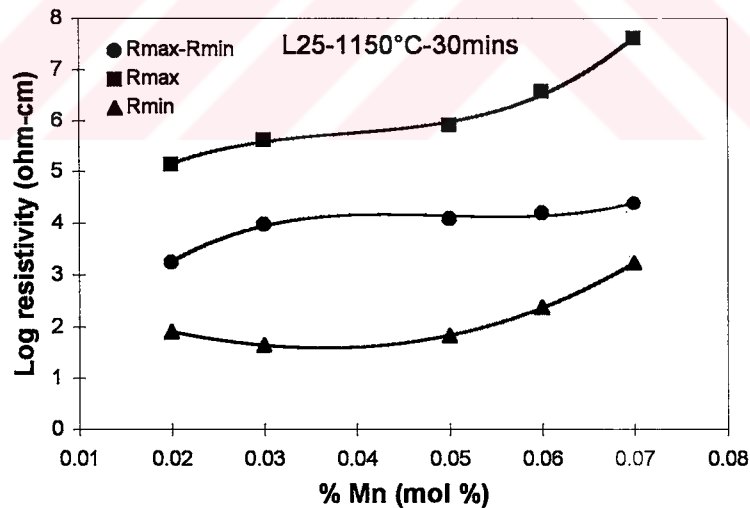
Figure 4.5. The plot of log R$_{min}$, log R$_{max}$ and (log R$_{max}$-log R$_{min}$) of 0.25 atomic percent La^{+3} doped BaTiO$_3$ as a function of Mn^{+2} concentration after annealing at 1150°C for 30 minutes.
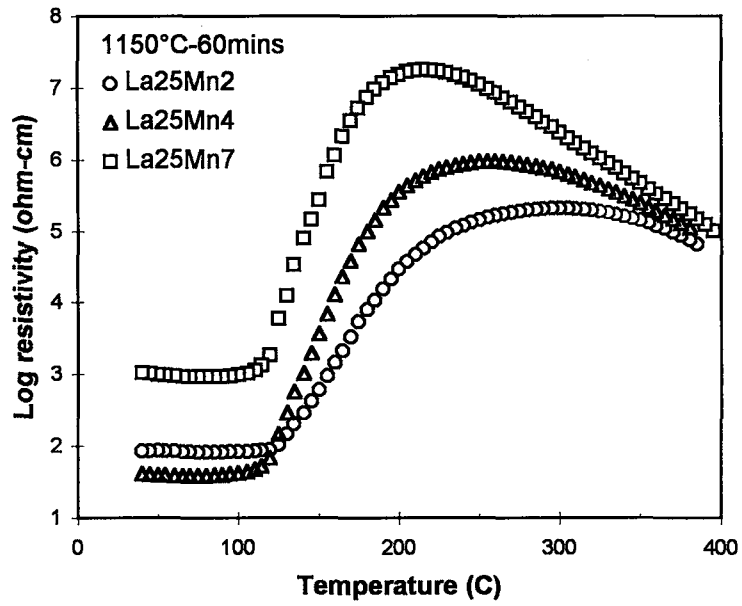
Figure 4.6. The resistivity versus temperature behavior of 0.25 percent La^{+3} doped $BaTiO_3$ after annealing at 1150°C for 60 minutes at various Mn^{+2} concentration levels.
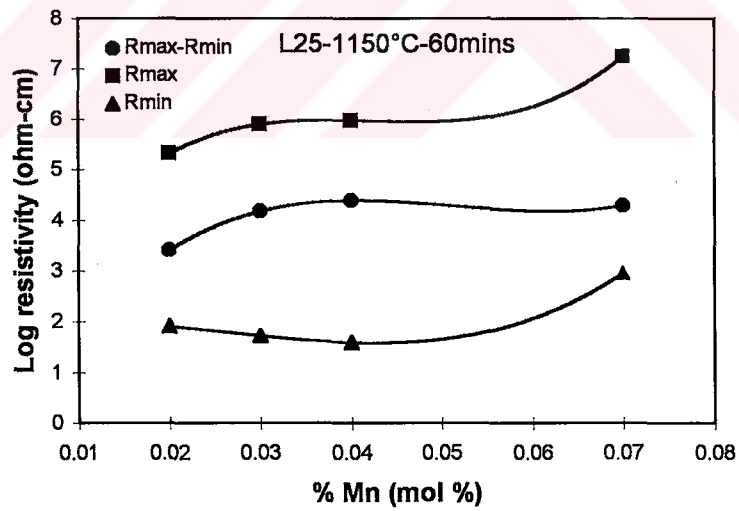
Figure 4.7. The plot of log R_{min}, log R_{max} and (log R_{max}-log R_{min}) of 0.25 atomic percent La^{+3} doped $BaTiO_3$ as a function of Mn^{+2} concentration after annealing at 1150°C for 60 minutes.
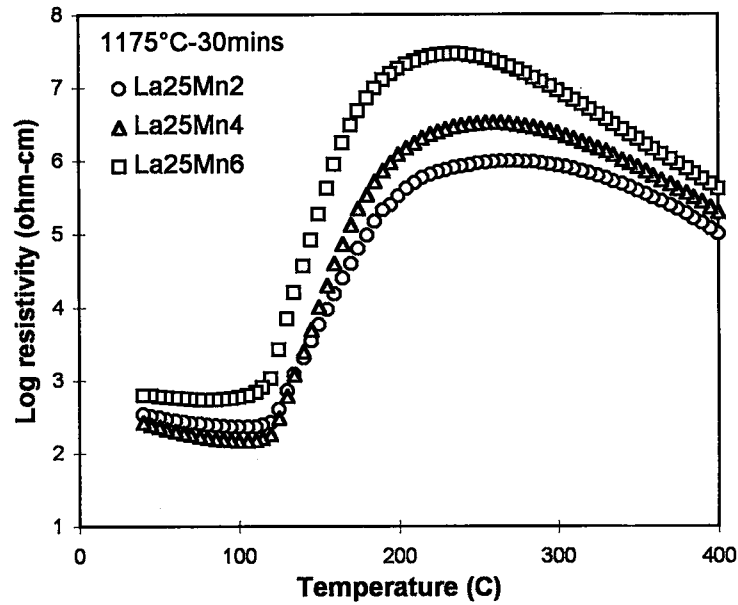
Figure 4.8. The resistivity versus temperature behavior of 0.25 percent La^{+3} doped $BaTiO_3$ after annealing at 1175°C for 30 minutes at various Mn^{+2} concentration levels.
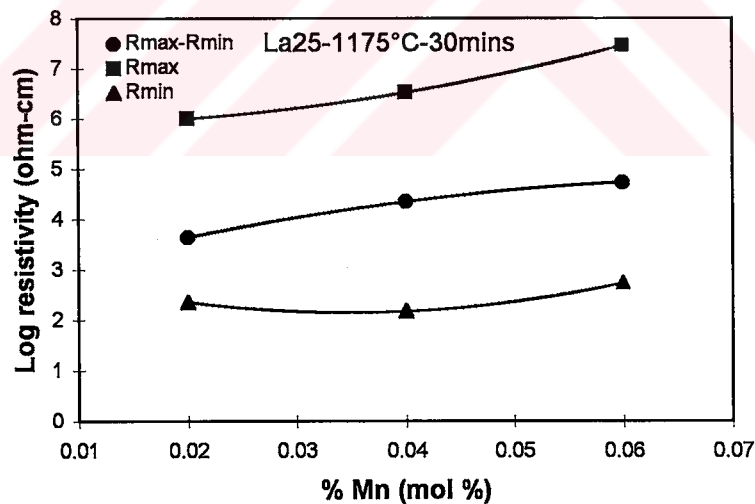
Figure 4.9. The plot of log R_{min}, log R_{max} and (log R_{max}-log R_{min}) of 0.25 atomic percent La^{+3} doped $BaTiO_3$ as a function of Mn^{+2} concentration after annealing at 1175°C for 30 minutes.
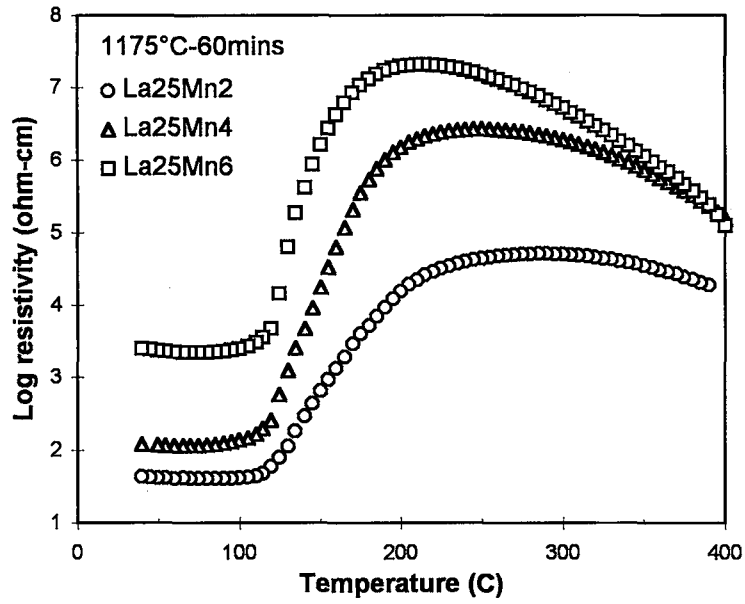
Figure 4.10. The resistivity versus temperature behavior of 0.25 percent La^{+3} doped BaTiO$_3$ after annealing at 1175°C for 60 minutes at various Mn^{+2} concentration levels.
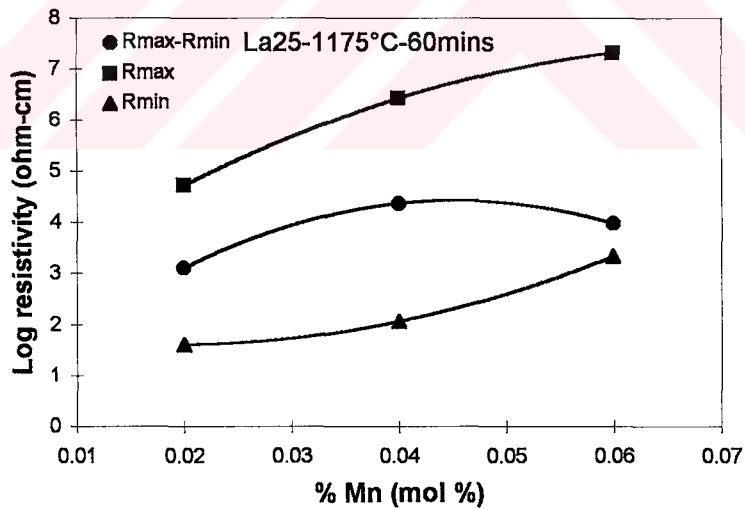
Figure 4.11. The plot of log R$_{min}$, log R$_{max}$ and (log R$_{max}$-log R$_{min}$) of 0.25 atomic percent La^{+3} doped BaTiO$_3$ as a function of Mn^{+2} concentration after annealing at 1175°C for 60 minutes.
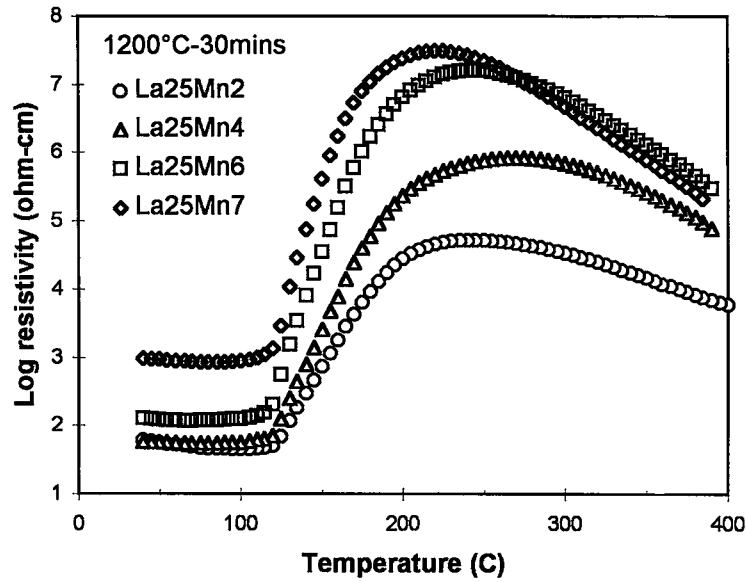
Figure 4.12. The resistivity versus temperature behavior of 0.25 percent La^{+3} doped $BaTiO_3$ after annealing at 1200°C for 30 minutes at various Mn^{+2} concentration levels.
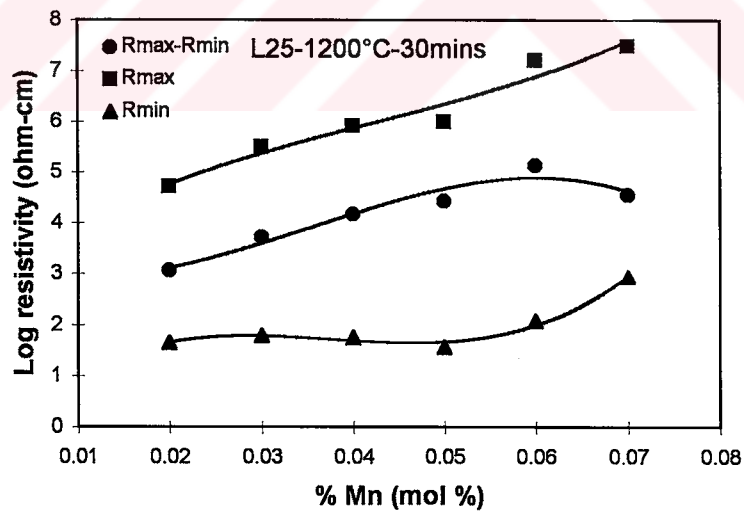
Figure 4.13. The plot of log R_{min}, log R_{max} and (log R_{max}-log R_{min}) of 0.25 atomic percent La^{+3} doped $BaTiO_3$ as a function of Mn^{+2} concentration after annealing at 1200°C for 30 minutes.

Figure 4.14. The resistivity versus temperature behavior of 0.25 percent La^{+3} doped BaTiO$_3$ after annealing at 1200°C for 60 minutes at various Mn^{+2} concentration levels.

Figure 4.15. The plot of log R$_{min}$, log R$_{max}$ and (log R$_{max}$-log R$_{min}$) of 0.25 atomic percent La^{+3} doped BaTiO$_3$ as a function of Mn^{+2} concentration after annealing at 1200°C for 60 minutes.

Figure 4.16. The resistivity versus temperature behavior of 0.25 percent La^{+3} doped $BaTiO_3$ after annealing at 1225°C for 30 minutes at various Mn^{+2} concentration levels.

Figure 4.17. The plot of log R_{min}, log R_{max} and (log R_{max}-log R_{min}) of 0.25 atomic percent La^{+3} doped $BaTiO_3$ as a function of Mn^{+2} concentration after annealing at 1225°C for 30 minutes.

Figure 4.18. The resistivity versus temperature behavior of 0.25 percent La^{+3} doped BaTiO$_3$ after annealing at 1225°C for 60 minutes at various Mn^{+2} concentration levels.

Figure 4.19. The plot of log R$_{min}$, log R$_{max}$ and (log R$_{max}$-log R$_{min}$) of 0.25 atomic percent La^{+3} doped BaTiO$_3$ as a function of Mn^{+2} concentration after annealing at 1225°C for 60 minutes.

4.2.2. Effect of Annealing on PTCR Behavior

One of the objectives of this work was to study the effect of annealing on the magnitude of the PTCR anomaly. For this purpose, the sintered samples were annealed at certain selected temperature and time combinations. The annealing temperature was varied from 1150°C to 1225°C and the annealing durations at each annealing temperature were 30 or 60 minutes. The annealing stage was designed to allow oxygen to diffuse into the grain boundaries.

The resistivity curves given in Figures 4.20 through 4.39 belong to the heat treated samples as explained above and in Chapter 3. The temperature-time combinations selected for annealing heat treatment are indicated on these figures. It is clear that, the annealing treatment enhanced the PTC anomaly with respect to the sample which did not receive this treatment. As an example, let us consider the resistivity curves plotted in Figure 4.20. Comparing the behavior of the resistivity curve given in Figure 4.20 indicated as "not annealed" with the one others in the same figure one sees that the PTC anomaly enhanced. The PTC anomaly for heat treated samples were one order of magnitude higher than the not annealed samples.
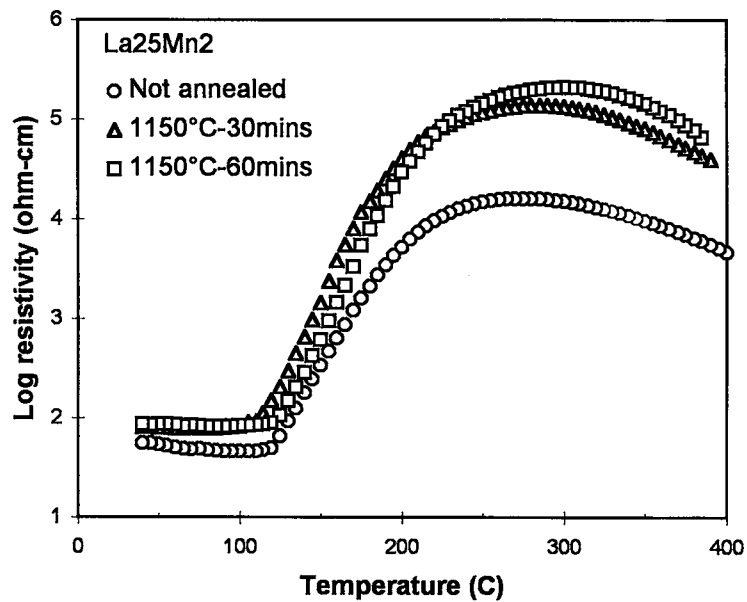
Figure 4.20. The resistivity behavior of 0.25 percent La^{+3} and 0.02 percent Mn^{+2} doped $BaTiO_3$ before and after annealing at 1150°C.
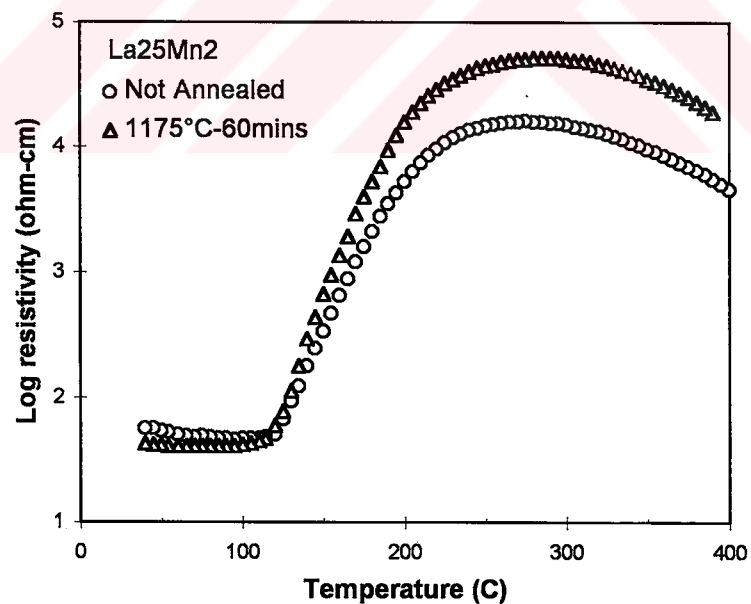
Figure 4.21. The resistivity behavior of 0.25 percent La^{+3} and 0.02 percent Mn^{+2} doped $BaTiO_3$ before and after annealing at 1175°C.

Figure 4.22. The resistivity behavior of 0.25 percent La^{+3} and 0.02 percent Mn^{+2} doped BaTiO$_3$ before and after annealing at 1200°C.

Figure 4.23. The resistivity behavior of 0.25 percent La^{+3} and 0.02 percent Mn^{+2} doped BaTiO$_3$ before and after annealing at 1225°C.
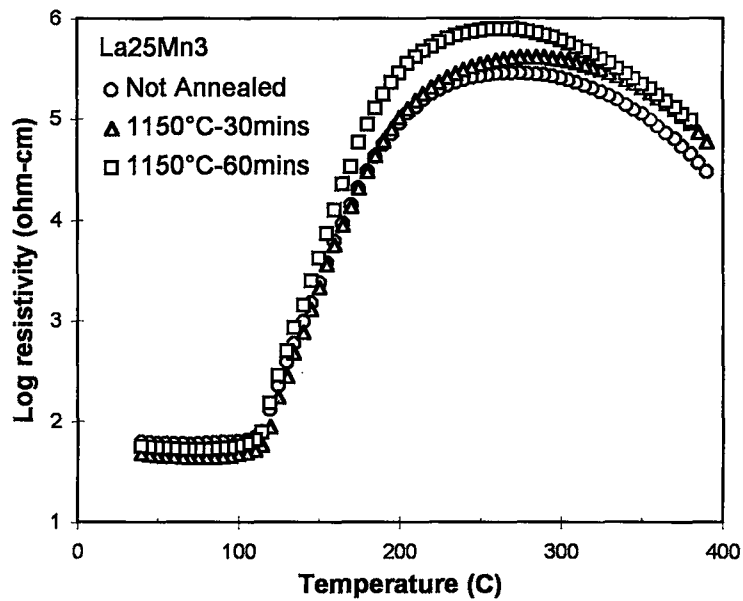
Figure 4.24. The resistivity behavior of 0.25 percent La^{+3} and 0.03 percent Mn^{+2} doped BaTiO$_3$ before and after annealing at 1150°C.
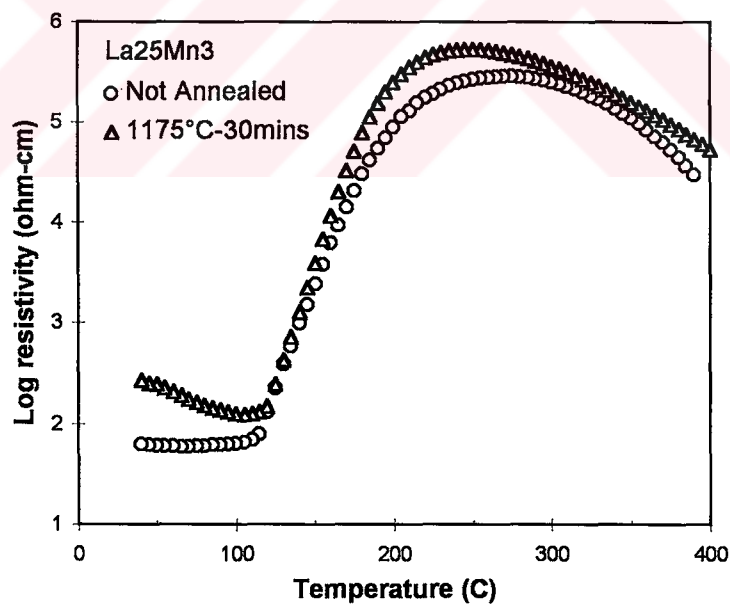
Figure 4.25. The resistivity behavior of 0.25 percent La^{+3} and 0.03 percent Mn^{+2} doped samples before and after annealing at 1175°C.
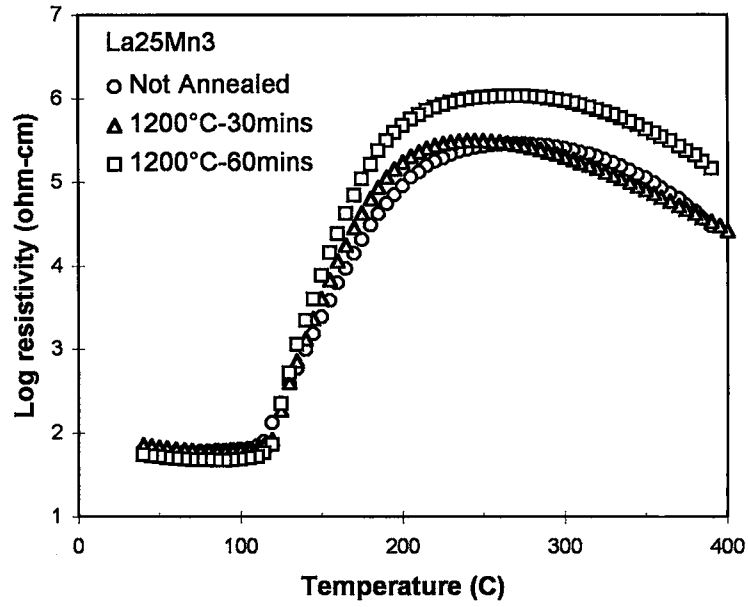
Figure 4.26. The resistivity behavior of 0.25 percent La^{+3} and 0.03 percent Mn^{+2} doped $BaTiO_3$ before and after annealing at 1200°C.
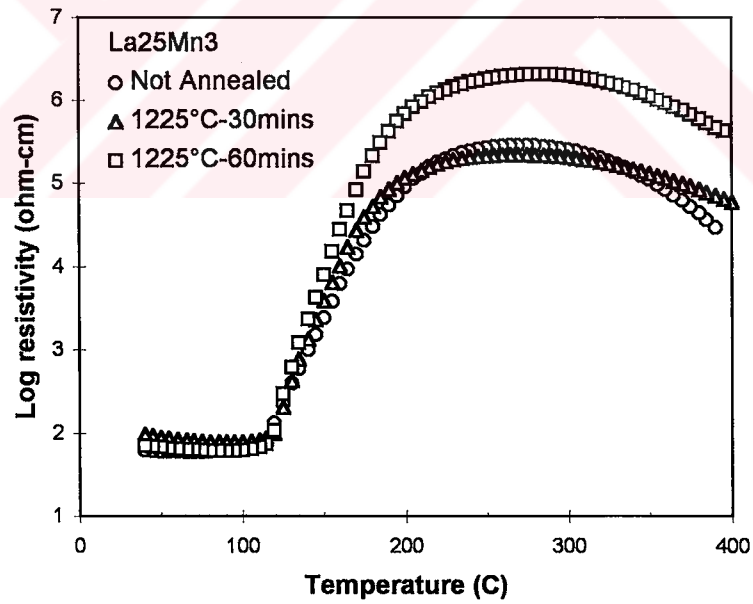
Figure 4.27. The resistivity behavior of 0.25 percent La^{+3} and 0.03 percent Mn^{+2} doped $BaTiO_3$ before and after annealing at 1225°C.
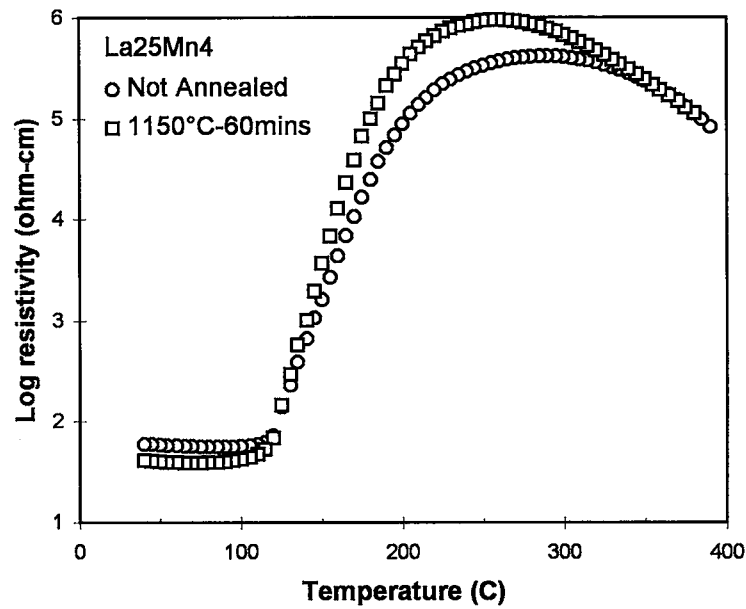
Figure 4.28. The resistivity behavior of 0.25 percent La^{+3} and 0.04 percent Mn^{+2} doped $BaTiO_3$ before and after annealing at 1150°C.
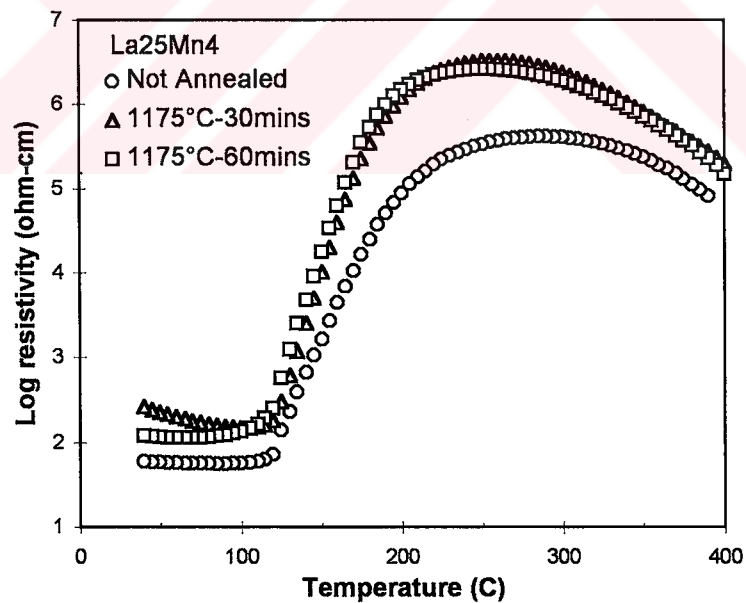
Figure 4.29. The resistivity behavior of 0.25 percent La^{+3} and 0.04 percent Mn^{+2} doped $BaTiO_3$ before and after annealing at 1175°C.
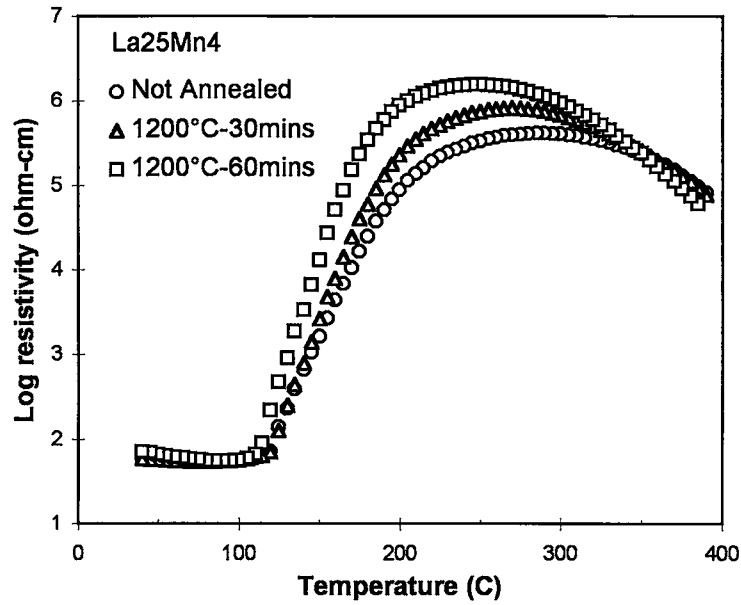
Figure 4.30. The resistivity behavior of 0.25 percent La^{+3} and 0.04 percent Mn^{+2} doped $BaTiO_3$ before and after annealing at 1200°C.
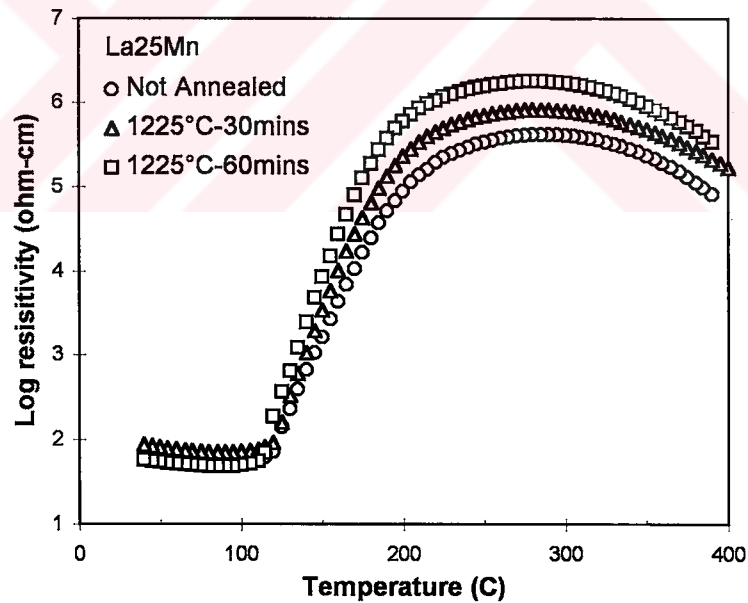
Figure 4.31. The resistivity behavior of 0.25 percent La^{+3} and 0.04 percent Mn^{+2} doped $BaTiO_3$ before and after annealing at 1225°C.
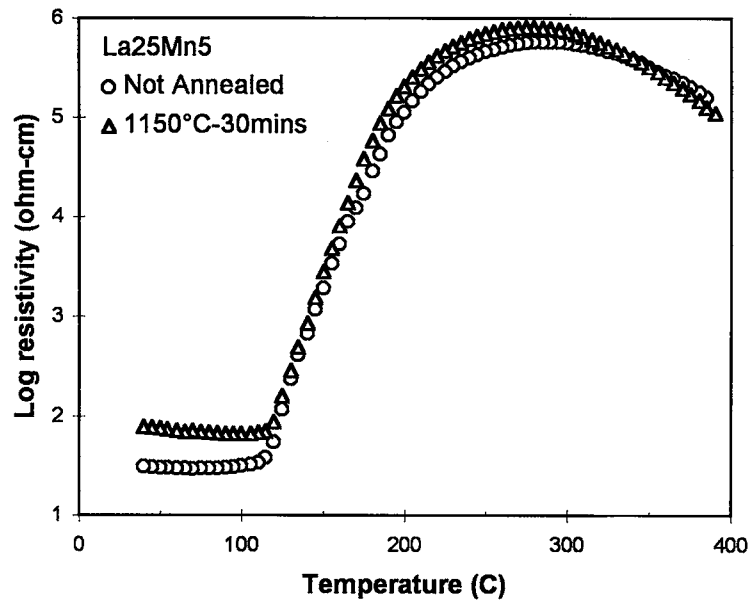
Figure 4.32. The resistivity behavior of 0.25 percent La^{+3} and 0.05 percent Mn^{+2} doped $BaTiO_3$ before and after annealing at 1150°C.
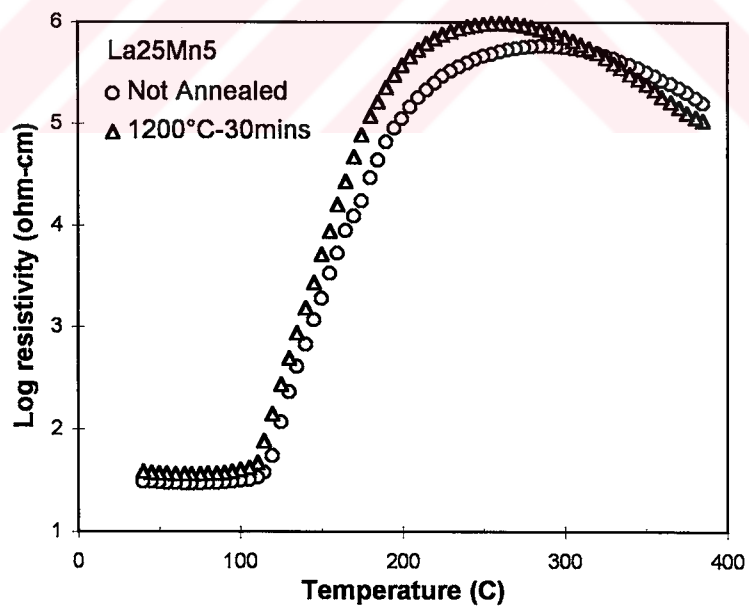
Figure 4.33. The resistivity behavior of 0.25 percent La^{+3} and 0.05 percent Mn^{+2} doped $BaTiO_3$ before and after annealing at 1200°C.
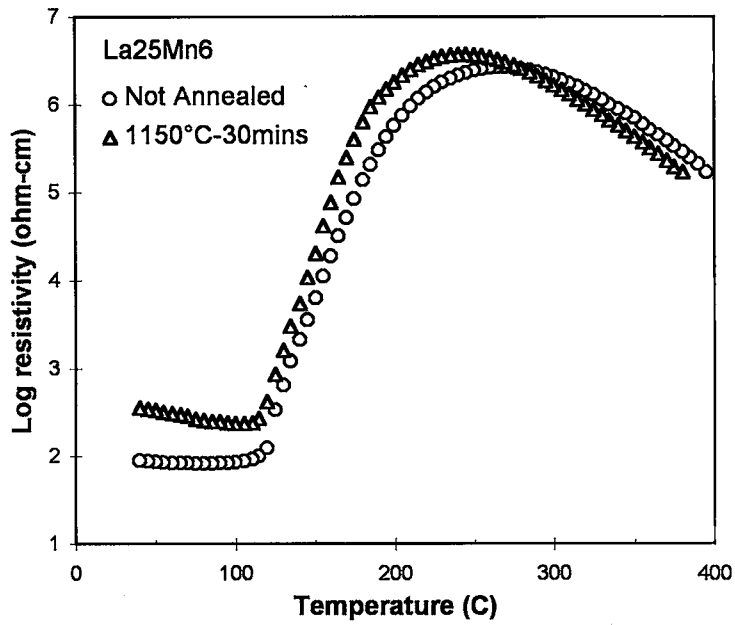
Figure 4.34. The resistivity behavior of 0.25 percent La^{+3} and 0.06 percent Mn^{+2} doped $BaTiO_3$ before and after annealing at 1150°C.
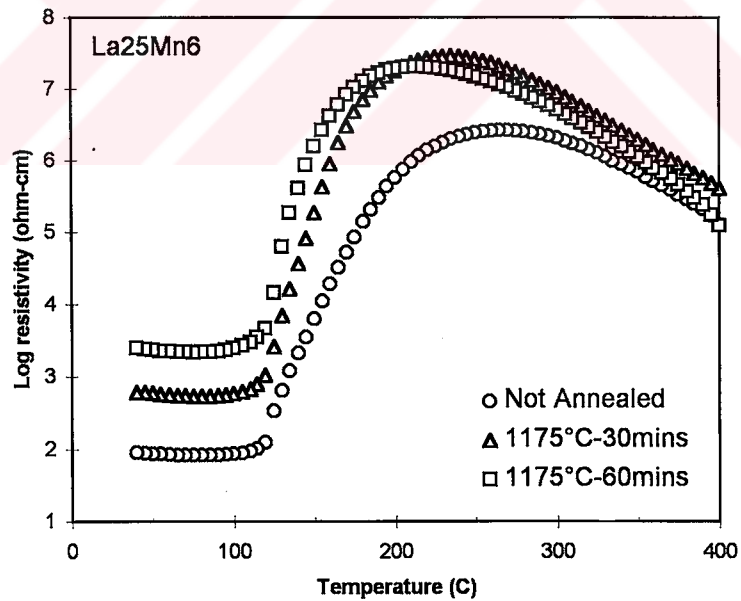
Figure 4.35. The resistivity behavior of 0.25 percent La^{+3} and 0.06 percent Mn^{+2} doped $BaTiO_3$ before and after annealing at 1175°C.
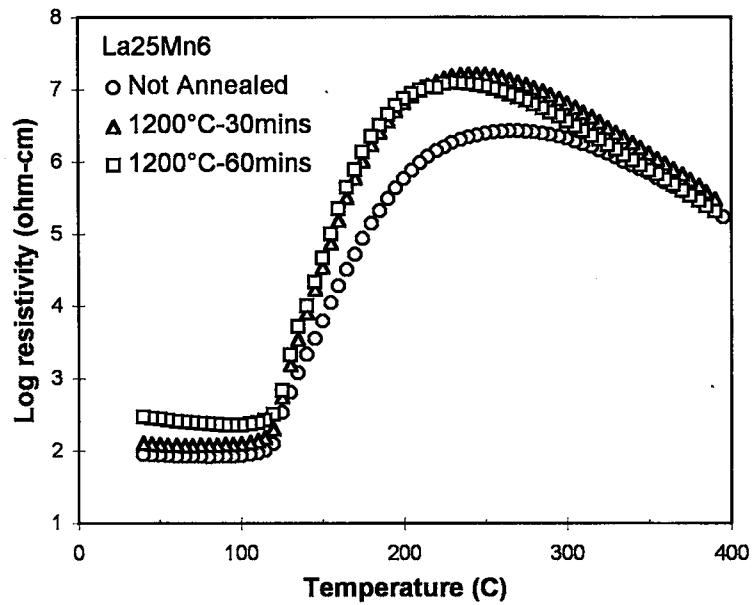
Figure 4.36. The resistivity behavior of 0.25 percent La^{+3} and 0.06 percent Mn^{+2} doped BaTiO$_3$ before and after annealing at 1200°C.
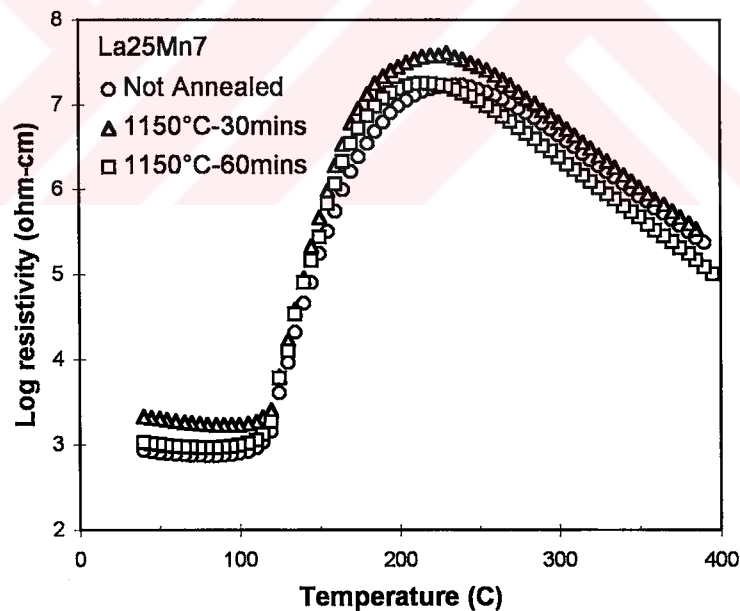
Figure 4.37. The resistivity behavior of 0.25 percent La^{+3} and 0.07 percent Mn^{+2} doped BaTiO$_3$ before and after annealing at 1150°C.
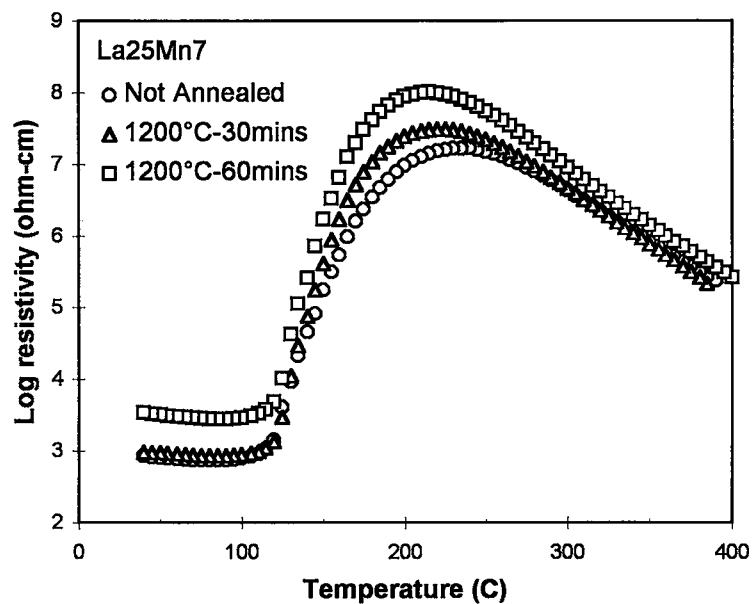
Figure 4.38. The resistivity behavior of 0.25 percent La^{+3} and 0.07 percent Mn^{+2} doped BaTiO$_3$ before and after annealing at 1200°C.
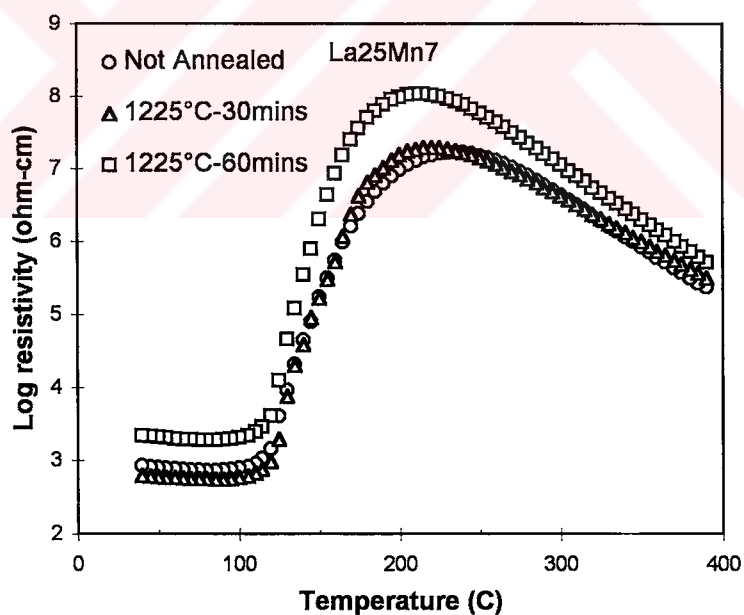
Figure 4.39. The resistivity behavior of 0.25 percent La^{+3} and 0.07 percent Mn^{+2} doped BaTiO$_3$ before and after annealing at 1225°C.

4.3. Ceramics with 0.2 Atomic Percent Lanthanum Additions

Referring back to the U-shaped curve, it may be seen that the barium titanate ceramics doped with 0.2 atomic percent La^{+3} exhibited a considerably low resistivity at room temperature. Because of this feature, this particular composition was regarded as a candidate for PTCR application and its electrical conductivity was examined in full detail like it was done for the PTCR ceramics with 0.25 atomic percent lanthanum.

The resistivity data for the PTCR ceramics of the group containing 0.2 atomic percent lanthanum and modified by 0.02, 0.03 and 0.04 atomic percent manganese are given in Table B1 of the Appendix. These data are shown with the resistivity curves in Figure 4.40. The initial resistivity of the ceramic with 0.02 atomic percent manganese was close to 10^2 ohm-cm, and the PTC anomaly was about 2. The magnitude of the PTC anomaly increased considerably, to about 3.5, when the manganese content was increased to 0.03 atomic percent. Further increase of manganese to 0.04 atomic percent a shift in the maximum resistivity $\rho_{max} = 10^6$ ohm-cm, but there was a decline in the PTC magnitude due to an increase of the initial resistivity. Curves in Figure 4.41 summarize the effect of manganese additions on the minimum and maximum resistivities and on the magnitude of PTC anomaly. 0.2 atomic percent lanthanum containing samples doped with manganese higher than 0.04 atomic percent did not exhibit substantial semiconductivity.

The resistivity data belonging to these compositions but annealed at different temperatures are given in Table B of the Appendix. The graphical display of these data are shown in Figures 4.42, 4.44, 4.46, 4.47, 4.49. In Figures 4.43, 4.48, 4.50 the effect of manganese additions on the minimum and maximum resistivities and on the magnitude of PTC anomaly are summarized.

88
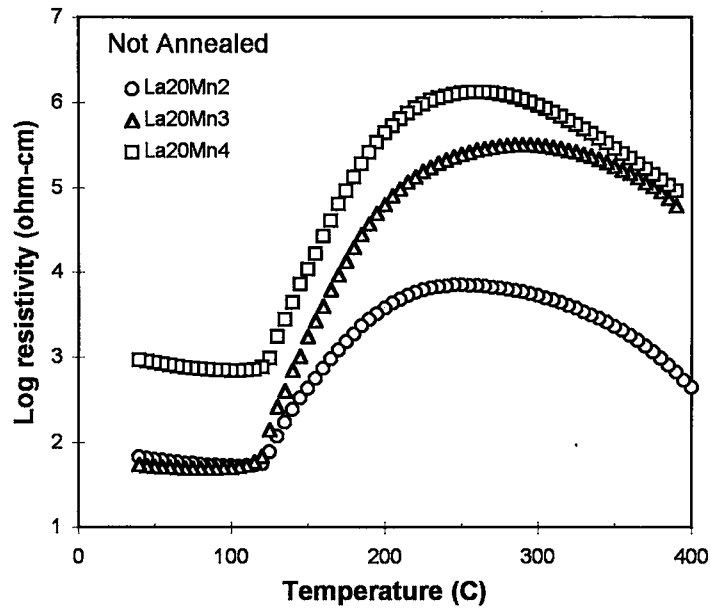
Figure 4.40. The resistivity versus temperature behavior of 0.20 percent La^{+3} doped $BaTiO_3$ without any annealing treatment at various Mn^{+2} concentration levels.
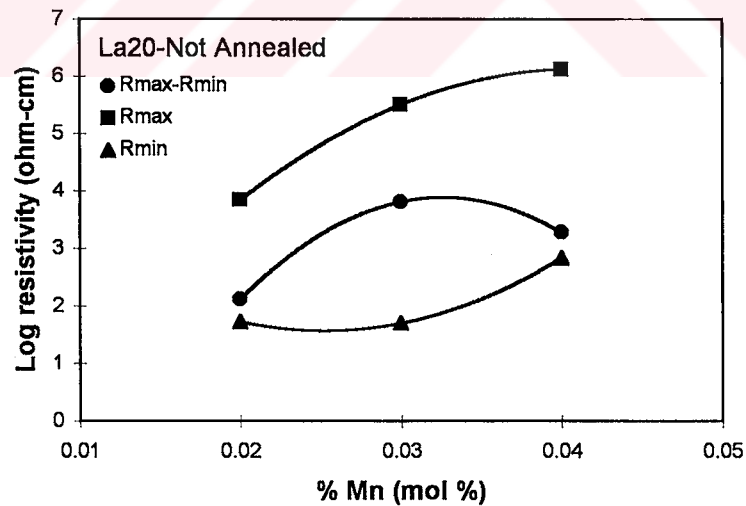

Figure 4.41. The plot of log R_{min}, log R_{max} and (log R_{max}-log R_{min}) of 0.20 atomic percent La^{+3} doped $BaTiO_3$ as a function of Mn^{+2} concentration.
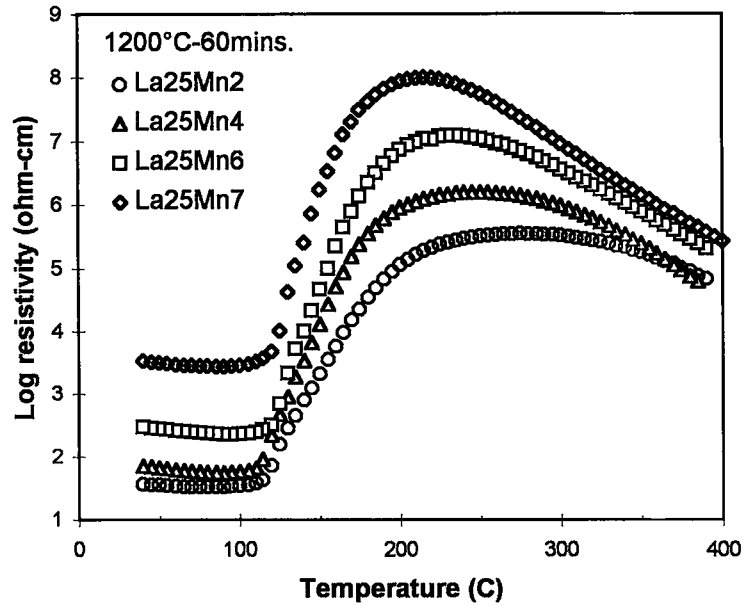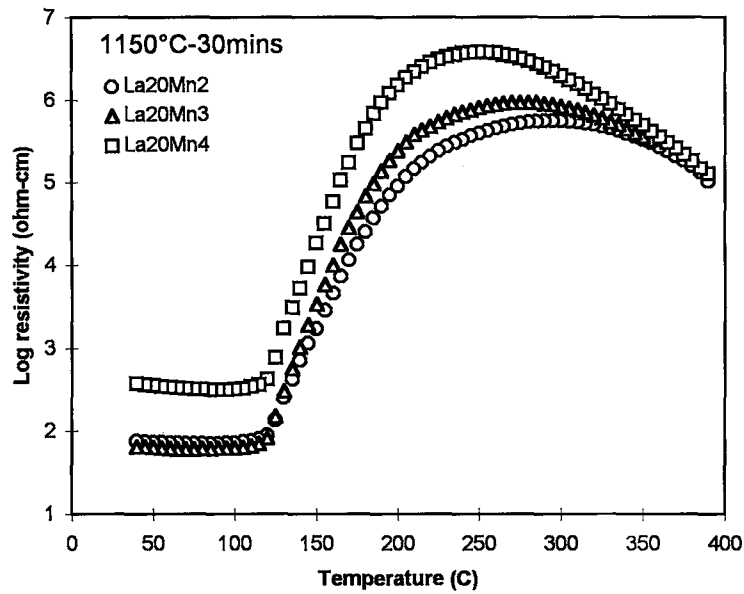
Figure 4.42. The resistivity versus temperature behavior of 0.20 percent La^{+3} doped $BaTiO_3$ after annealing at 1150°C for 30 minutes at various Mn^{+2} concentration levels.
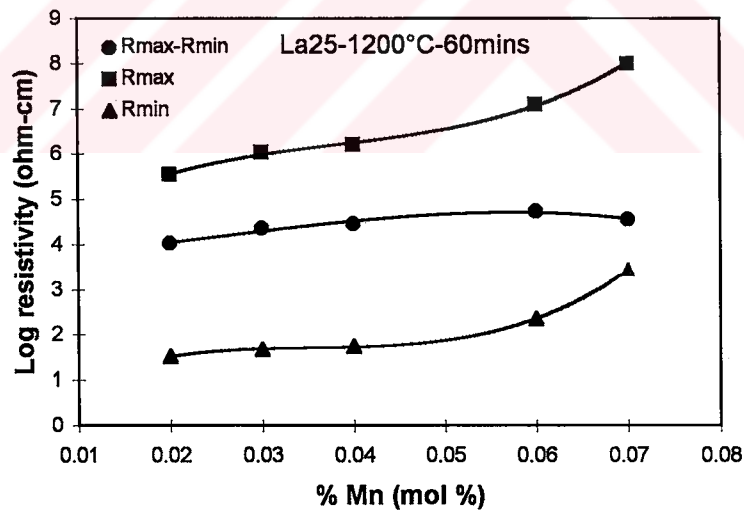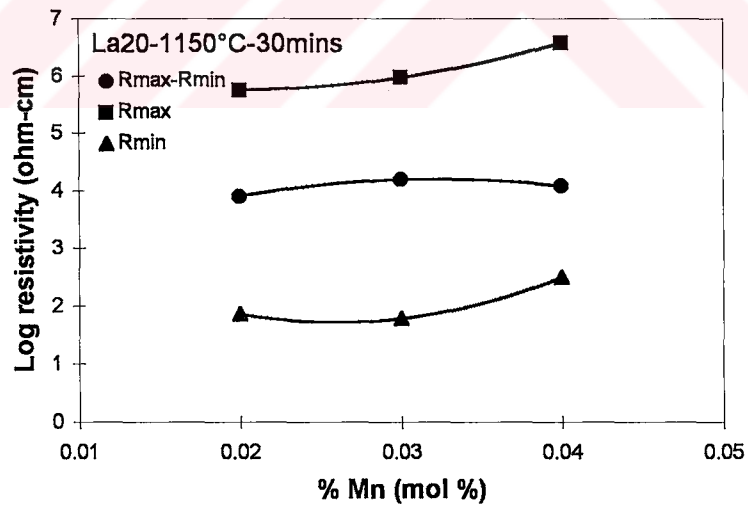

Figure 4.43. The plot of log R_{min}, log R_{max} and (log R_{max}-log R_{min}) of 0.20 atomic percent La^{+3} doped $BaTiO_3$ as a function of Mn^{+2} concentration after annealing at 1150°C for 30 minutes.
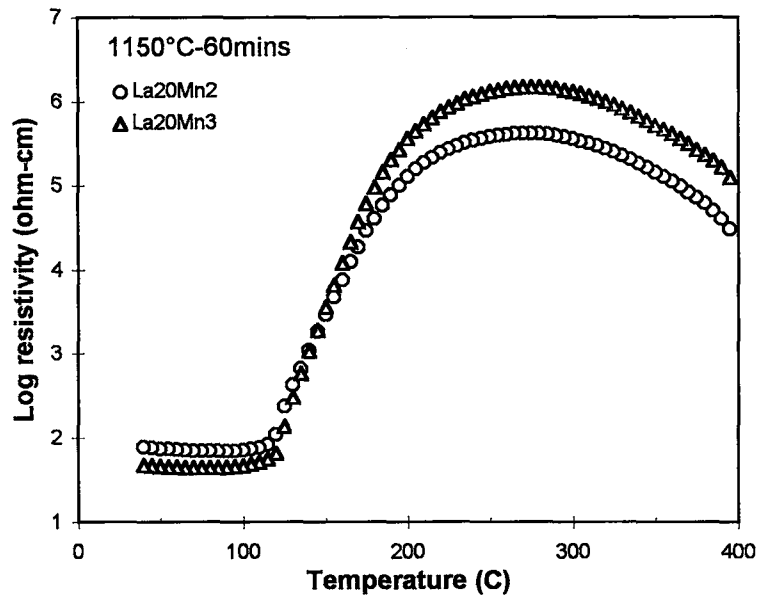
Figure 4.44. The resistivity versus temperature behavior of 0.20 percent La^{+3} doped $BaTiO_3$ after annealing at 1150°C for 60 minutes at various Mn^{+2} concentration levels.
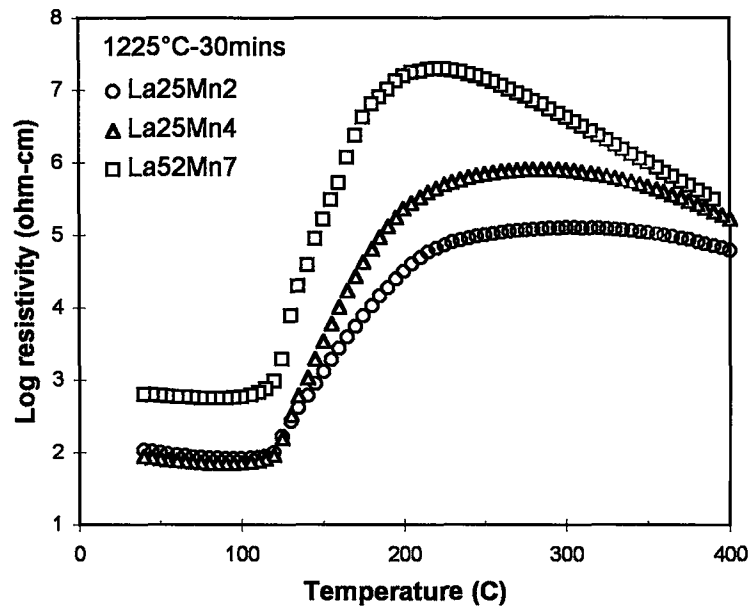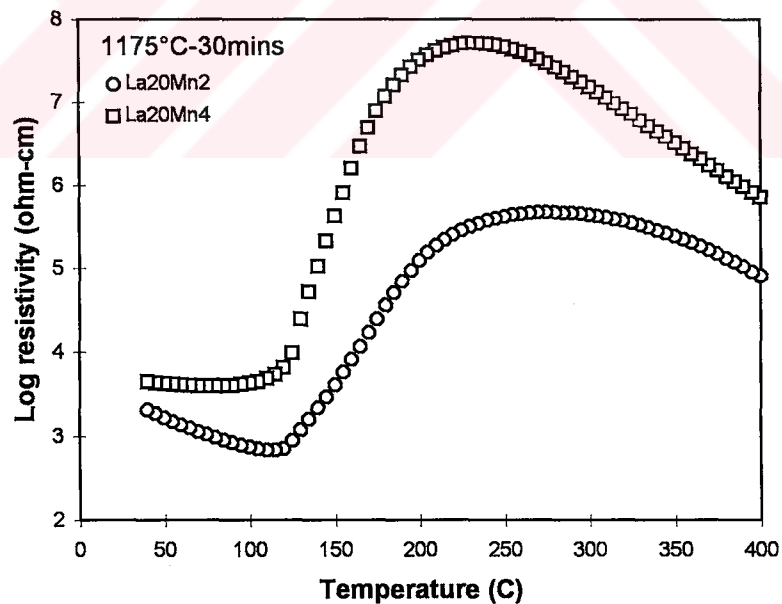

Figure 4.45. The resistivity versus temperature behavior of 0.20 percent La^{+3} doped $BaTiO_3$ after annealing at 1175°C for 30 minutes at various Mn^{+2} concentration levels.
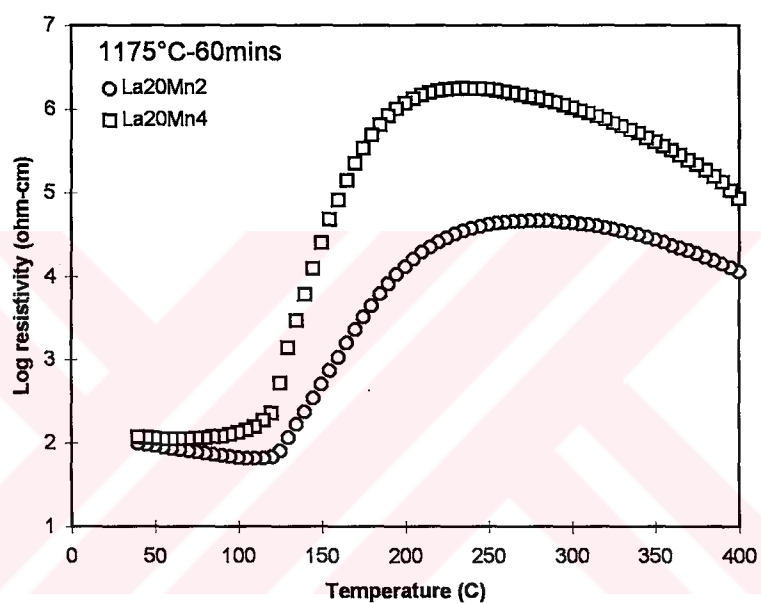
Figure 4.46. The resistivity versus temperature behavior of 0.20 percent La^{+3} doped $BaTiO_3$ after annealing at 1175°C for 60 minutes at various Mn^{+2} concentration levels.
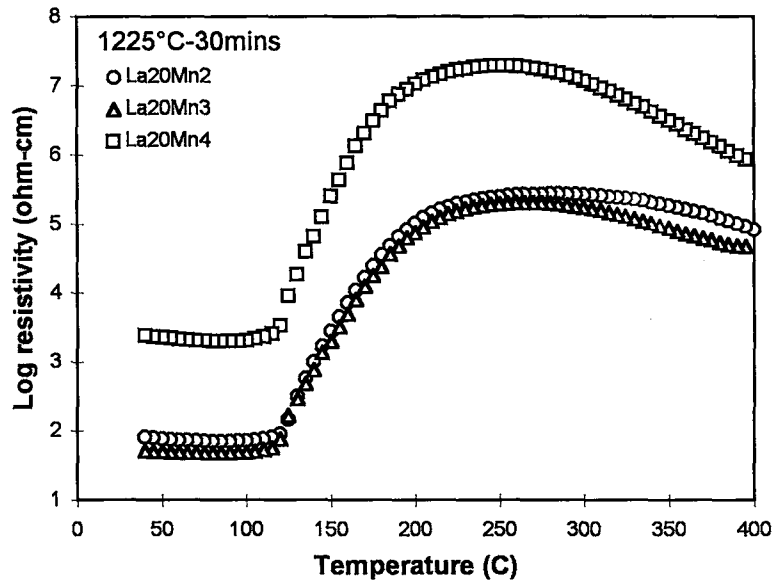
Figure 4.47. The resistivity versus temperature behavior of 0.20 percent La^{+3} doped $BaTiO_3$ after annealing at 1225°C for 30 minutes at various Mn^{+2} concentration levels.
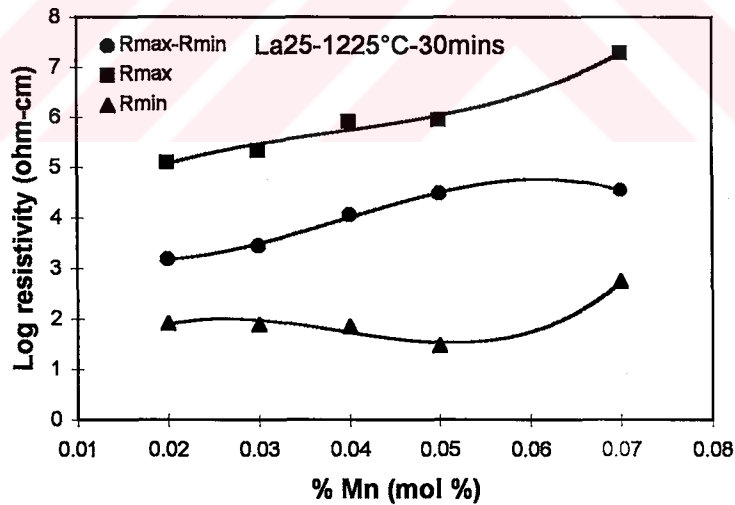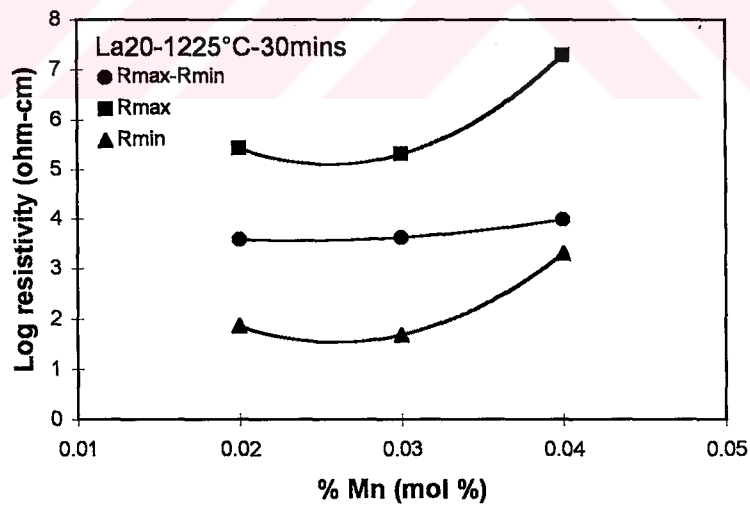

Figure 4.48. The plot of log R_{min}, log R_{max} and (log R_{max}-log R_{min}) of 0.20 atomic percent La^{+3} doped $BaTiO_3$ as a function of Mn^{+2} concentration after annealing at 1225°C for 30 minutes.
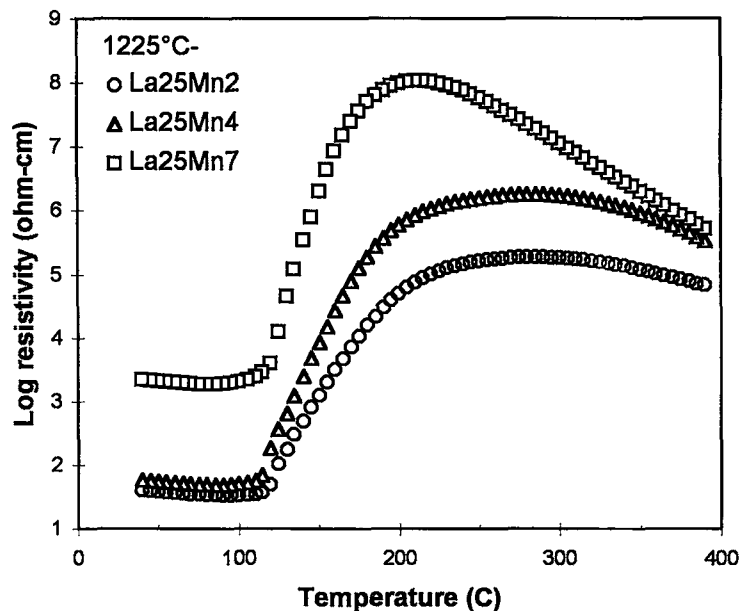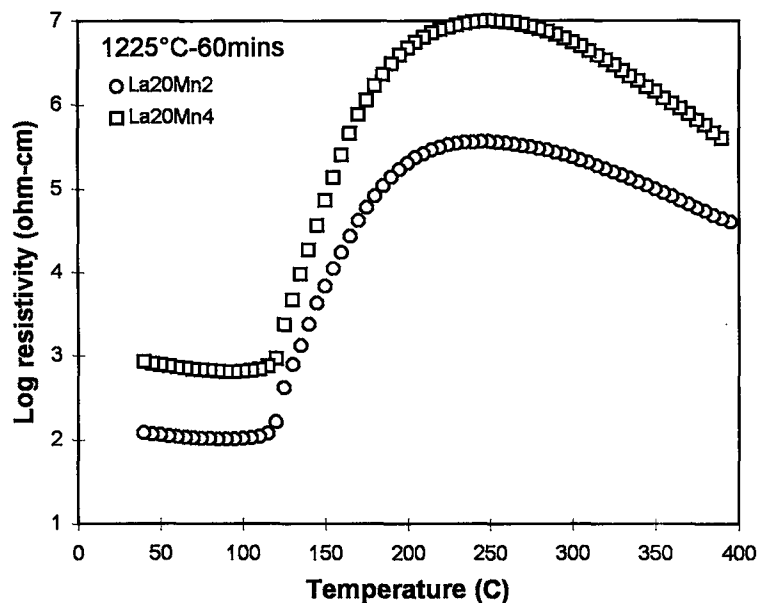
Figure 4.49. The resistivity versus temperature behavior of 0.20 percent La^{+3} doped BaTiO$_3$ after annealing at 1225°C for 60 minutes at various Mn^{+2} concentration levels.
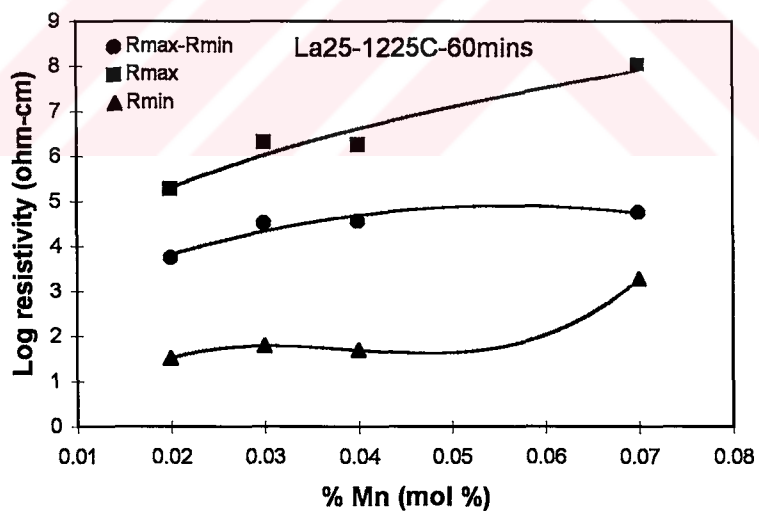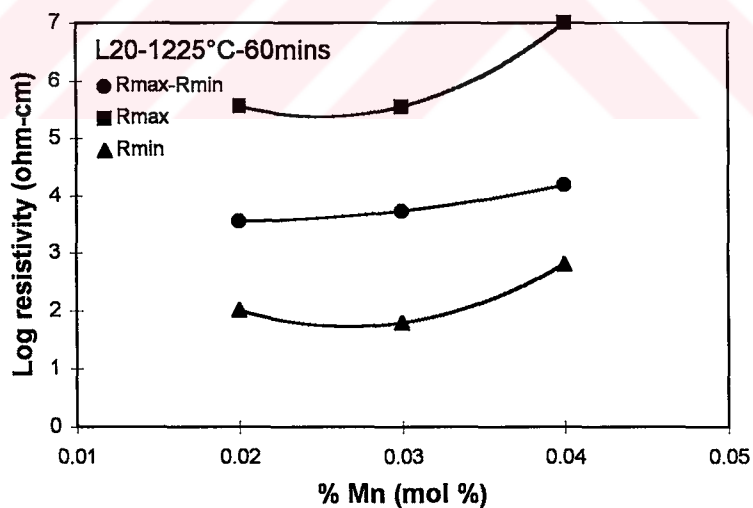

Figure 4.50. The plot of log R$_{min}$, log R$_{max}$ and (log R$_{max}$-log R$_{min}$) of 0.20 atomic percent La^{+3} doped BaTiO$_3$ as a function of Mn^{+2} concentration after annealing at 1225°C for 60 minutes.

The effects of annealing on the PTCR ceramics containing 0.2 atomic percent La^{+3} were studied in the temperature interval of 1150°C to 1225°C. The resistivity data belonging to these samples are given in Table B of the Appendix. The graphical display of these data are shown in Figures 4.51 through 4.60.

For the interpretation of the results, consider the resistivity curves given in Figure 4.51. In this figure each of the resistivity curves had 0.20 atomic percent La^{+3} ion, 0.02 percent manganese and annealed at 1150°C. The difference being just the annealing time. The lowest curve in Figure 4.50 belong to the sample that is directly cooled to the room temperature after sintering. The PTCR effect was found to be around about 2. After thermal treatment at 1150°C for 30 or 60 minutes, the PTC anomaly improved from about 2 to about 3.5 orders of magnitude.
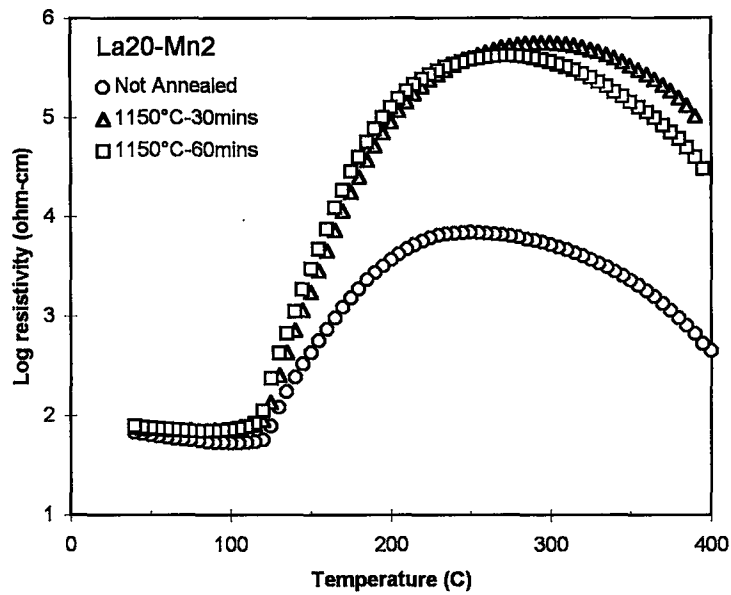
Figure 4.51. The resistivity behavior of 0.20 percent La^{+3} and 0.02 percent Mn^{+2} doped BaTiO$_3$ before and after annealing at 1150°C.
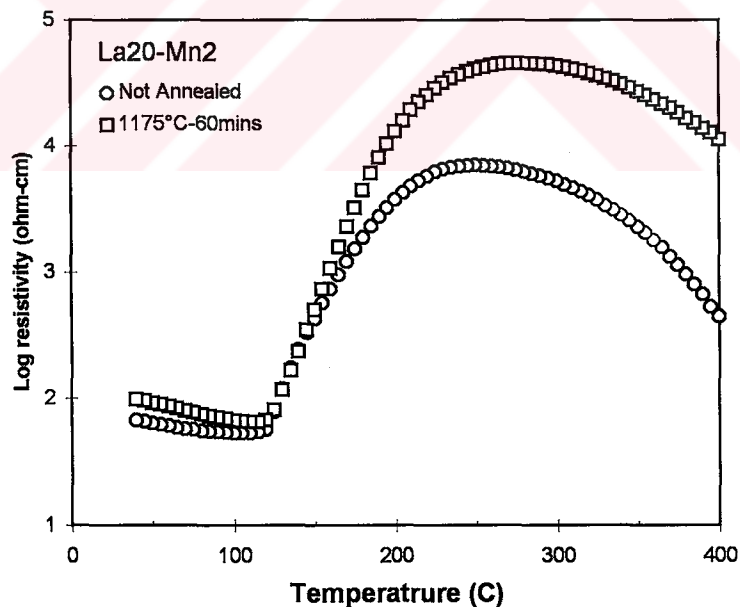
Figure 4.52. The resistivity behavior of 0.20 percent La^{+3} and 0.02 percent Mn^{+2} doped BaTiO$_3$ before and after annealing at 1175°C.
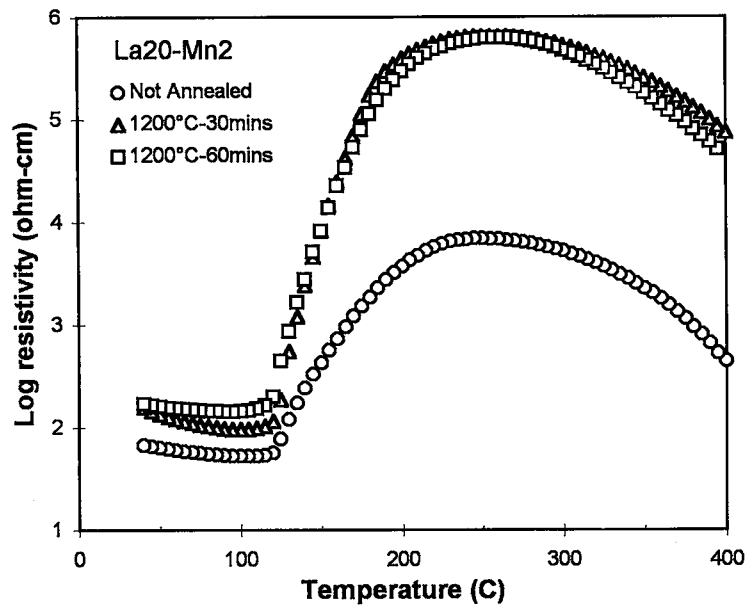
Figure 4.53. The resistivity behavior of 0.20 percent La^{+3} and 0.02 percent Mn^{+2} doped BaTiO$_3$ before and after annealing at 1200°C.
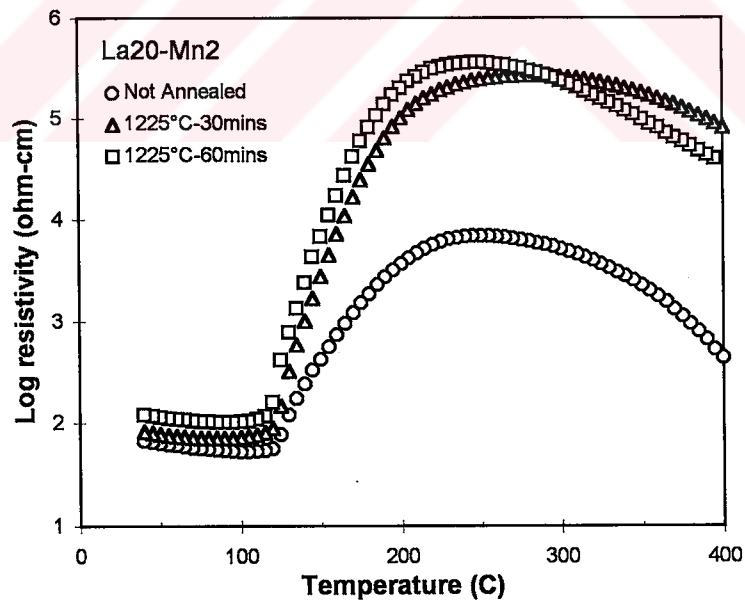
Figure 4.54. The resistivity behavior of 0.20 percent La^{+3} and 0.02 percent Mn^{+2} doped BaTiO$_3$ before and after annealing at 1225°C.
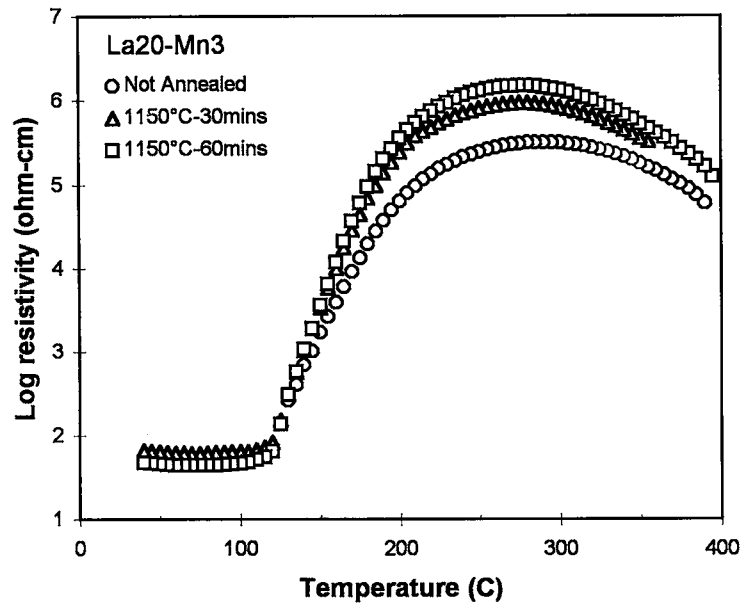
Figure 4.55. The resistivity behavior of 0.20 percent La^{+3} and 0.03 percent Mn^{+2} doped $BaTiO_3$ before and after annealing at 1150°C.
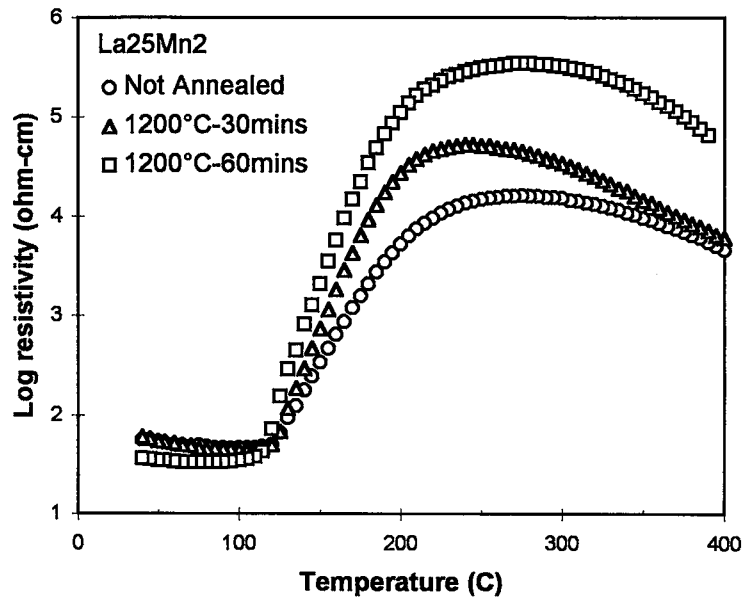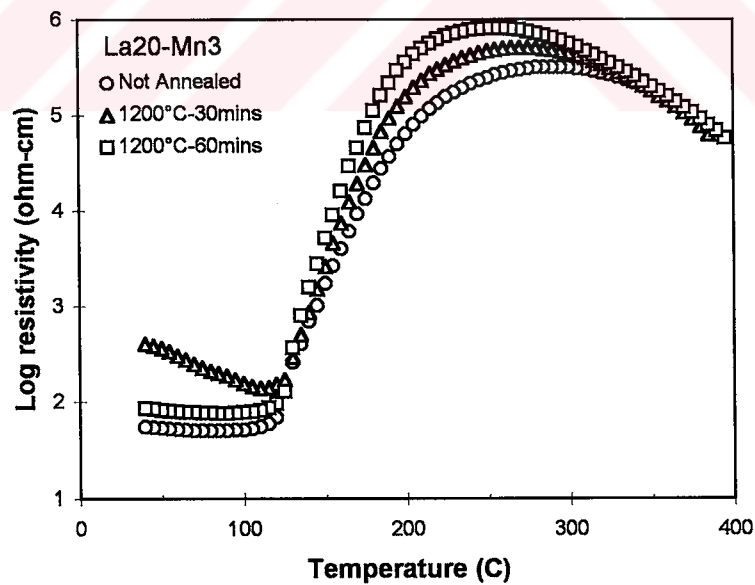

Figure 4.56. The resistivity behavior of 0.20 percent La^{+3} and 0.03 percent Mn^{+2} doped $BaTiO_3$ before and after annealing at 1200°C.
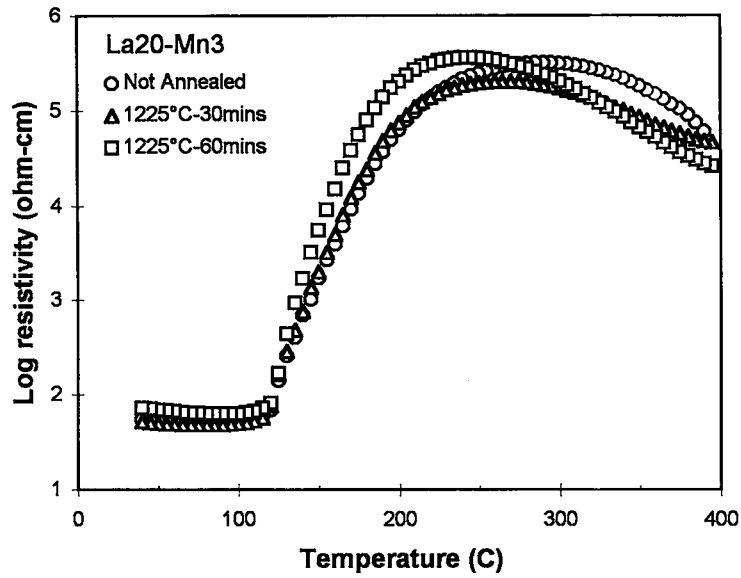
Figure 4.57. The resistivity behavior of 0.20 percent La^{+3} and 0.03 percent Mn^{+2} doped BaTiO$_3$ before and after annealing at 1225°C.
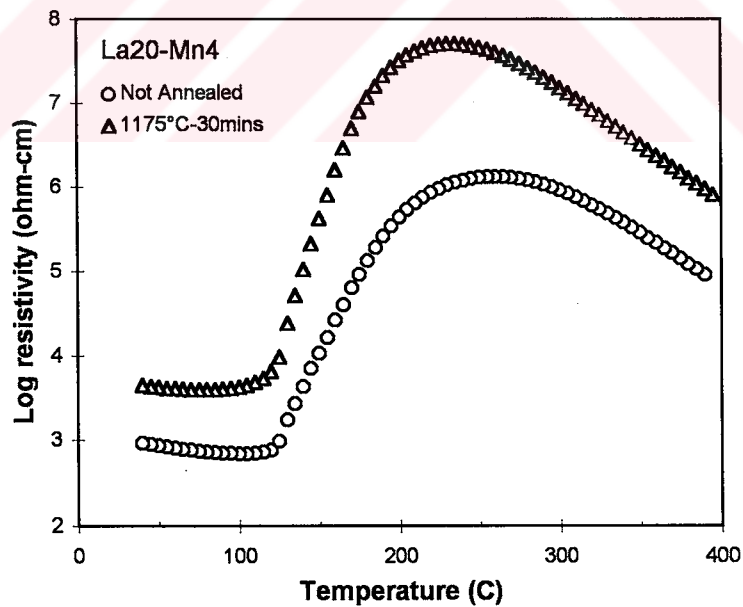
Figure 4.58. The resistivity behavior of 0.20 percent La^{+3} and 0.04 percent Mn^{+2} doped BaTiO$_3$ before and after annealing at 1175°C.
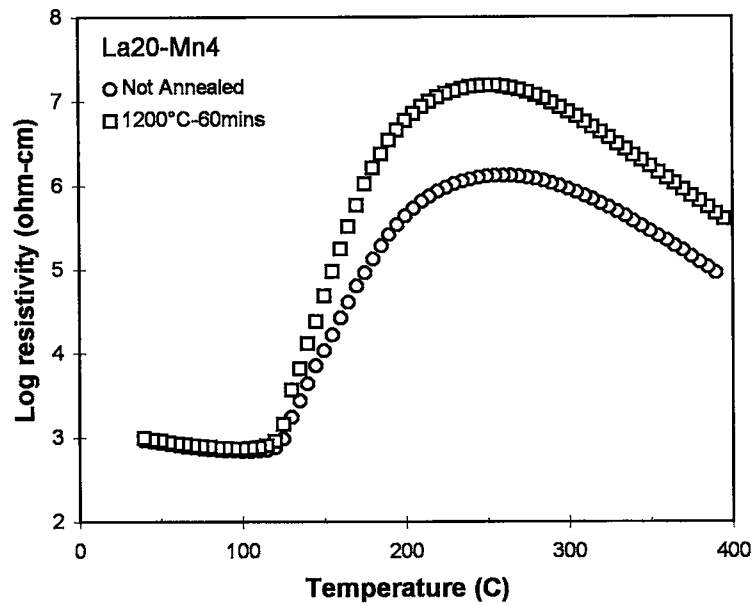
Figure 4.59. The resistivity behavior of 0.20 percent La^{+3} and 0.04 percent Mn^{+2} doped $BaTiO_3$ before and after annealing at 1200°C.
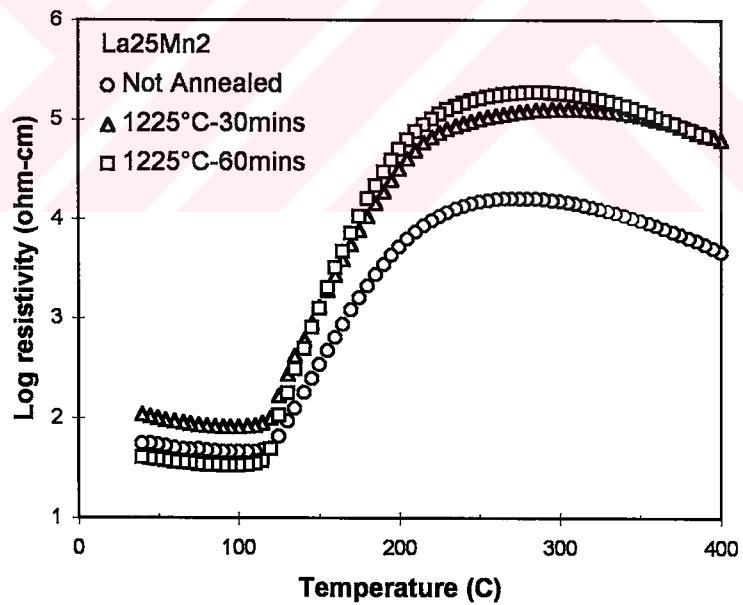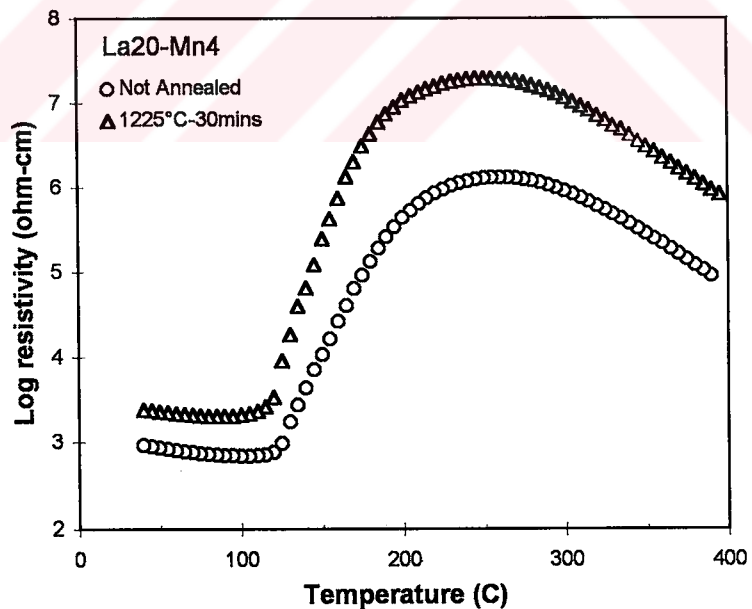

Figure 4.60. The resistivity behavior of 0.20 percent La^{+3} and 0.04 percent Mn^{+2} doped $BaTiO_3$ before and after annealing at 1225°C.

100

4.4. Electrical Resistivity of (Ba,Pb)TiO$_3$ Solid Solution

The electrical resistivity of lead containing PTCR compositions were studied in solid solution range up to 50 mol percent PbTiO$_3$. These selected compositions were made semiconductor by incorporation of 0.35 atomic percent lanthanum and they were modified by 0.02 percent manganese additions. Sintering of these samples took place at 1200°C or 1250°C for 30 minutes. The electrical resistivity versus temperature data related to these compositions are summarized in the Table C of the Appendix. These data were used to construct the curves given in Figure 4.61 for samples sintered at 1200°C for 30 minutes and in Figure 4.62 for samples sintered at 1250°C for 30 minutes.

The resistivity versus temperature curves shown in Figure 4.61 indicated that up to 30-40 percent lead the material may be regarded as a semiconductor. The negligible PTCR anomalies could be noted in all the compositions studied. The 10 percent lead titanate containing composition was the only composition among the ten compositions studied that showed appreciable PTCR effect. The $\Delta\log\rho$ was approximately 3 orders of magnitude. The resistivity of 50 percent lead titanate containing sample showed a continuos decline with increasing temperature. Therefore, this material could not be classified as a PTCR ceramic, rather it was a NTC material. The resistivity of the same lead titanate containing samples sintered at 1250°C for 30 minutes are given in Figure 4.62. The degradation in the PTCR effect of 10 percent lead titanate containing sample from about 3 to 1 order of magnitude was the marked change with increasing sintering temperature. The negligible PTC anomaly that was not encountered in Figure 4.61 became for 50 percent lead titanate containing sample as shown in Figure 4.62.
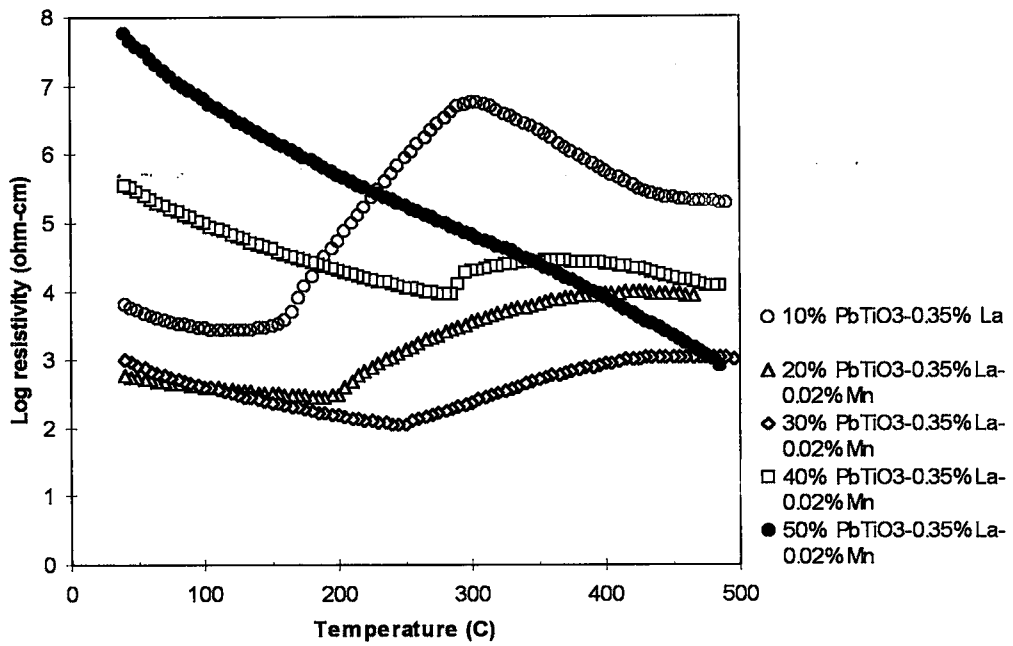
Figure 4.61. Resistivity versus temperature plots of PbTiO₃ containing samples sintered at 1200°C.
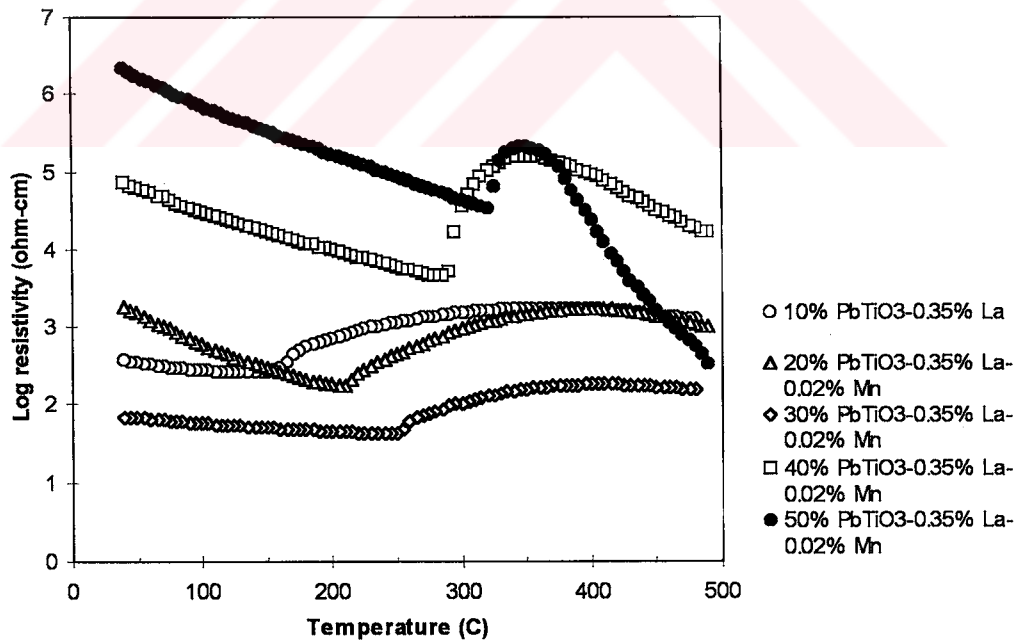
Figure 4.62. Resistivity versus temperature plots of PbTiO₃ containing samples sintered at 1250°C.

CHAPTER 5

DISCUSSION AND CONCLUSIONS

The present thesis work was undertaken with the aim of generating information on processing of PTCR barium titanate ceramics. The outstanding features of this type of ceramics are their low resistance at room temperature and the display of very high resistivity jump above the Curie point. Thus the material functions as a semiconductor at low temperatures and becomes an insulator at temperatures above the Curie point. Although numerous publications exists on both of these matters some of the information is still of proprietary nature. Therefore, in order to be able to manufacture these ceramics, part of the information unrevealed in open literature or patents had to be uncovered by research of our own.

Pure barium titanate is normally an insulator. However, its resistivity can be lowered significantly by doping with suitable cations. Among the common used doping agents suggested in the literature, lanthanum was chosen in this study as the additive for producing semiconductor barium titanate. In addition, manganese was used as an acceptor dopant for enhancing the magnitude the PTCR action. The results obtained in the present work on the combined effects of lanthanum and manganese were in accordance of the observations made in similar earlier studies published in the literature. (Amarakoon, Ching et al).

In the present study, the semiconductor grade barium titanate powder used in the production of PTCR ceramic samples were manufactured in the

laboratory by the thermochemical method known as mixed oxide route. The procedure followed in the thesis for powder synthesis permitted to obtain substantially spherical submicron spherical powders with a narrow size distribution. The optimum amount of lanthanum added to obtain the lowest room temperature resistance in the ceramics was 0.25 atomic percent. Good results could also be displayed with ceramics doped by 0.2 or 0.3 atomic percent lanthanum, in some sacrifice from room temperature conductivity. Figure 5.1 shows the example of a SEM photograph taken from a typical powder batch having 0.25 atomic percent La^{+3}, and 0.03 percent manganese in its composition. The powder had a quite uniform size distribution and the particle size was about 0.25 micron.

The sintering temperature selected in the present study was 1360°C, and the ceramics were soaked at this temperature for 2 hours. The sintering schedule suggested by Amarakoon [30] was found to be equally effective for the kind of powders produced in the present study. The sintering mechanism involved was essentially that of liquid phase sintering; excess TiO_2 and excess SiO_2 introduced into the ceramic powder mixtures as liquid phase sintering aids were instrumental in obtaining highly dense barium titanate ceramics.

For the first time in literature, Ching et al. showed that the process of imparting semiconductivity to barium titanate by using lanthanum as the dopant depended critically on the level of manganese additions. Present study confirmed their findings. At the sintering temperature of 1360°C manganese additions up to 0.06 atomic percent enhanced the PTC anomaly without much degradation in the room temperature conductivity of the ceramics. When manganese additions exceed this limit, however, the room temperature resistance tended to rise in an exponential manner. These ceramics also exhibited considerable PTCR activity. Hence the present study showed that advantage could be taken from high manganese additions in applications where PTCR ceramics with lower heating rate were required.
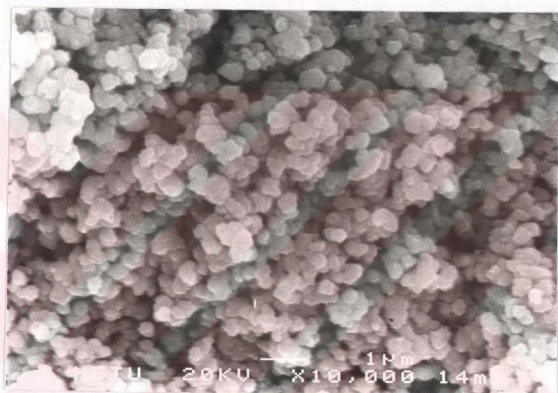
Figure 5.1. SEM photograph 0.25 atomic percent La^{+3}, and 0.03 percent
manganese doped barium titanate powder sample calcined at
1075°C for 8 hours.

In the present study, the annealing process, which enhances the PTC anomaly upon oxidation of the grain boundaries of the ceramic, was conducted for short durations like 30 minutes to 1 hour. The results of annealing at different annealing temperatures were all similar; i.e., the magnitude of the PTC anomaly was increased to higher $\Delta\log \rho$ values upon heat treatment. The increase in PTC anomaly was similar to that predicted by Al-Allak, et al. [46] who carried out prolonged annealing treatments up to 30 hours.

The problem encountered during the experimental part of the study were of two kinds. (1) The manufacture of non-ohmic contacts, and (2) The issue of reproducibility. The former was solved quite efficiently by adopting the procedure of electroless nickel plating suggested in the literature [44] specifically for the PTCR barium titanates. It should perhaps be stressed here that the same procedure should be used in electroding PTCR ceramics. Otherwise unduely high contact resistances develop which render the ceramic useless.

The issue of reproducibility is also related to closely with the reliability of the PTCR ceramics. The reproducibility in the electrical behavior of commercial PTCR ceramics has been stated to be 60 percent [40]. This rather a low yield, because that means about 40 percent of the manufactured PTCR ceramics are unreliable and should be discarded. Therefore, a rather close quality control practice must be established in order to eliminate the unqualified ceramics.

The problem of reproducibility is linked with the uniform distribution of the liquid phase additives in the powder mixture. special emphasis has been placed on SiO_2 (Amarakoon, Abicht), because this ingredients is the main agent which is responsible for the development of the liquid phase that operates in the sintering of PTCR barium titanate. Since TiO_2 and SiO_2 are used only in very small quantities as sintering additives great care must be

exercised in achieving their uniform distribution throughout the microstructure. This is necessary for obtaining uniform microstructure, free from abnormal grain growth, and also for uniform diffusion of oxygen to the grain boundaries, that is so crucial for obtaining a proper PTC anomaly.

The grain structure of the PTCR ceramics produced in the present work were studied by SEM examinations. In all ceramic samples examined the average grain size was typically in the order of 10 microns. Figure 5.2 shows the SEM micrograph of the ceramic sample with 0.25 atomic percent La^{+3} and 0.04 atomic percent Mn^{+2} additions. The liquid phase enveloping the grain boundaries of the sample was removed by exposing it to molten KOH. The micrograph of the etched sample, shown in Figure 5.3 is evidence to the fact that the grain size was quite uniform with no exaggerated grain growth occurrence.

In order to shift the Curie point of barium titanate ceramics to higher temperatures, in the present study the $BaTiO_3$ compositions were alloyed with $PbTiO_3$. Additions of lead were indeed instrumental in extending the room temperature conductivity to temperatures above 120°C. But the PTC anomaly degraded considerably to the extend that the lead-based compositions could be regarded as simple ceramic heaters but not as PTCR elements. The main reasons for the loss of PTC behavior could be related with the powder preparation technique. In the literature, the PTCR grade barium-lead titanate powders are reported to be manufactured by the so-called titanyl-oxalate precipitations [47, 48] which involve the use of highly expensive chemicals for this purpose.

Figure 5.2. SEM micrograph of the ceramic sample with 0.25 atomic percent La^{+3} and 0.04 atomic percent Mn^{+2} additions.
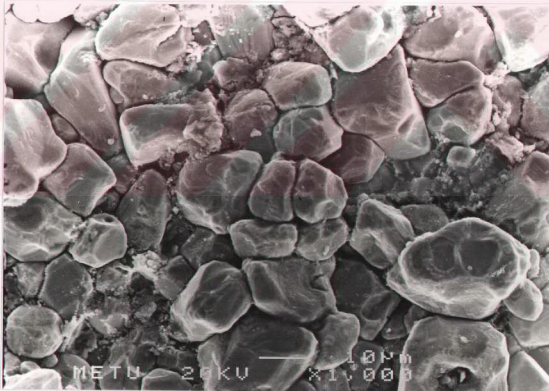
Figure 5.3. SEM micrograph of the ceramic sample with 0.25 atomic percent La^{+3} and 0.02 atomic percent Mn^{+2} additions.

REFERENCES

[1] S. Saito, "Fine Ceramics", Elsevier Publ. Co. (Tokyo), pp. 286-291, (1988).

[2] B. Jaffe, W. R. Cook, and H. Jaffe, "Piezoelectric Ceramics", Academic Press, pp. 49-109, (1971).

[3] L. L. Hench, and J. K West, "Principles of Electronic Ceramics", Willey-Interscience Publication, pp. 237-281, (1989).

[4] Encyclopedia of Chem. Tech., vol. 10, pp. 1-30.

[5] a) J. Daniels and K. H. Hardtl, "Electrical Conductivity at High Temperatures of Donor-Doped Barium Titanate Ceramics", Philips Res. Repts., 31, pp. 489-504, (1976).

b) J. Daniels, "Defect Equilibria in Acceptor Doped Barium Titanate", Philips Res. Repts., 31, pp. 505-515, (1976).

c) D. Hennings, "Thermogravimetric Investigations", Philips Res. Repts., 31, pp. 516-525, (1976).

d) R. Wernicke, "The Kinetics of Equilibrium Restoration in Barium Titanate Ceramics", Philips Res. Repts., 31, pp. 526-543, (1976).

    e) J. Daniels and R. Wernicke, "New Aspects of an Improved PTC
    Model", <u>Philips Res. Repts., 31,</u> pp. 544-559, (1976).

[6] R. E. Newham, "Electroceramics", <u>Rep. Prog. Phys., 52,</u> pp 123-156,
    (1989).

[7] J. Daniels, K. H. Hardtl and R. Wernicke, "The PTC Effect of Barium
    Titanate", <u>Philips Technical Review, 38,</u> 73-82, (1978/79).

[8] R. C. Buchanan, Ceramic Materials for Electronics, pp. 249-347, (1991),

[9] H. Ueoka, "The Doping Effect of Transition Elements on the PTC
    Anomaly of Semiconductive Ferroelectric Ceramics", <u>Ferroelectrics, 7,</u>
    pp. 351-53, (1974).

[10] H. A. Sauer and J. R. Fisher, "Processing of Positive Temperature
    Coefficient Thermistors", <u>J. Am. Ceram. Soc.,</u> vol. <u>43,</u> pp. 297-301;
    June, (1960).

[11] O. Saburi and K. Wakino, "Processing Techniques and Applications of
    Positive Temperature Coefficient Thermistors", <u>IEEE Transactions on
    Component Parts,</u> pp. 53, (1963).

[12] H. Ueoka and M. Yodogawa, "Ceramic Manufacturing Technology for
    the High Performance PTC Thermistors", <u>IEEE Transactions on
    Manufacturing Technology,</u> vol. <u>3,</u> pp. 77-82, (1974).

[13] W. Y. Howng and C. McCutcheon, "Electrical Properties of
    Semiconducting $BaTiO_3$ by Liquid Phase Sintering", <u>Ceramic Bulletin,
    62,</u> pp 231-33, (1983).

[14] H. Ueoka, "The Doping Effect of Transition Elements on the PTC Anomaly of Semiconductive Ferroelectric Ceramics", Ferroelectrics, 7, pp. 351-53, (1974).

[15] T. Fukami, and H. Tsuchiya, "Dependence of Resistivity on Donor Dopant Content in Barium Titanate Ceramics", Jpn. J. Appl. Phys., 18, pp. 735-38, (1979).

[16] H. Ihrig, "PTC Effect in BaTiO$_3$ as a Function of Doping with 3d Elements", J. Am. Ceram. Soc., 64, pp. 617-20, (1981).

[17] C. J. Ting, C. J. Peng, H. H. Lu, and S. T. Wu, "Lanthanum-Magnesium and Lanthanum-Manganese Donor-Acceptor-Codoped Semiconducting Barium Titanate", J. Am. Ceram. Soc., 73, pp 329-34, (1990).

[18] J. G. Fagan, V. R. W. Amarakoon, "Reliability and Reproducibility of Ceramic Sensors: Part II, PTC Thermistors", Am. Ceram. Bull. Soc., 72, pp. 69-76, (1993).

[19] a) Y. M. Chiang, and T. Takagi, "Grain Boundary Chemistry of Barium Titanate and Strontium Titanate: I, High-Temperature Equilibrium Space Charge", J. Am. Ceram. Soc., 73, pp 3278-85, (1990).

   b) Y. M. Chiang, and T. Takagi, "Grain Boundary Chemistry of Barium Titanate and Strontium Titanate: II, Origin of Electrical Barriers in Positivie Temperature Coefficient Thermistors", J. Am. Ceram. Soc., 73, pp 3286-91, (1990).

[20] W. Heywang, "Semiconducting Barium Titanate", J. Mater. Sci., 6, pp 1214-1226, (1971).

[21] A. Amin, "Phenomenological Description of Stress Related Grain Boundary Properties in Semiconducting Perovskites", Ferroelectrics, 87, pp 41-53, (1988).

[22] H. Brauer, J. Phys. C, 11, pp 819, (1978).

[23] T. R. N. Kutty and P. Murugaraj, Mater. Lett., 3, pp 195, (1985).

[24] J. H. Lee, S. H. Kim and S. H. Cho, "Valence Change of Mn Ions in BaTiO$_3$ PTCR Materials", J. Am. Ceram. Soc., 78, pp 2845-48, (1995).

[25] G. H. Jonker, "Halogen Treatment of Barium Titanate Semiconductors", Mat. Res. Bull., 2, pp. 401-07, (1967).

[26] H. F. Cheng, T. F. Lin, C. T. Hu, and I. N. Lin, "Effect of Sintering Aids on Microstructures and PTCR Characteristics of (Sr$_{0.2}$Ba$_{0.8}$)TiO$_3$ Ceramics", J. Am. Ceram. Soc., 76, pp 827-32, (1993).

[27] T. Negas, R. S. Roth, H. S. Parker, and D. Minor, "Subsolidus Phase Relation in the BaTiO$_3$-TiO$_2$ System", J. Solid State Chem., 9, pp 297-307, (1974).

[28] R. K. Sharma, N. H. Chan, and D. M. Smyth, "Solubility of TiO$_2$ in BaTiO$_3$", J. of the American Ceram. Soc., 64, pp 448-51, (1981).

[29] D. E. Rase and R. Roy, J. Am. Ceram. Soc., 38, 393, (1955).

[30] K.R. Udayakumar, K.G. Brooks, J.A.T. Taylor and V.R.W. Amarakoon, "Effect of Liquid Phase on the PTCR Behavior of BaTiO$_3$", Ceram. Eng. Sci. Proc., 8[9-10], pp 1035-1043(1987).

[31] M. Kahn, "Effect of Heat Treatment on the PTCR Anomaly in Semiconducting Barium Titanate", Ceramic Bulletin, vol. 50, no 8, pp 676-680, (1981).

[32] R. T. Thomas, R. H. Tredgold and R. H. Williams, "Influnce of Gaseous Adsorption on the Metal-BaTiO$_3$ Contact", Proc. Phys. Soc., London, Solid-State Phys., Ser. 2, 5, pp 1370-75, (1968).

[33] W. Heywang, "Barium Titanate as a Semiconductor with Blocking Layers", Solid State Electron., 3, pp. 51-58, (1961).

[34] W. Heywang and H. Thomann, "Positive Temperature Coefficient Resistors", Electronic Ceramics, pp 29-47, 1990

[35] F. M. Ryan and E. C. Subbarao, "Hall Effect in Semicondunting Barium Titanate", Appl. Phys. Lett., 1, pp. 69-71, (1962).

[36] G. H. Jonker, "Some Aspects of Semiconducting Barium Titanate," Solid-State Electronics, vol. 7, 895-903, (1964).

[37] M. Kuwabara, "Influence of Stoichiometry on the PTCR Effect in Porous Barium Titanate Ceramics", J. Am. Ceram. Soc., vol. 64, pp. C170-71; June, (1981).

[38] G. V. Lewis, C. R. A Catlow and R. E. W. Casselton, "PTCR Effect in Barium Titanate", J. Am. Ceram. Soc., vol. 68, pp 555-558, (1982).

[39] G. H. Jonker and E. E. Havinga, "The Influence of Foreign Ions on the Crystal Lattice Barium Titanate", Mater. Res. Bull., 17, pp 345, (1982).

[40] M. Kuwabara, "Determination of the Potential Barrier Height in Barium Titanate Ceramics", Solid State Electronics, 27, pp 925-935, (1984).

[41] O. Saburi, "Semiconducting Bodies in the Family of Barium Titanates", J. Am. Ceram. Soc., 44, pp. 54-63, (1961).

[42] B. Jaffe, W. R. Cook Jr. and H. Jaffe, Piezoelectric Ceramics, Academic, London, pp. 94-101, (1971)

[43] Y. I. Gol'tsov, O. I. Prokopalo and L. A. Belova, "Positive Temperature Coefficient of Resistance in Doped Lead Titanate", Soviet Physics-Solid State, 14, pp 805-06, (1972).

[44] K. H. Yoon, H. S. Park. S. O. Yoon, and H. I. Song, "Electroless Nickel Electrode on N-Type Semiconducting Barium Titanate", J. of Mater. Sci. Lett., 8, pp 1442-44, (1989).

[45] D. R. Turner, and H. A. Sauer, "Ohmic Contacts to Semiconducting Ceramics", J. of Electrochem. Soc., 107, pp 250-51, (1960).

[46] H. M. Al-Allak, G. J. Russel and J. Woods , "The Effect of Annealing on the Characteristics of Semiconducting BaTiO₃ Positive Temperature Coefficient of Resistance Devices", J. Phy. D: Appl. Phys, 20, pp 1645-1651, (1987).

[47] M. Kuwabara, S. Suemura, and M. Kawabara, "Preparation of High Curie Point Barium Lead Titanates and Their PTCR Characteristics", Am. Ceram. Soc. Bull., 64, pp 1394-98, (1985).

[48] M. Kuwabara, K. Nakao, and K. Okazaki, "Instability of the Characteristics of the Positive Temperature Coefficient of Resistivity in High-Curie-Point Barium-Lead Titanate Ceramics and Their Grain Structures", Comm. of the Am. Ceram. Soc., 71, pp C110-112, (1988).

Table A.1. Electrical Resistivity versus Temperature Data for Un-Annealed 0.25 Percent La^{+3} Doped BaTiO$_3$

Temperature (°C)	Electrical Resistivity (ohm-cm)						
	La25Mn2	La25Mn3	La25Mn4	La25Mn5	La25Mn6	La25Mn7	La25Mn8
350	9618	111458	236768	319962	697726	834753	1109036
340	10748	138020	281238	381584	888884	1163483	1553697
330	11925	170533	321809	440290	1133424	1599436	2234625
320	13074	202303	360356	492171	1438769	2243577	3049850
310	14128	229497	388996	536603	1747838	3179531	4368485
300	14964	254404	409393	566087	2069809	4389770	6111016
290	15626	272224	417206	578808	2338324	6030900	8577702
280	15992	283730	414045	574504	2554665	8041200	11763706
270	15992	287318	399420	551935	2656643	10434414	15989503
260	15615	281835	373915	513427	2619112	13017190	20715960
250	14749	267539	338415	461318	2448623	15164200	25143799
240	13416	245726	294895	398303	2164754	16964338	29200689
230	11620	214342	245636	328812	1796222	16726923	30957121
220	9573	177502	193010	252932	1388732	15395037	29754631
210	7396	131272	138364	180962	961311	12889570	25652942
200	5200	90050	88152	112231	575508	9667178	19490164
190	3461	55105	51318	66327	302510	6245778	12429576
180	2112	30481	24656	29214	139695	3487364	6890874
170	1200	14132	10578	12383	52329	1624134	3173254
160	640	6218	4355	5311	19015	551252	1247666
150	341	2421	1623	1917	6254	174484	428327

Table A.1. (Continued)

Temperature (°C)	Electrical Resistivity (ohm-cm)						
	La25Mn2	La25Mn3	La25Mn4	La25Mn5	La25Mn6	La25Mn7	La25Mn8
140	180	991	667	672	2138	45336	149042
130	94	393	231	234	652	9226	55081
120	50	131	72	55	125	1431	25357
110	46	69	59	34	93	913	21799
100	46	64	57	32	86	790	21500
90	46	62	56	30	83	747	22062
80	48	60	56	30	83	739	23494
70	48	59	57	30	83	749	25534
60	51	60	58	30	85	771	28371
50	54	61	58	30	87	804	31979
40	56	62	59	31	89	854	37345

116

Table A.2. Electrical Resistivity versus Temperature Data for 0.25 Percent La^{+3} Doped BaTiO$_3$ After Annealing at 1150°C for 30 Minutes.

Temperature (°C)	Electrical Resistivity (ohm-cm)				
	La25Mn2	La25Mn3	La25Mn5	La25Mn6	La25Mn7
350	85557	201029	321720	427746	1058231
340	98766	244490	399763	574484	1480481
330	111476	286832	481829	758048	2149769
320	122296	327025	568470	1016746	3069844
310	130756	362591	653620	1320042	4311875
300	136330	390737	732426	1668100	6158559
290	138141	407483	778432	2129843	8586791
280	137230	411401	798495	2598581	11926098
270	132002	402373	792368	3028606	16884139
260	123384	381448	757497	3429988	22344809
250	111776	348323	696216	3670775	28140232
240	97837	305612	618395	3707961	33959060
230	82175	258524	518955	3524348	40282649
220	67391	206528	416419	3098187	37708617
210	49383	151812	307662	2494840	34307954
200	32133	103098	204229	1804367	27905077
190	19340	60403	122943	1220096	21451655
180	11779	30416	58900	637363	13477026
170	5529	13691	23542	249727	6047036
160	2375	5667	8068	76943	1909388
150	978	2143	2779	20239	465229

117

Table A.2. (Continued).

Temperature (°C)	Electrical Resistivity (ohm-cm)					
	La25Mn2	La25Mn3	La25Mn5	La25Mn6	La25Mn7	
140	446	771	851	5440	89981	
130	209	283	284	1611	16922	
120	112	88	87	420	2523	
110	91	52	68	243	1852	
100	81	47	66	239	1706	
90	80	45	67	251	1685	
80	79	44	68	258	1717	
70	79	44	72	287	1788	
60	80	44	71	309	1883	
50	81	46	76	336	1996	
40	82	48	78	360	2136	

118

Table A.3. Electrical Resistivity versus Temperature Data for 0.25 Percent La^{+3} Doped BaTiO$_3$ after Annealing at 1150°C for 60 Minutes.

Temperature (°C)	Electrical Resistivity (ohm-cm)			
	La25Mn2	La25Mn3	La25Mn4	La25Mn7
350	141560	220660	243962	469009
340	161913	282306	309695	632640
330	180445	358184	383653	873277
320	195952	439097	472040	1227104
310	206357	519001	573533	1698617
300	209015	601918	673219	2376362
290	205742	678161	768348	3253579
280	197636	738917	854235	4584351
270	183688	778502	912103	6256883
260	165507	786527	939375	8422727
250	143698	764844	927055	10991822
240	119956	709704	870006	13686932
230	96132	631827	783246	16267896
220	70744	527068	660635	17649608
210	46922	415766	509463	17605948
200	29351	285475	351245	15388550
190	15328	175689	212276	11763974
180	7883	87442	99561	7299697
170	3312	33609	38417	3484555
160	1437	12663	12852	1152584
150	608	4227	3658	271390
140	287	1426	1017	79522
130	149	501	295	12378
120	90	151	68	1863
110	85	65	47	1130
100	83	57	42	982
90	82	54	40	927
80	82	53	39	921
70	84	53	39	927
60	85	53	39	952
50	86	54	40	992
40	86	56	41	1051

Table A.4. Electrical Resistivity versus Temperature Data for 0.25 Percent La^{+3} Doped $BaTiO_3$ After Annealing at 1175°C for 30 Minutes.

Temperature (°C)	Electrical Resistivity (ohm-cm)		
	La25Mn2	La25Mn4	La25Mn6
350	389331	817616	1972680
340	478597	1035647	2682056
330	577508	1341868	3661413
320	674133	1662149	4992836
310	776916	2009464	6768999
300	861952	2384311	9050684
290	931464	2719880	11904101
280	976069	3005225	15470759
270	990013	3213224	19194063
260	973327	3302553	23235890
250	924012	3257276	26555302
240	843077	3062185	28631902
230	750010	2734612	28836904
220	651324	2293596	26970229
210	498568	1756097	23258253
200	332857	1220248	18183089
190	212971	726443	12665265
180	97883	347293	7149504
170	39828	133742	3062779
160	15332	39559	895012
150	5824	10098	184892
140	2022	2487	36670
130	723	607	7004
120	265	182	1060
110	231	152	681
100	228	148	584
90	235	154	549
80	244	164	541
70	261	180	548
60	280	201	566
50	307	227	594
40	339	265	615

Table A.5. Electrical Resistivity versus Temperature Data for 0.25 Percent La^{+3} Doped $BaTiO_3$ After Annealing at 1175°C for 60 Minutes.

Temperature (°C)	Electrical Resistivity (ohm-cm)		
	La25Mn2	La25Mn4	La25Mn6
350	35054	719493	1110364
340	38945	914218	1567023
330	42770	1145399	2148575
320	45864	1379235	2923159
310	48446	1633603	3931012
300	50265	1889095	5202406
290	51118	2122466	6657217
280	51046	2328265	8551081
270	49918	2488134	10589951
260	47491	2591671	12771572
250	44290	2625817	15029173
240	40067	2581600	17260883
230	34584	2462008	19099976
220	28797	2258351	20312465
210	22462	1916341	20622150
200	15713	1481781	19642087
190	9267	989079	17082527
180	5193	531465	13109146
170	2901	203263	8358922
160	1339	62871	4209019
150	655	17482	1587928
140	292	4712	409323
130	113	1242	63046
120	59	252	4701
110	44	164	3003
100	41	136	2499
90	41	123	2273
80	40	116	2195
70	41	114	2193
60	41	114	2241
50	41	116	2339
40	43	120	2476

Table A.6. Electrical Resistivity versus Temperature Data for 0.25 Percent La^{+3} Doped BaTiO$_3$ After Annealing at 1200°C for 30 Minutes.

Temperature (°C)	Electrical Resistivity (ohm-cm)					
	La25Mn2	La25Mn3	La25Mn4	La25Mn5	La25Mn6	La25Mn7
350	14615	80391	258088	244102	1297966	777779
340	17630	99238	327820	308312	1828122	1101359
330	20957	120408	414495	392770	2520323	1575948
320	25105	144413	505062	495575	3484473	2279275
310	29339	171576	598628	602781	4780723	3231312
300	33776	200532	686928	710007	6457544	4684353
290	38393	229982	759410	810546	8373976	6573033
280	42548	257772	809908	897760	10383731	9460858
270	46471	283091	826825	956486	12480445	13116189
260	49515	302027	807842	977376	14600296	17414373
250	51594	312478	755785	960218	15984807	22282329
240	51935	312118	681019	902698	16184119	26892466
230	50082	298368	579989	808770	15225411	30120685
220	45503	270918	471943	686890	12787845	31027545
210	37766	228816	351469	537023	9722594	29088323
200	27706	173666	231318	374826	6506097	24350731
190	17473	113355	131948	227552	3666572	17878325
180	9251	63151	59525	117581	1701135	10971717
170	4297	28428	24397	46587	591329	5314110
160	1820	11431	7838	15897	155352	1740387
150	733	4014	2609	5182	35223	414592

Table A.6. (Continued).

Temperature (°C)	Electrical Resistivity (ohm-cm)						
	La25Mn2	La25Mn3	La25Mn4	La25Mn5	La25Mn6	La25Mn7
140	298	1322	788	1542	8062	75538
130	116	401	250	492	1567	10972
120	50	82	70	140	202	1374
110	46	66	62	47	137	995
100	45	61	56	40	126	891
90	46	60	55	38	123	856
80	46	60	55	37	120	856
70	49	62	55	36	117	877
60	52	64	56	37	119	905
50	55	68	57	37	122	949
40	60	72	59	38	127	975

Table A.7. Electrical Resistivity versus Temperature Data for 0.25 Percent La^{+3} Doped $BaTiO_3$ After Annealing at 1200°C for 60 Minutes.

Temperature (°C)	Electrical Resistivity (ohm-cm)				
	La25Mn2	La25Mn3	La25Mn4	La25Mn6	La25Mn7
350	175121	426507	243424	753390	1428352
340	208519	523205	330580	1041923	2007698
330	240645	633489	458732	1461802	2883939
320	272748	730123	605258	1989318	4214301
310	299731	839167	764956	2654221	6258480
300	322403	929725	950552	3574480	9105146
290	337097	994090	1128087	4746724	13345287
280	344958	1050664	1294279	6159795	19599990
270	344014	1072462	1435240	7752565	28567037
260	333963	1068031	1525886	9387291	40816171
250	315922	1033854	1562903	10922759	55787676
240	290386	979028	1545407	11943993	71643121
230	254786	891253	1464235	12345472	87257647
220	211323	776167	1323828	10645733	97929446
210	164577	636609	1128087	9794074	98997767
200	113277	473376	892057	7401064	87538219
190	67419	309908	605258	4431708	66400941
180	34401	161338	347208	2219201	42012941
170	14915	69667	153315	773216	20226141
160	5689	23843	51042	221585	6623938
150	2113	7580	12943	46344	1731831

124

Table A.7. (Continued).

Temperature (°C)	Electrical Resistivity (ohm-cm)				
	La25Mn2	La25Mn3	La25Mn4	La25Mn6	La25Mn7
140	809	2196	3367	10028	255868
130	285	522	903	2120	42078
120	72	73	219	320	4776
110	38	52	66	246	3296
100	34	48	57	230	2905
90	33	47	55	228	2781
80	33	47	56	236	2792
70	33	48	58	247	2866
60	34	49	62	260	2988
50	35	51	66	278	3158
40	36	55	71	298	3374

Table A.8. Electrical Resistivity versus Temperature Data for 0.25 Percent La^{+3} Doped BaTiO$_3$ After Annealing at 1225°C for 30 Minutes.

Temperature (°C)	Electrical Resistivity (ohm-cm)					
	La25Mn2	La25Mn3	La25Mn4	La25Mn5	La25Mn6	La25Mn7
350	109003	131453	474794	634284	4384548	1001761
340	115837	147949	549536	718110	6140663	1316338
330	121553	164747	624431	795175	8851824	1748011
320	125261	179653	691586	855252	13104655	2359338
310	126548	193076	749572	892233	18826110	3200584
300	126983	204372	789958	903108	26415916	4216394
290	125261	212907	810931	889312	38266449	5486134
280	121553	218202	812729	853014	52127407	7184006
270	115837	220240	793378	799073	71082828	9108835
260	109326	218454	755754	727728	94586022	11637703
250	100962	213389	699505	649446	117876047	14156026
240	91465	204261	629795	550713	138800789	16670223
230	80681	190927	541419	454070	156478842	18772121
220	66580	169180	445913	357480	155346578	19625399
210	49269	141831	334740	255503	152024195	18451230
200	31938	114672	231695	162362	136379845	15700319
190	18805	83838	133288	93149	172286667	10255553
180	10618	53062	64874	44661	84076464	6501816
170	5474	27358	27191	19759	51216885	2359338
160	2695	10142	10098	7181	24034153	534979
150	1301	3842	3400	2708	8885354	166702

Table A.8. (Continued).

Temperature (°C)	Electrical Resistivity (ohm-cm)						
	La25Mn2	La25Mn3	La25Mn4	La25Mn5	La25Mn6	La25Mn7
140	604	1338	1062	920	2538672	38379
130	273	420	329	331	579193	7575
120	100	99	93	107	105664	964
110	85	82	76	38	35434	670
100	82	78	72	33	28502	585
90	82	77	71	31	25497	555
80	84	79	72	30	24666	559
70	87	81	74	30	25196	569
60	93	84	77	30	26180	583
50	100	89	82	31	27925	599
40	109	96	88	32	29958	628

Table A.9. Electrical Resistivity versus Temperature Data for 0.25 Percent La^{+3} Doped BaTiO$_3$ After Annealing at 1225°C for 60 Minutes.

Temperature (°C)	Electrical Resistivity (ohm-cm)				
	La25Mn2	La25Mn3	La25Mn4	La25Mn5	La25Mn7
350	119972	1108391	893274	947189	1955594
340	135664	1318087	1092600	1304136	2763296
330	150138	1514572	1271198	1787149	3847479
320	163735	1704225	1443282	2497471	5487516
310	174256	1854343	1586138	3527463	7942457
300	182055	1975796	1697107	4825303	11271038
290	186489	2039131	1766261	6591264	16072900
280	186891	2049127	1784138	8639901	22393406
270	182951	2013870	1754540	11366269	31511835
260	175077	1931454	1683063	14129340	43670742
250	162916	1806268	1566405	16802960	58165314
240	146012	1648537	1420791	19403722	76087400
230	125768	1448591	1253124	20842792	92078650
220	100907	1219231	1057637	21118172	104073570
210	75461	953144	847465	20152960	107364434
200	50453	678922	592846	18048063	98062100
190	30028	418022	372933	14782720	76949580
180	15991	212040	187657	10836485	50209245
170	7192	82660	79402	6968421	25221172
160	3198	27815	27259	3744379	8650701
150	1246	7973	8448	1618614	2006145

Table A.9. (Continued).

Temperature (°C)	Electrical Resistivity (ohm-cm)				
	La25Mn2	La25Mn3	La25Mn4	La25Mn5	La25Mn7
140	489	2337	2471	572128	349141
130	178	607	648	150613	45729
120	49	108	185	26892	4024
110	35	68	56	21014	2445
100	34	62	50	19703	2059
90	34	61	49	19887	1931
80	34	62	49	20775	1896
70	35	63	50	22123	1926
60	37	65	52	24172	1996
50	39	67	55	26640	2089
40	40	71	57	29634	2203

Table B.1. Electrical Resistivity versus Temperature Data for Un-Annealed 0.20 Percent La^{+3} doped $BaTiO_3$.

Temperature (°C)	Electrical Resistivity (ohm-cm)		
	La20Mn2	La20Mn3	La20Mn4
350	2266	180029	288828
340	2815	215554	381027
330	3373	248773	490120
320	4010	275680	610306
310	4621	300172	756306
300	5220	313787	918655
290	5750	318604	1069897
280	6196	314126	1201802
270	6560	299553	1290169
260	6835	276467	1319271
250	6957	246243	1290169
240	6811	212714	1189580
230	6462	173680	1047541
220	5691	133902	858010
210	4722	96534	641547
200	3709	63304	438110
190	2726	37062	261106
180	1862	19606	133941
170	1210	9224	63689
160	732	3943	26525
150	425	1725	10798
140	243	698	4332
130	120	259	1729
120	56	68	765
110	53	54	695
100	53	51	691
90	54	50	702
80	55	50	725
70	57	50	755
60	60	51	801
50	63	53	854
40	67	55	923

Table B.2. Electrical Resistivity versus Temperature Data for 0.20 Percent La^{+3} doped $BaTiO_3$ After Annealing at 1150°C for 30 Minutes.

Temperature (°C)	Electrical Resistivity (ohm-cm)		
	La20Mn2	La20Mn3	La20Mn4
350	328458	357764	492860
340	391574	448397	669479
330	452840	543390	889050
320	502397	648112	1171588
310	541200	752906	1555088
300	560176	838416	1983462
290	557829	900798	2464302
280	535396	931286	2919690
270	501136	922769	3359595
260	451305	877299	3671908
250	396629	804968	3792794
240	333115	708825	3681687
230	270967	600532	3347393
220	204718	480426	2824256
210	145238	383124	2178839
200	90774	242522	1510900
190	51804	136954	921649
180	25183	68788	443812
170	11412	28446	173678
160	4528	10055	58829
150	1722	3374	18482
140	711	1033	5237
130	254	305	1703
120	89	83	423
110	76	66	341
100	73	63	319
90	71	62	315
80	71	62	317
70	71	61	325
60	72	61	336
50	74	64	352
40	76	66	374

Table B.3. Electrical Resistivity versus Temperature Data for 0.20 Percent
La^{+3} doped $BaTiO_3$ After Annealing at 1150°C for 60 Minutes.

Temperature (°C)	Electrical Resistivity (ohm-cm)	
	La20Mn2	La20Mn3
350	142450	521149
340	180756	660877
330	227156	829100
320	274147	1002209
310	318848	1159335
300	361278	1315399
290	394400	1422053
280	411220	1484552
270	414881	1483747
260	403506	1420576
250	379931	1309105
240	341845	1144782
230	295279	946723
220	243156	751657
210	185431	535427
200	127104	358588
190	77460	200295
180	39890	93700
170	18568	36383
160	7517	11896
150	2947	3614
140	1101	1086
130	422	304
120	110	65
110	76	51
100	72	47
90	70	45
80	70	44
70	70	44
60	72	44
50	74	46
40	77	47

Table B.4. Electrical Resistivity versus Temperature Data for 0.20 Percent
La^{+3} doped $BaTiO_3$ After Annealing at 1175°C for 30 Minutes.

Temperature (°C)	Electrical Resistivity (ohm-cm)	
	La20Mn2	La20Mn4
350	242753	3238982
340	285956	4439406
330	329929	6085136
320	372070	8336063
310	409490	11267815
300	439636	15195453
290	459953	20176057
280	469598	26250782
270	466541	33074680
260	449002	40169249
250	418579	46327600
240	372844	50459284
230	317083	51335989
220	252861	48525625
210	185553	41680317
200	122707	32232779
190	69709	21239651
180	36119	11663177
170	16822	4933589
160	8162	1601930
150	4058	423440
140	2165	105107
130	1183	24464
120	700	6534
110	681	4835
100	740	4255
90	831	4023
80	963	3951
70	1130	3963
60	1352	4060
50	1650	4214
40	2073	4439

Table B.5. Electrical Resistivity versus Temperature Data for 0.20 Percent
La^{+3} doped $BaTiO_3$ After Annealing at 1175°C for 60 Minutes.

Temperature	Electrical Resistivity (ohm-cm)	
(°C)	La20Mn2	La20Mn4
350	27098	396389
340	31039	503925
330	34361	610269
320	37890	741930
310	40998	883618
300	43434	1026137
290	44865	1178157
280	45538	1327501
270	45173	1468448
260	43674	1592503
250	40956	1692035
240	36864	1751425
230	31712	1747816
220	25325	1656784
210	19166	1469296
200	12902	1172728
190	8041	818270
180	4426	478350
170	2263	220713
160	1067	81045
150	502	24828
140	235	6045
130	116	1370
120	67	228
110	65	156
100	67	131
90	70	120
80	75	114
70	80	112
60	86	111
50	92	114
40	98	117

Table B.6. Electrical Resistivity versus Temperature Data for 0.20 Percent La^{+3} doped BaTiO$_3$ After Annealing at 1200°C for 60 Minutes.

Temperature (°C)	Electrical Resistivity (ohm-cm)		
	La20Mn2	La20Mn3	La20Mn4
350	181814	197686	1685637
340	228619	255494	2284039
330	285566	315349	3121693
320	345307	387135	4269231
310	411037	469718	5662906
300	472661	558565	7407693
290	535255	647859	9451195
280	581670	721480	11564753
270	615752	779021	13501707
260	629271	808793	14863593
250	624287	810513	15303442
240	597093	779021	14704112
230	552128	714712	13177147
220	488026	621438	11096544
210	401611	498614	8591995
200	296580	356020	5869050
190	199914	217930	3421781
180	113814	110739	1617019
170	53891	45841	588164
160	22845	16006	174022
150	8275	5106	48170
140	2749	1574	12990
130	864	369	3640
120	200	95	908
110	152	81	759
100	144	77	737
90	143	76	743
80	144	76	770
70	147	77	804
60	153	79	851
50	159	81	914
40	168	85	982

Table B.7. Electrical Resistivity versus Temperature Data for 0.20 Percent La^{+3} doped $BaTiO_3$ After Annealing at 1225°C for 30 Minutes.

Temperature (°C)	Electrical Resistivity (ohm-cm)		
	La20Mn2	La20Mn3	La20Mn4
350	182074	85638	3104503
340	202961	101438	4157665
330	223523	117982	5449511
320	239816	136765	7146899
310	252914	155573	9219716
300	261739	172134	11647809
290	267336	186371	13998743
280	268484	197342	16232585
270	265820	202428	18057550
260	258492	201834	19193245
250	246272	195378	19562346
240	229262	183021	19073287
230	206197	164314	17742593
220	176090	138209	15649877
210	141537	108655	13443727
200	101922	74498	10670370
190	64668	47892	7389167
180	35185	23988	4268148
170	16819	12327	2021011
160	7213	4989	749810
150	2787	2012	248917
140	1011	764	65488
130	321	289	18619
120	90	76	3365
110	76	53	2317
100	72	50	2070
90	71	48	2000
80	71	48	2010
70	72	48	2063
60	74	49	2154
50	77	50	2271
40	82	52	2405

Table B.8. Electrical Resistivity versus Temperature Data for 0.20 Percent La^{+3} doped $BaTiO_3$ After Annealing at 1225°C for 60 Minutes.

Temperature (°C)	Electrical Resistivity (ohm-cm)		
	La20Mn2	La20Mn3	La20Mn4
350	98872	66421	1433585
340	120716	85081	1941165
330	144859	106833	2571862
320	173508	134192	3416354
310	206667	166977	4387778
300	239390	201658	5560220
290	272721	239213	6849748
280	302082	276709	8031430
270	329923	308806	9035358
260	349548	336507	9740244
250	360889	353819	9916061
240	359639	357266	9637715
230	343003	344227	8918016
220	312384	313498	7870341
210	261281	268385	6417638
200	202107	202897	4743953
190	139039	136977	3107182
180	81745	79738	1683057
170	41861	38075	760872
160	17390	15074	252227
150	6815	5475	72474
140	2403	1684	18749
130	785	441	4695
120	161	82	919
110	109	67	685
100	102	63	648
90	101	62	646
80	102	63	662
70	105	64	687
60	109	66	725
50	113	68	776
40	120	72	840

Table C.1. Electrical Resistivity versus Temperature Data for Barium-Lead Titanate Samples Sintered 1200°C.

Temperature (°C)	Electrical Resistivity (ohm-cm)				
	P10La35	P20La35Mn2	P30La35Mn2	P40La35Mn2	P50La35Mn2
450	231768	8929	1105	15381	2203
440	251705	9162	1087	17397	2852
430	282632	9357	1053	19745	3654
420	343353	9408	1004	21839	4761
410	444136	9333	941	23546	6097
400	574236	9114	873	24991	7868
390	748018	8751	798	26045	9967
380	977753	8276	724	26845	12697
370	1279568	7781	648	27295	15832
360	1693385	7176	573	27378	19729
350	2215732	6498	507	27027	24630
340	2842468	5858	439	26102	30901
330	3527886	5191	381	24614	39581
320	4416710	4581	327	23047	45050
310	5313025	4024	282	21511	54960
300	5620700	3461	241	20156	65990
290	4858920	2890	210	12531	80655
280	3448402	2487	180	8827	99155
270	2261054	2092	159	9406	120226
260	1406168	1720	139	10181	147971

Table C.1. (Continued).

Temperature (°C)	Electrical Resistivity (ohm-cm)				
	P10La35	P20La35Mn2	P30La35Mn2	P40La35Mn2	P50La35Mn2
250	861354	1398	113	11234	179777
240	507584	1114	114	12444	216258
230	301702	879	122	13837	264233
220	173775	692	131	15582	325485
210	99736	497	141	17568	404546
200	55891	312	153	19877	502906
190	31089	293	166	22611	634857
180	16444	295	180	25932	820306
170	7880	301	198	30268	1012430
160	3772	311	218	34327	1291018
150	3131	322	241	40495	1665469
140	2847	336	266	47217	2090888
130	2714	351	291	56616	2757873
120	2691	369	326	67491	3555669
110	2746	388	365	78764	4703219
100	2869	408	406	96080	6422760
90	3099	428	462	117501	8474082
80	3401	453	522	143927	11450099
70	3823	487	602	179189	16873830
60	4359	517	699	221905	25178229
50	5182	553	815	283976	37978611
40	6317	583	994	359455	59370885

Table C.2. Electrical Resistivity versus Temperature Data for Barium-Lead Titanate Samples Sintered 1250°C.

Temperature (°C)	Electrical Resistivity (ohm-cm)				
	P10La35	P20La35Mn2	P30La35Mn2	P40La35Mn2	P50La35Mn2
450	1398	1382	168	32521	1654
440	1469	1487	172	39977	2579
430	1536	1582	177	48436	3945
420	1596	1651	179	62180	7141
410	1649	1689	180	76879	12196
400	1683	1712	180	91059	23425
390	1704	1704	178	106157	42492
380	1719	1674	175	122684	79510
370	1726	1616	170	137045	139679
360	1726	1549	164	160564	185404
350	1711	1464	157	157602	204678
340	1690	1377	148	152897	193201
330	1662	1278	138	134349	138278
320	1622	1170	128	101176	34541
310	1572	1054	117	68984	37655
300	1518	940	106	35143	43113
290	1453	824	95	5280	49934
280	1388	704	83	4662	57344
270	1316	601	72	4913	65213
260	1235	516	60	5385	75585

Table C.2. (Continued).

Temperature (°C)	Electrical Resistivity (ohm-cm)				
	P10La35	P20La35Mn2	P30La35Mn2	P40La35Mn2	P50La35Mn2
250	1144	448	43	5904	87226
240	1074	379	42	6504	99149
230	988	315	43	7265	112964
220	890	247	44	8003	129203
210	800	178	45	8966	147135
200	712	179	45	10143	167389
190	629	190	46	10671	191412
180	545	209	47	11708	218179
170	454	229	48	13092	249367
160	293	262	49	14582	286521
150	269	289	50	17074	331822
140	262	327	51	18883	380009
130	260	379	52	21155	443140
120	263	435	54	23741	516167
110	269	511	55	26870	598336
100	274	584	57	30241	705546
90	282	710	58	34147	836943
80	293	837	60	37766	979739
70	306	998	62	48151	1188075
60	325	1200	65	53216	1455810
50	345	1505	68	61712	1759362
40	369	1803	70	73566	2233657